Imperial College London
The Blackett Laboratory
Quantum Optics & Laser Science Group

Formation and dynamics of structural defects in ion chains

Ramil Nigmatullin

Thesis submitted in partial fulfillment of the
requirements for the degree of
Doctor of Philosophy
of Imperial College London
and the Diploma of Membership of Imperial College.

Declaration of Originality

Unless specifically mentioned the work presented in this thesis is my own. The figures in this thesis that are not my own are appropriately referenced and the permission to use them has been granted to me by their authors.

Copyright Declaration

Abstract

Non-adiabatic crossing of symmetry breaking phase transitions results in formation of a domain structure and topological defects. The average density of domains depends on the quench rate of the phase transition. Kibble-Zurek mechanism predicts the scaling of the number of domains with quench rate. Phase transitions are ubiquitous in Nature and formation of domains and defects occurs in many different systems. One example of such system is Coulomb crystals of trapped ions, where structural defects can form as a result of symmetry breaking structural transitions between different crystal configurations. In the thesis, we investigate the Kibble-Zurek mechanism using the linear to zigzag structural phase transition in trapped ion Coulomb crystals. First, we analyse the equilibrium properties of crystals in the vicinity of the critical point of the linear to zigzag transition. Next, we show how to derive Kibble-Zurek scaling laws by transforming the equations of motion into a universal form. This mathematical derivation of the scaling laws is generalized for finite and inhomogeneous systems. Two experiments measuring the defect scaling in small trapped ion crystals are described, whose results agree with molecular dynamics simulations. In order to understand and predict defect dynamics we develop the technique for calculating the effective potential in which the defects move. Using this technique we show that heavy molecular ions stabilize the structural defects in zigzag chains and suggest a way of controlling kink motion using the application of electric fields. Finally, conclusions are drawn and possibilities for future work are suggested.

Contents

Acknowledgments

First of all I would like to thanks my supervisors, Martin Plenio and Alex Retzker, for their advice. They have guided me into interesting topics and have constantly challenged me to independently tackle difficult research problems.

It was very exciting to collaborate with the experimental groups and witness the physical realizations of our theoretical ideas. I am grateful to teams of Optical Metrology With Trapped Ions group in Physikalisch-Technische Bundesanstalt (PTB) and Cold Ions and Experimental Quantum Information group in the University of Mainz for the great effort that they have put into their experiments. I would like to especially thank Tanja Mehlstäubler for her enthusiasm, insight and excellent management of the project. Much of the content of the thesis was stimulated by the results of her experiments and our discussions.

I would like to thank Adolfo del Campo for many interesting discussions in Ulm and in Los Alamos National Laboratory. I very much appreciate him and Wojciech Zurek hosting me in LANL for two productive and enjoyable months. I am grateful to Wojciech for advice concerning the analysis of the ion chain in thermodynamic equilibrium. Concerning the Kibble-Zurek problem, I would like to acknowledge Gor Nikoghosyan for his insights. It was a pleasure to work with him.

During my PhD, I have been working in two Universities and two countries: Imperial College London (UK) and the University of Ulm (Germany). Along the way, I have benefited from interactions with many people both scientifically and personally. Indeed, much productive thinking took place in conversations during the coffee breaks, walks in the forest and trips to the pub. Many thanks to the first Cohort of the Controlled Quantum Dynamics DTC; I hope that we will keep in contact. I would also like to thank Ms Lilian Wanjohi and Frau Bender-Palm for their friendly advice and help in administrative tasks; they really made my life easier.

My friends and family have been very supportive. I was fortunate that Mischa Woods came also to Ulm from Imperial and we have become close friends during the past three years. My parents, Rinat and Alla, my sister, Yulia, were always there for me. Their advice and encouragement was invaluable. Finally, I am very grateful to my fiancee, Tania Gasanova, for her love and support.

Publications

Parts of this thesis are based on material published in the following papers

- Nikoghosyan G, Nigmatullin R and Plenio M B, Universality in the dynamics of second-order phase transitions, arXiv:1311.1543 (2013)
- Partner H L, Nigmatullin R, Burgermeister T, Pyka K, Keller J, Retzker A, Plenio M B and Mehlstäubler T E, Dynamics of topological defects in ion Coulomb crystals, *New J. Phys.*, 15, 103013 (2013)
- Pyka K, Keller J, Partner H L, Nigmatullin R, Burgermeister T, Meier D M, Kuhlmann K, Retzker A, Plenio M B, Zurek W H, del Campo A and Mehlstubler T E, Topological defect formation and spontaneous symmetry breaking in ion Coulomb crystals, *Nat. Commun.*, 4, 2291 (2013)
- Ulm S, Rossnagel J, Jacob G, Degunther C, Dawkins S T, Poschinger U G, Nigmatullin R, Retzker A, Plenio M B, Schmidt-Kaler F and Singer K, Observation of the Kibble-Zurek scaling law for defect formation in ion crystals, *Nat. Commun.*, 4, 2290 (2013)

Chapter 1

Introduction

> *"... the task of theory is to try and understand the universal aspects of the natural world; first of all to identify the universals; then to clarify what they are about, and to unify and inter-relate them; finally, to provide some insights into their origin and nature." M. Fisher*

The main objective of the present thesis is to contribute to our understanding of the dynamical non-equilibrium phase transition phenomena. In particular, we will focus on the process of creation of topological defects following a phase transition. In the literature, this scenario of defect formation following a dynamic symmetry breaking is often referred to as the Kibble-Zurek mechanism. One of the main goals of our work was to provide an experimental verification of Kibble-Zurek theory. This has been done in collaboration with experimental groups (PTB and the University of Mainz) using structural phase transitions of Coulomb crystals in ion traps (Chapter 4). The experimental study was carried out on small inhomogeneous systems and the extrapolation of the results to thermodynamic limit is not trivial. In order to understand the finite size Kibble-Zurek scaling, we develop a mathematically rigourous perspective on the physics behind the Kibble-Zurek mechanism (Chapter 3). In the Chapter 5, we develop models for understanding the dynamics of defects in ion crystals - novel collective structures whose dynamics is yet to be fully explored. In this chapter, we briefly review the important ideas from the phase transition theory as well as provide the necessary background information on Coulomb crystals in ion traps.

1.1 Thermodynamics and statistical mechanics

Since ancient times people have observed that different materials have varying properties and that matter can transform from one state to another. However, a theoretical understanding of matter and phase transition started to develop only recently. The understanding of fundamental properties of matter is the subject of statistical physics developed initially in the second half of the 18th century (for a historical review see

for example [67]). The main breakthrough at that time was the realization that matter is composed of a large number of small particles in continuous random motion. These theory is known as the *kinetic model* of matter. Using the kinetic model it was possible to explain many phenomena, for example, liquid to gas phase transitions. Starting with this work, the theory of matter and phase transition has developed into a collection of many sophisticated ideas. A wide variety of phases of matter have been predicted and discovered, for example, ferromagnets, antiferromagnets, superconductors, quantum Hall phases, Bose-Einstein condensates and many more. Materials in various phases are put to practical uses - for instance, electric conductors and insulators constitute an essential part of human economic infrastructure.

A fundamental observation for the development of thermodynamics and statistical mechanics is that systems with many degrees (ideally infinitely) of freedom flow irreversibly towards unchanging state of statistical equilibrium. These observation is encompassed in the second law of thermodynamics - the physical systems tend to the state of thermodynamic equilibrium or states of maximum entropy. The statistical ensemble of possible states of a system that is in thermal equilibrium with a heat bath is called the *canonical ensemble*. The canonical ensemble is constructed by assigning a probability of finding a system in a particular microstate j in the small volume of phase space $d\Omega$ by

$$p_j = e^{-(E_j - F)/k_B T} d\Omega, \tag{1.1}$$

where E_j is the energy of the jth microstate, k_B is the Boltzmann constant, T is the temperature of the heat bath and F is the free energy. The free energy constant F can be determined by requiring that all probabilities sum to unity

$$e^{-F/k_B T} = \int d\Omega e^{-E_j/k_B T}. \tag{1.2}$$

In theory, construction and analysis of the canonical ensembles allows one to calculate all of the thermodynamic properties of the system, though this task is often computationally challenging and necessitates the use of approximate methods.

1.2 Mean field approximation and Ginzburg-Landau theory

Matter in systems in thermodynamic equilibrium organizes itself into structures known as *thermodynamic phases*. There is a wide variety of possible phases exhibited by different systems and remarkably the same system can undergo transformation from one phase into the other when the specific parameters such as pressure are varied. The existence of distinct phases and *phase transitions* are studied using statistical mechanics by analyzing the canonical ensemble. Since matter is composed of a huge number of interacting particles it is difficult to theoretically predict the topology of the phase diagram and even more difficult to predict the precise details of the phase diagram such as locations of critical points. One of the most useful approximations that in most cases allows one to predict the general features of the phase diagram is the *mean field theory*. The idea of the mean field is to describe the effect of all the particles on any given individual particle by a single approximate quantity. This way the many-body problem is effectively reduced to a one body problem. Early examples of mean field theories in the context of phase transitions are van der Waals theory of gases and liquids and Weiss's theory of magnetism.

For the construction of a free energy functional it is very useful to consider the symmetries present in the system. Symmetry considerations are important because phase transitions are accompanied by changes of symmetries in the system (except in recently discovered topological phase transitions [84]). For example in the case of liquid/solid phase transition there is a change in the rotational symmetry of the system. The observation that each phase transition is a manifestation of symmetry breaking was exploited very effectively by Lev Landau in the theoretical framework that has become known as *Ginzburg-Landau's (GL) theory* of phase transitions. Landau's theory writes the free energy as an integral over space of an order parameter field, which respects the symmetries of the system. In general, the free energy is of the following form

$$-\mathcal{F}/k_BT = \int \left\{ A\phi(\mathbf{r}) + B\phi(\mathbf{r})^2 + C\phi(\mathbf{r})^4 + D\left[\nabla\phi(\mathbf{r})\right]^2 + \ldots \right\} d^d\mathbf{r}, \tag{1.3}$$

where A, B, $C, \ldots$ are parameters that depend on the microscopic structure of the system and the externally imposed conditions, $\phi(\mathbf{r})$ is the order parameter, $\mathbf{r}$ is the spatial position and d is the dimensionality of the system. By construction the order parameter is small in the vicinity of the critical point and therefore near the critical

point the first several terms of the series expansion (1.3) accurately describe the free energy of the system. In order to determine the structure of the phase of the system in a thermal equilibrium for a given set of parameters $\mathcal{Q} = \{A, B, C \ldots\}$ one needs to find $\phi(\mathbf{r})$ that minimizes the free energy functional $\mathcal{F}$. Thus by minimizing the functional (1.3) it is possible to determine the critical points and the nature of the phases for given $\mathcal{Q}$. It also possible to determine *the order* of a particular phase transition. The phase transition is said to be of nth order if $(\partial^n \mathcal{F}/\partial h^n)_{\mathcal{Q}}$ is discontinuous, where h is the parameter the variation of which induces the phase transition. In practice most phase transitions are either of first or second order. In the case of the first order phase transition, the two phases are separated by an energy gap and thus a transition between them requires an influx of certain amount of energy known as latent heat. Second order phase transition are continuous and do not require latent heat. Critical points of the second order phase transition are of particular theoretical interest. The reason for this is that near the critical point the system exhibits *scale invariant* properties with many intriguing implications. One of the implication of the scale invariance are power divergences of thermodynamic quantities. The correlation length ξ in particular diverges

$$\xi = \xi_0 \left|\delta\right|^{-\nu}, \tag{1.4}$$

where the system is in the critical state when $\delta = 0$, ξ_0 is a constant that depends on the microscopic structure of the system and ν is the exponent of divergence of the correlation length. Divergence of the correlation length indicates a reorganization of the atoms and generation of long range order.

The exponents characterizing the powerlaw divergences depend intricately on the symmetries of the order parameter and the dimensionality of space. One of the principle tasks of the study of phase transition is the determination of the critical exponents. All of the thermodynamic properties, including critical exponents can be calculated from the partition function

$$Z = \int D\phi e^{-\mathcal{F}[\phi]/k_B T}, \tag{1.5}$$

where $\int D\phi$ denotes a functional integral over all possible order parameter configurations $\phi(\mathbf{r})$. The functional integral (1.5) can be done analytically only for specific functionals $\mathcal{F}[\phi]$, notably when $\mathcal{F}[\phi]$ is quadratic in ϕ. $\mathcal{F}[\phi]$ can be made quadratic by considering only the lowest order perturbation theory in fluctuations around the ground

state. Effectively the lowest order perturbation theory is the mean field theory. The mean field theory calculation gives the critical exponent of $\nu = 1/2$, which has been experimentally measured in many physical systems. The details of the derivation of the mean field exponent $\nu = 1/2$ are presented in Chapter 2.

The beauty of the Landau's approach is that it connects phase transitions in seemingly unrelated physical systems, since the free energy functional is constructed chiefly by considering the symmetry properties of the system rather than the specific microscopic details of the system. For example, it is well known that the liquid/gas and paramagnetic/ferromagnetic phase transitions can be described by GL free energy functional of the same form and thus topologically the phase diagrams of these two completely disparate systems are equivalent. Of course, the detailed structure of these two phase diagrams is different but in the vicinity of the critical point properties of the systems and, in particular, the critical exponents are identical. Thus to understand second order phase transitions it is sufficient to analyze a small set of GL free energies; the vast majority of phase transitions in real physical systems can then be understood simply by mapping the system to an appropriate GL theory using symmetry arguments. Each kind of distinct critical point is characterized by a set of critical exponents and dictates a particular *universality class*.

In many cases the mean field theory can accurately describe the behavior of a system. By construction the Ginzburg-Landau free energy accurately describes the system near the critical point. For this reason, we may expect that the mean field theory will be accurate near the critical point but will fail away from the critical point. Surprisingly it was demonstrated that the mean field theory also fails right at the critical point; in the close proximity to the critical point the effect of the fluctuations of the order parameter can be greater than the effect of the average of the order parameter. The failure of the mean field theory was predicted be analyzing exactly solvable models such as one dimensional and two dimensional Ising models [7]. Experimentally discrepancies with the mean field theory predictions were observed in measurements of critical exponents for specific heat in classical fluids of argon, oxygen and nitrogen [3, 29, 121] (for detailed review of the experimental measurements of critical exponents in fluids and magnets see [43]). It can be shown that in dimensions greater than four fluctuations always have a negligible effect and the mean field is always valid. For the dimensions less than four, the mean field approximation is only faithful sufficiently far from the critical point. The regime of validity of the mean field approximation is described by the Ginzburg criterion [56, 1, 73]. Mean field theory may also be valid for systems of dimensionality

less than four but containing long range interactions.

Many statistical models do not belong to the mean field universality class and also do not have a known exact solution. A technique known as the renormalization group have been developed that allows one to calculate in many instances the critical exponents without solving the complete model (see [23, 68, 50, 67, 57] for reviews). Renormalization group is a refinement of the scaling argument and it involves analyzing the behavior of the Hamiltonian under scaling transformations.

Phase transitions can occur at zero temperature in which case they are driven by quantum rather than thermal fluctuations. Such phase transitions are referred to as quantum phase transitions [122, 114]. In the current thesis we will be concerned with classical thermal phase transitions, but many of the ideas can be applied equally well to the quantum phase transitions.

1.3 Computers and numerical methods

The difficulty of applying statistical mechanical theory is that often the constructed models have no known analytic solutions. A simple example with no known analytical solution is the three dimensional Ising model which describes magnetism in three dimensional materials. In fact, the vast majority of statistical mechanical models cannot be solved exactly.

The models that have no analytic solutions can, nevertheless, be studied algorithmically using computational engines. Early numerical calculations were performed mentally by teams of humans. The mechanical automation of calculations goes back to the work of Charles Babbage in the 18th century. More recently, the invention of transistor and integrated circuits has lead to creation of electronic computers that are capable of many millions of operations per second. The computational power of modern computers makes it feasible to explore numerically statistical mechanical models.

One of the most common algorithmic strategies for solving statistical mechanical problems are the so called Monte Carlo methods. These methods are essentially systematized trial and error approaches for solving optimization problems. For instance if one wants to find a ground state of a particular Hamiltonian, one can try many different trial configurations and check which particular configuration are the most optimal. Apart from probabilistic algorithms, there are also extremely useful deterministic algorithms. For instance, ordinary and partial differential equations can be solved numerically on the computer by converting the differential equations into systems of difference equations

and sequentially evaluating them. This way one may compute statics and dynamics of systems of particles and fields.

It is important to note the limitations of computers. First of all, in the case of complex optimization problems it may well be that the found solutions are not globally optimal. In the case of deterministic algorithms as in the solution of differential equations there are errors coming from the discretization. Thus, one must be careful and take into account possible errors resulting from the computation. Secondly, even though computers are powerful they are not sufficiently powerful in many interesting and important instances. Real materials can easily contain 10^{23} mutually interacting components and currently even the most powerful computers could not treat systems with so many degrees of freedom in an economically viable timeframe. If the system is quantum mechanical, the number of degrees of freedom that need to be considered growths very quickly with the number of particles and computational power becomes a limiting factor fairy quickly.

In order to be able to gain insight into these systems using the available computing power one limits the number of degrees of freedom to a manageable number. Thus, instead of considering infinitely many interacting particles one considers a finite cell of the material and computes the desired quantities on a finite system. Such calculations lead to artifacts coming from the fact that the number of degrees of freedom is finite and from the boundaries of the cells. This means that one has to be particularly careful when interpreting the results of computations on the finite size systems. For instance, the singularities that should be present at the critical point of the second order phase transition will no longer be there. The correlation length cannot divergence to infinity at the critical points as it is limited by the finite size of the sample. Thus all of the sharp features that are expected at criticality in the thermodynamic limit will be washed out in the system of finite size (figure 1.1). Strictly speaking there are no true phase transitions in finite systems since there are no mathematical singularities in thermodynamic quantities for finite size systems. However, as one increases the system size there is often a rapid convergence towards the thermodynamic limit and the computed properties of even moderately sized system could be identical to properties of infinite systems. When making measurements on a finite size system one has to make sure that the results are not sensitive to the system size. For this reason, one typically makes the same measurements for systems of several sizes. The way the results depend on the system size is not arbitrary and by analysing such results it is possible to extrapolate the behavior of the system in the thermodynamic limit. For a review of

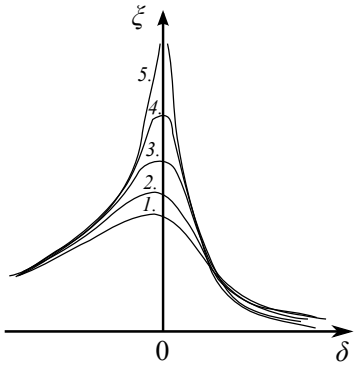

Figure 1.1: Cartoon illustrating how the sharp features at a critical point of a phase transition become smooth in finite size systems. The five curves 1 to 5 show the correlation length ξ in the vicinity of the critical point for different systems, curve 1 corresponding to the smallest system and curve 5 corresponding to the largest system.

the finite size scaling theory refer for instance to [19].

1.4 Experiments in atomic physics - model emulation

Recent advanced in quantum optics and atomic physics provide a possibility for studying phase transition phenomena in a way complementary to the computational investigations. The key development was the invention of laser cooling and trapping technologies for the spectroscopic and metrological applications. The clouds of trapped atoms at ultralow temperatures can organize into a myriad number of phases and can transform from one phase into the other by specific applications of laser light and external electromagnetic fields. For instance, by using neutral atoms trapped in optical lattices prototypical models of condensed matter systems such as Bose-Hubbard model can be realized [14]. The advantage of investigating statistical mechanics in atomic systems is that in atomic systems it is often possible to engineer Hamiltonians in a clean precise way and perform measurements that are typically not possible in condensed matter systems. However, just as in computer calculations the experimental atomic systems are of finite size. Thus one has to carefully extrapolate the information obtained in atomic experiments to the thermodynamic limit using the finite size scaling theories. In trapped atomic systems in addition to the finite size effects there are also often complications arising from the inhomogeneities of the systems. Typically the atomic gas is trapped in a harmonic confining potential, which results in a spatial dependence

of parameters of the Hamiltonian (such as coupling strengths). The artifact of inhomogeneity must be considered during the interpretation of the results of such atomic experiments. The necessity for taking the trapping potential into the account has lead to the development of the trap-size scaling theory [22, 26, 130, 33, 32, 25, 106, 35].

1.5 Non-equilibrium phase transitions and the coarsening problem

The discussion so far was focused exclusively on the approaches to investigate the structure and thermodynamic properties of systems in thermodynamic equilibrium. The majority of processes in Nature drive the system out of the thermal equilibrium, and for this reason it is important to understand non-equilibrium dynamics. The theories of non-equilibrium thermodynamics are under active development.

One important task in non-equilibrium thermodynamics is to understand how the system transforms from one phase in a given finite time. A time dependence of a critical parameter that induces the phase transition is known as *quench*. If the duration of the quench is much greater than the inverse of the frequency gap between the ground state and the first eigenstate then the quench is *adiabatic*. On the other hand if the quench is comparable or faster than the inverse of the frequency gap then the quench is *non-adiabatic*. Non-adiabatic processes always lead to creation of excitations and in the case of phase transition these excitations can manifest themselves in forming topologically stable defect structures. Topological defects are formed in symmetry breaking phase transitions. In the symmetry broken state there are several possible ground states and the order parameter can select locally different ground states. When this happens a domain structure develops with the accompanying topological defects, whose nature depends on the dimensionality of space and the type of order parameter. For example, for the Ginzburg-Landau field theory in d dimensions and an n-component vector parameter field, the defects are domain walls if $d = n$, strings if $d = n - 1$ and monopoles if $d = n - 2$. The defects are topologically stable because they cannot be removed by local deformations of the order parameter field [87]. The process of domain growth during non-equilibrium phase transitions is known as *coarsening* [21].

Coarsening process is relevant in condensed matter theory and also in cosmology. The vast majority of phase transitions are non-adiabatic processes and real material nearly always contain topological defects. The topological defects influence the prop-

erties of the materials and sometimes even dominate their thermodynamic properties. For this reason, understanding the process of formation of topological defects and ways to either enhance or suppress their production is an important problem. In the field of cosmology certain theories assert that there were symmetry breaking phase transitions in the fundamental forces during the early stages of the evolution of the universe. If this is the case than one may expect to see the signatures of these transitions in the topological defect structures. The defect formation in the context of cosmology was examined in particular by Tom Kibble [72], but this physics will not be considered further in the current thesis.

Even though for all non-equilibrium processes the systems are not in *global thermodynamic equilibrium* (GTE) sometimes they can be in the so-called *local thermodynamic equilibrium* (LTE). The system in GTE is a system with all intensive thermodynamic quantities being homogeneous throughout the whole system. The system in LTE are system where the intensive parameters vary in space and time throughout the system but a selected small part of the system is in the thermodynamic equilibrium with neighbouring regions. The analysis of many problems and in particular the coarsening problem is much more manageable if the LTE assumption is invoked. The assumption of LTE leads to generalization of Ginzburg-Landau theory to the description of dynamic phase transition phenomena [62]. The idea of the approaches reviewed in [62] is the construction of stochastic differential equations that describe the evolution of the order parameter in the vicinity of the critical point, given that the system has to maintain LTE. Such dynamical equations are often referred to as time dependent Ginzburg-Landau (TDGL) equations of motion. One possible way to construct TDGL equation is to take the rate of change of the order parameter to be proportional to the local thermodynamic force

$$\frac{\partial\phi(x,t)}{\partial t} = -\Gamma\frac{\delta\mathcal{F}[\phi,t]}{\delta\phi(x,t)} + \theta(x,t), \tag{1.6}$$

where Γ is the constant determining the rate of change of energy between the system and the reservoir and $\theta(x,t)$ a white noise stochastic force with

$$\langle\theta(x,t)\rangle = 0 \tag{1.7}$$

$$\langle\theta(x,t)\theta(x',t')\rangle = 2\Gamma k_B T\delta(x-x')\delta(t-t'). \tag{1.8}$$

Dynamics specified by equation (1.6) is known as model A dynamics according to the classification scheme introduced in [62]. Model A can describe for example superconductors [82], anisotropic alloys and magnets [62]. Other dynamical models can be constructed (for example conserved model dynamics) and are reviewed in [62]. These models are usually phenomenological in the sense that they are constructed using symmetry and conservation law arguments. In certain cases these equations can be derived from the microscopic description of the system. Once the equations are constructed they can be analyzed using analytical or numerical methods. Analytically one can calculate the linear response of the system. The linear response theory allows one to determine how the system relaxes toward thermal equilibrium after it has been externally perturbed. The characteristic time scale that determines how long it takes for the system to equilibrate is known as the *relaxation time*. It can be shown that the relaxation time τ has a power law divergence in the vicinity of the critical point

$$\tau = \tau_0 \delta^{-\nu z}, \tag{1.9}$$

where at the critical point $\delta = 0$ and the exponent z is the dynamic critical exponent. The dynamic critical exponents determine the *dynamic universality class* of the phase transition. Just as the divergence of correlation length leads to various anomalous properties of static thermodynamic properties at the critical point, the divergence of the relaxation time leads to anomalous properties in the dynamic properties such as the transport coefficients. Linear response theory cannot be used to describe processes that are far from equilibrium. In particular, formation of topological defects cannot be accounted for by the linear response theory. In dealing with problems which are far from equilibrium but still in LTE one often resorts to directly simulating the equations of motion such as the equation (1.6).

The principle subject of this thesis is the study of coarsening during *slow* (so that LTE assumption is valid) but non-adiabatic quenches. The final number of domains formed as a result of finite rate quench depends on the quench rate $1/\tau_Q$, where τ_Q is the characteristic quench time. The final number of domains should tend to one as the quench rate $1/\tau_Q \to \infty$ and quench dynamics tends to the adiabatic limit. On the other hand as $1/\tau_Q \to 0$ (sudden quench limit) the number of defects will tend to a specific non-zero limit. The coarsening during slow quenches is commonly known as the Kibble-Zurek scenario, recognizing the work of Tom Kibble in connection to cosmology and the work of Wojciech Zurek who suggested that the average number of topological

defects is connected to the quench rate via a simple scaling law [138, 139]. In the next section, we review Zurek's argument that predicts the defect scaling with quench rate.

1.6 Kibble-Zurek mechanism

Suppose that the critical parameter δ varies in time such that the system undergoes a quench from a symmetric phase to the symmetry broken phase. For simplicity we take the quench to start at $t = -\infty$, crossing the critical point at $t = 0$ and ending at $t = \infty$. At the critical point the quench is taken to be an nth degree power law

$$\delta = -\left(\frac{t}{\tau_Q}\right)^n \text{sign}(t)\delta_0 \tag{1.10}$$

In the initial stages of the quench the order parameter adapts to its equilibrium value. This is because far from the critical point the relaxation time in the system is short. On the approach to the equilibrium point the relaxation time increases as given by equation (1.9) and eventually the system cannot adapt to its equilibrium state. In KZ theory the time instance when the system falls out of the equilibrium is known as the *freeze-out time* $\hat{t}$. Strictly speaking the freeze-out time does not refer to a particular instance but rather to a time scale at which the system falls out of the equilibrium. In Chapter 3 we will show that this time scale makes the equations of motion describing the coarsening quench independent and hence universal. In KZ theory, the length scale at the freeze-out time dictates the typical size of the domains after the system settles to the thermal equilibrium in the symmetry broken phase.

Figure 1.2 illustrates pictorially the idea of KZ theory. KZ theory obtains the freeze-out time scale by taking it to be the time when the inverse of the relaxation time and the rate of change of the critical parameter are equal i.e.

$$\tau(\hat{t}) = \left.\frac{\dot{\delta}}{\delta}\right|_{t=\hat{t}}. \tag{1.11}$$

Using equations (1.4), (1.9) and (1.10) the condition (1.11) gives

$$\hat{t} \propto \tau_Q^{\frac{\nu z}{1+\nu z}}. \tag{1.12}$$

Inserting (1.12) into (1.4) gives the "freeze-out" correlation length

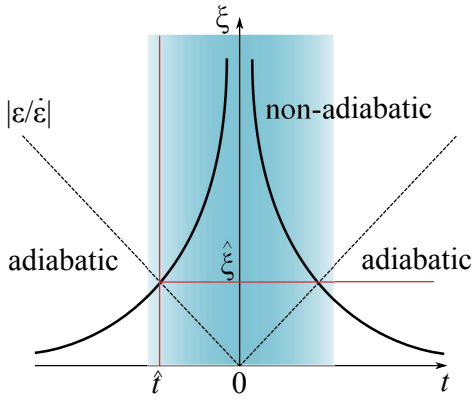

Figure 1.2: Graphical illustration of the KZ theory. The coarsening dynamics is split roughly into three stages - adiabatic dynamics in the symmetric phase, non-adiabatic dynamics during the non-equilibrium transition and finally adiabatic dynamics in the symmetry broken phase. The final length scale is dictated by the correlation length at the freeze-out time $\hat{t}$, which is obtained by equating the relaxation time to the quench time scale.

$$\hat{\xi} \propto \left(\frac{1}{\tau_Q}\right)^{\frac{\nu}{1+\nu z}}. \tag{1.13}$$

According to KZ theory the typical size of domains is dictated by $\hat{\xi}$. The number of domains (or defects) in d dimensions is thus expected to scale with quench time as

$$\begin{aligned} n_d &\propto \frac{1}{\hat{\xi}^d} \\ &\propto \tau_Q^{\frac{d\nu}{1+\nu z}}. \end{aligned} \tag{1.14}$$

One should note that the scaling (1.14) is expected to fail at fast and slow quenches. At very fast quenches the defect density will become so high that the defects will start to deform due to their mutual interactions. The structure of defects and their interactions are specific to the physical system and are in this sense not universal. KZ theory does not account for the expected plateau in the scaling at fast quenches. For very slow quenches the scaling is also expected to flatten. In this case, the reason is that $\hat{\xi}$ becomes of the order of the size of the system and hence the non-equilibrium dynamics will be heavily influenced by the boundaries of the system. This finite size effect coming from system boundaries is not universal and is not accounted for by the KZ theory. Note that if the system is truly infinite then the flatting of the KZ scaling

at slow quenches should not occur.

We have mentioned before that by the Ginzburg criterion many physical systems will effectively be in a mean field universality class near the critical point. The measured critical exponent is typically $\nu = 1/2$ and it is often difficult to resolve experimentally the regime where the fluctuations dominate the dynamics of the system. Thus one may expect to measure the "mean-field" KZ scaling in numerical simulations and physical experiments

$$n_d^{(MF)} \propto \tau_Q^{\frac{d}{2+z}}. \tag{1.15}$$

Very few works have been able to demonstrate KZ scaling beyond mean field regime. One demonstration of non-mean field scaling is presented in [75], where authors shown using time-dependent matrix product states (tMPS) calculations that, for quenches in a finite one dimensional Ising model, the spin-spin correlation function follows the predictions of KZ theory. More demonstrations of non-mean field KZ scaling law should be provided to give a more solid support of KZ theory. On the other hand, many papers demonstrate mean field KZ scaling given by (1.15) albeit the most compelling demonstrations are provided by computer experiments rather than physical experiments. One of the principle aims of this thesis is to advance the understanding of KZ theory, which may eventually lead to either confirmation or rejection of the conjecture (1.14). Our methodology will be numerical simulations, experiments in ion traps and analytic scaling analysis of the equations of motion. Before moving to the ion trap systems, which will serve as a model system for exploration of KZ physics let us review existing work that attempts to verify (1.14).

1.7 Experimental and numerical tests of Kibble-Zurek mechanism

The derivation of KZ scaling given by equation (1.13) is qualitative and cannot be regarded as a rigourous mathematical proof. All physical theories require experimental verification and even more so when the mathematical framework of the theory is incomplete such as in the case of KZ theory. Thus much effort has been put into testing KZ scaling using numerical simulations and physical experiments.

For the real one dimensional ϕ^4 GL theory, the KZ scaling was measured using numerical simulations for model A dynamics [76] and underdamped dynamics [77].

KZ scaling was tested for the quench in the complex two dimensional gauged field in [137]. Quenches inducing Bose-Einstein-Condensation were investigated by numerically solving the Gross-Pitaevskii equation in [34]. In these three works the scaling was found to be consistent with (1.14) assuming the mean field critical exponent of $\nu = 1/2$.

Kibble-Zurek physics was also investigated in the quantum Ising model - a prototypical model for exploring quantum phase transitions. In [45] an analytic solution for quench dynamics in a one dimensional quantum Ising model is presented. The scaling functions extracted from this solution is in agreement with KZ theory. The dynamics of the one dimensional Ising model was also calculated numerically in [141, 75]. KZ physics in the context of quantum phase transition is reviewed in [105].

There were many experiments in a wide variety of systems aimed at producing topological defects and studying KZ scaling laws. For a recent reviews of the experimental progress refer to [71, 38, 39]. The early experiments investigating Kibble-Zurek mechanism were carried out in the liquid crystal systems [31, 18] and liquid ^{3}He [6, 113]. In these experiments defects were indeed created via quench through a second order phase transition but a scaling of defects with quench rate was not measured. Quench experiment in ^{4}He was believed to have generated defects, but they were later attributed to inadvertent stirring [42]; attempts to see quench-generated defects in ^{4}He were so far unsuccessful. Defects were also created via non-adiabatic quenches in superconducting films [85, 58]. First experiments in Bose-Einstein condensates [115, 133] confirm defect production, but not the scaling. KZM scaling was recently measured in multiferroic materials [59, 27]. Interpretation in terms of KZM is suggestive, but is based on theoretical predictions that have not been confirmed by measurement of equilibrium critical exponents; the authors compare the results with the mean field KZ prediction. In tunnel Josephson junctions, scaling of the probability to trap a single flux line has been measured [92, 90, 91], but with exponents that require additional assumptions (about e.g. external fields) in order to be consistent with KZ mechanism.

KZ mechanism was also studied experimentally in ion trap system using linear to zigzag structural transition [108, 129, 49] following a theoretical proposal [37, 30]. Experiments [108, 129] form an integral part of this thesis. All three experiments [108, 129, 49] have measured the defect scaling as a function of quench rate, however, as we will see in detail in later chapters the scaling is not of simple KZ scaling form. The scaling is complicated by the fact that the experiment is done in a harmonic trap (and hence the phase transition is inhomogeneous). Moreover the experiments were limited to fairy small ion chains where the finite size effect are expected to play a

significant role. The same problem of harmonic confinement and finite size is present in the experiment measuring KZ scaling in the BEC system [78]. The experiments in BEC are further complicated by the fact that in these experiments phase transition is induced by varying the chemical potential, which is in practice difficult to do in a precise fashion. In contrast, in the case of linear to zigzag phase transition in ion trap the quench functions (which are related to electrode voltages) are measured precisely.

1.8 KZ scaling in inhomogeneous and finite size systems

Experiments in ultracold atomic and ionic lattices for the purpose of studying phase transition have advantages and disadvantages as compared to condensed matter materials. The advantage of studying trapped atomic lattices is that these systems can be easily engineered in desired ways using quantum optical techniques and tuning the trap parameters. The atomic lattices are also much cleaner than their solid state counterparts, which may contain impurities and intrinsic lattice defects. The complication present in trapped atomic lattices is that they are typically smaller than condensed matter systems and inhomogeneous because of the trapping potential. For the study of both equilibrium and non-equilibrium critical phenomena the finite size effects and inhomogeneity of the system must be taken into account.

In the present thesis, we will show that the KZ scaling exponent can be measured in the finite size system/harmonic traps if at the same time one is allowed to vary the system size/trap potential [53]. There is also another approach of treating the effect of inhomogeneity on the KZ scaling suggested in [46]. The idea is to show that even though a powerlaw KZ scaling will not exist in a harmonic trap for all quench values there could be a quench range with a specific powerlaw. Moreover, this inhomogeneous KZ (IKZ) power law will be steeper than the homogeneous power law. The argument for deriving IKZ powerlaw is qualitative - it states that the defects are produced via regular KZ mechanism but in the reduced region that is dictated by the phase transition front velocity. The argument was applied to BECs [140], ion traps [37, 30] and Ising chains [47, 48]. This approach should be treated with caution since the derivation is based on physical intuition rather than mathematical rigour. In the present thesis we will not use this approach to derive any results.

1.9 Rescaling and the universal equations

Most of the work concerning KZ scaling has been aimed at verifying the scaling given by (1.14) using numerical simulations or experiments. It is true that the ultimate test of a physical theory is the experiment. However, in this case the KZ theory is also a mathematical conjecture which should be possible to prove. Recently, A. Chandran *et al* postulated that the scaling on quench rates holds not only for defects but other thermodynamic quantities [28]. This could be justified by realizing that the equations of motion during the quench can be mathematically transform into a universal quench independent equation. We pursue this approach in [53] and Chapter 3. This method formalizes the KZ problem and can be used to arrive additional results such as finite size KZ scaling. Both works [28] and [53] concern chiefly the mean field scaling limit, but the approach has the potential to provide a mathematical proof of the existence of a non-mean field scaling.

1.10 Model system - repulsive particles in a confining external potential

We will now introduce the model system that will be used to study non-equilibrium statistical mechanics and in particular the KZ scenario. Mathematically the system will consist of a number of particles moving in external confining potential. Each particle interact repulsively with every other particles and the interaction force scales as an inverse powerlaw of the separation between particles $F_{int} \sim r^{-\alpha}$; with $\alpha = 2$ the interaction follows Coulomb law. If the kinetic energy of the particles is sufficiently small then the particles organize into crystal-like lattice structures. The structure of the crystal is influenced by the external potential and thus by varying the external potential one can induce structural phase transition in the crystal. If the structural phase transitions are non-adiabatic then lattice defects such as dislocations may form - a process that we will use for the study of the KZ scenario.

There are a number of physical systems that consist of mutually repulsive particles in an external potentials, for example, electrons in quantum wires [103], colloidal particles [127, 124], microfluidic crystals [9, 8], dusty plasmas [93] and trapped ions [117]. In the electronic system organization into crystal like structures was predicted by Eugene Wigner [134] and is now known as Wigner crystallization. Wigner crystals are hard to realize experimentally because the long de Broglie wavelength of electrons implies

that quantum fluctuations can easily destroy the crystal. In order to observe Wigner electron crystals the density of electrons has to be extremely low. First experimental observations of Wigner crystallization was on the surface of liquid Helium [60]. Wigner crystallization was then realized in GaAs/GaAlAs quantum wells [2] and recently in carbon nanotubes [40]. Wigner crystal of electrons is an interesting system but the difficulty in its generation and observation makes this system too challenging for our present objective of studying KZ mechanism. It is much simpler to obtain crystals in systems where particles are more massive than electrons and hence have a short de Broglie wavelength. Such systems may be regarded as purely classical particles since the quantum corrections to their dynamics can be completely neglected. In the current work we have chosen to focus on the trapped ion Coulomb crystals. A number of features makes trapped ions an excellent system for studying KZ mechanism: the external trapping potentials in this system can be controlled with high precision, the individual particles are known to have identical masses, particles interact via a precise Coulomb law and the thermalization is easily achieved via laser cooling. Moreover, another advantage of ion Coulomb crystals is that in this system it is possible to enter a regime where the quantum correction to the dynamics of ions become important [110, 4, 5]. Thus, in the longer term, experiments in ion Coulomb crystals can shed light onto quantum non-equilibrium dynamics relevant for instance to the quantum energy transport [12, 97].

1.11 Coulomb crystals in ion traps

It is well known that a static globally confining potential cannot exist (Earnshaw's theorem). Traps that confine electrically charged plasmas must either use a time-varying electric field or a combination of electric and magnetic fields. A trap that uses a combination of a static electric field and a static magnetic field is known as a Penning trap [36, 102], and it can be used to successfully trap crystals of ions. In this thesis however, we will focus on the so-called Paul trap that uses a time varying electric potential to achieve an effective global harmonic confinement [101].

Let us briefly review how the ion confinement is achieved in Paul trap (for a detail treatment see for example [55]). Consider a potential of the following form

$$V(x,y,z,t) = (U_x - V\cos\Omega t)\,\frac{x^2}{2r_0^2} - (U_y - V\cos\Omega t)\,\frac{y^2}{2r_0^2} + \frac{m\omega_z^2}{2}z^2. \tag{1.16}$$

Equation (1.16) is a potential of an ideal linear quadrupole trap or Paul trap. In the z-direction the potential is static and in the x and y-direction the potential is oscillatory. We will often refer to the z-direction as axial direction because the linear ion crystals considered in the thesis will usually be aligned with the z-axis. The x and y directions will accordingly be referred to as the radial directions. A single particle of mass m and charge e moving in the potential (1.16) has the following equations of motion

$$\frac{d^2x}{dt^2} = -\frac{e}{mr_0^2}\left(U_x - V\cos\Omega t\right)x \tag{1.17}$$

$$\frac{d^2y}{dt^2} = \frac{e}{mr_0^2}\left(U_y - V\cos\Omega t\right)y \tag{1.18}$$

$$\frac{d^2z}{dt^2} = -\omega_z^2 z. \tag{1.19}$$

To see how equations (1.17)-(1.19) can correspond to a particle moving in a globally confining potential consider a substitution $\xi = \Omega t/2$. With this substitution the equations (1.17)-(1.19) become

$$\frac{d^2x}{d\xi^2} = -\left(a_x - 2q\cos 2\xi\right)x, \tag{1.20}$$

$$\frac{d^2y}{d\xi^2} = \left(a_y - 2q\cos 2\xi\right)y \tag{1.21}$$

$$\frac{d^2z}{d\xi^2} = -\left(\frac{2\omega_z}{\Omega}\right)^2 z, \tag{1.22}$$

where $a_x = 4eU_x/m\Omega^2r_0^2$, $a_y = 4eU_y/m\Omega^2r_0^2$ and $q = 2eV/m\Omega^2r_0^2$. Equations (1.20) and (1.21) are Mathieu differential equations that has been extensively analyzed. The parameter a and q are known as Mathieu parameters. Stable trapping of the charged particles is achieved for only certain values of a and q and the stability diagram for Mathieu equations is well known [55]. In the lowest stability zone, for $|a| \ll 1$ and $|q| \ll 1$, the solution of equation (1.20) and (1.21) have the approximate form

$$x(t) = x_0\cos\left(\omega_x t + \varphi_x\right)\left(1 - \frac{q}{2}\cos\Omega t\right), \tag{1.23}$$

$$y(t) = y_0\cos\left(\omega_y t + \varphi_y\right)\left(1 - \frac{q}{2}\cos\Omega t\right), \tag{1.24}$$

where x_0 and y_0 are determined by the initial conditions and

$$\omega_x = \frac{\Omega}{2}\sqrt{\frac{q^2}{2} + a_x}, \tag{1.25}$$

$$\omega_y = \frac{\Omega}{2}\sqrt{\frac{q^2}{2} + a_y} \tag{1.26}$$

Thus in the x and y directions the motion of the particle is that of a harmonic oscillators with frequencies ω_x and ω_y and their amplitude modulated at the frequency Ω. The rapid oscillatory motion at frequency Ω is known as the *micromotion* and the oscillations at frequencies ω_x and ω_y are known as the secular motions. If the important dynamics happens on the time scale of secular frequencies than the effect of micromotion can be neglected i.e. we can assume that the particle moves in an effective pseudo potential

$$V_p = \frac{1}{2}m\omega_x^2 x^2 + \frac{1}{2}m\omega_y^2 y^2 + \frac{1}{2}m\omega_z^2 z^2. \tag{1.27}$$

Now suppose that the trap contains N particles of mass m and charge e. The equations of motion for the jth particle are given by

$$m\frac{d^2\mathbf{r}_j}{dt^2} = -e\nabla_j V + \frac{e^2}{4\pi\epsilon_0}\nabla_j \sum_{j\neq k}^{N} \frac{1}{|\mathbf{r}_i - \mathbf{r}_k|}, \tag{1.28}$$

where $\nabla_j \equiv \left(\frac{\partial}{\partial x_j}, \frac{\partial}{\partial y_j}, \frac{\partial}{\partial z_j}\right)$ and V is given by equation (1.16). The equations of motion are of the same form as for a single ion but with important difference - there is Coulomb interaction between the ions which couples the motion of all of the ions in the system. It can be shown that a stable confinement of N particles in a Paul trap is possible. The set of Mathieu parameters a and q for which a stable confinement of N ions is possible is smaller than that for only a single ion. Nevertheless, a stable confinement is achievable when $|a| \ll 1$ and $q \ll 1$ and thus a pondermotive approximation can be used. The potential energy of N charged particles can thus be taken to be

$$V = \frac{1}{2}\sum_j \left(m\omega_x^2 x_j^2 + m\omega_y^2 y_j^2 + m\omega_z^2 z_j^2\right) + \frac{e^2}{4\pi\epsilon_0}\sum_{j<k}\frac{1}{|\mathbf{r}_j - \mathbf{r}_k|}. \tag{1.29}$$

From now on we will work with the equation (1.29), which ignores the effects of micromotion. The underlying assumption of all results (apart from the experimental results) developed in the thesis concerning ion crystals is that the trap parameters are

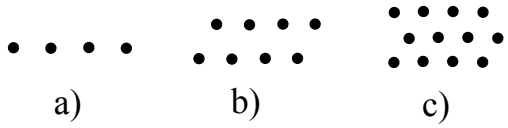

Figure 1.3: a) Linear chain b) two row (zigzag chain) c) three row chain

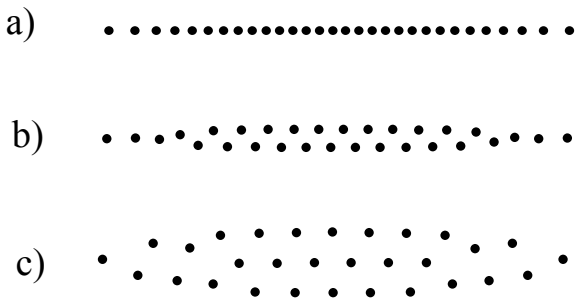

Figure 1.4: Inhomogeneous Wigner crystals in harmonic confining potential in all three directions. a) Inhomogeneous linear chain b) Inhomogeneous chain in zigzag phase in the central region and linear phase in the outer region c) Inhomogeneous chain in three row phase in the central region and the zigzag phase in the outer region

such that the effect of the micromotion is negligible. This assumption will be justified in more detail in Chapter 4.

If one minimized the potential energy given by (1.29) with respect to the positions of the particles, then one will obtain a crystal-like structure whose exact shape depends on the values of the secular frequencies. For simplicity, let us first consider a case of periodic boundary conditions in z-direction. In this case if ω_x and ω_y is large then all of the particles will lie on the z-axis in a linear chain configuration (figure 1.3a). If ω_x is reduced below a critical value, the system will undergo a structural transition from linear chain to a two row chain (zigzag chain) shown in figure 1.3b. Three row (figure 1.3c), four row, etc configurations are also possible if ω_y is kept high confining the structure to the xz-plane. The phase diagram for these structural phase transitions has been numerically evaluated in [103]. In the limit of infinite rows and infinite extent in the z-direction the system forms a true triangular lattice. If we start with a planar triangular lattice and reduce the confining potential, then the structure will undergo a transition to a three planar triangular lattice, then to a two planar square lattice, then to a three planar square lattice and so on. In the limit of infinite number of planes the crystal forms a 3 dimensional body centred cubic (bcc) lattice. Studies of the structural transition in Coulomb crystals are reviewed in [44].

Periodic boundary conditions can in principle be realized experimentally in ring

traps but such traps in practice are difficult to implement. The traps that are used most often are harmonic in all three directions. In such traps the linear chain can be realized by making the axial confinement much weaker than the radial confinement i.e. $\omega_z \ll \omega_x, \omega_y$. In this case, however, the spacing between ions will not be constant but will increase from the centre to the edges of the chain (figure 1.4a). The same applies for the zigzag phase and the three row phase (figure 1.4b-c). The crystals in the harmonic traps are always inhomogeneous but since they are locally nearly homogeneous, it is possible to use many of the results for the homogeneous crystals for their analysis.

Coulomb plasma is in the fluid state at high temperatures. Coulomb crystallization takes place at low temperatures when the correlations between charges increase and become important. A measure of the strength of the correlations is given by the so-called plasma parameter

$$\Gamma = \frac{e^2}{ak_BT}, \tag{1.30}$$

where a is the Wigner-Seitz radius i.e. $4\pi Na^3/3V \equiv 1$. The plasma parameters is the ratio of the interaction energy between neighbouring charges to the random energy per degree of freedom. According to [44], for an infinite plasma the first order phase transition from fluid to a bcc crystal takes place when

$$\Gamma \sim 174. \tag{1.31}$$

This condition is not very demanding for macroscopic particles such as charged microspheres. In fact, the first experimental demonstrations of Coulomb crystallization in Paul traps were done for a system of charged aluminum microspheres [136]. To achieve Wigner crystallization with ions, one has to typically reach mK temperatures. This has only became possible with the development of Doppler laser cooling [123]. First observations of Wigner crystallization in Paul traps were reported for small clusters [41, 135] and then for large crystals [131, 13]. Nowadays ion crystals are routinely created in dozens of labs around the world. The linear chain configuration is particularly well studied and serves as a workhorse for the development of quantum optical techniques - many of the proof-of-principle quantum computing experiments are performed using the linear ion chain system [61]. Zigzag and more complex configurations are also attracting an increasing interest in the quantum information community [11].

One should note that for certain values of Mathieu parameters, crystallization may not be possible even though the ion clouds have a stable confinement. In these cases

the micromotion destabilizes the crystal and the motion of ions becomes deterministic but chaotic [79]. In this thesis we will work with Coulomb crystals and so traps are assumed to have Mathieu parameters where a Coulomb crystal is dynamically stable.

With this background, we will now turn to a detailed examination of the linear to zigzag phase transition.

Chapter 2

Linear to zigzag phase transition

In this chapter we will focus on the equilibrium properties of the linear to zigzag structural phase transition. Later we will use this transition for studying the Kibble-Zurek (KZ) mechanism. The proposal for studying KZ mechanism using linear to zigzag phase transition was put forward in [37, 30]. In [37, 30] predictions are made by using the concept of diverging correlation length, but the critical behaviour was not explicitly evaluated in [37, 30], in particular finite size effects were not considered. In this chapter, we will review the Ginzburg-Landau description of the linear to zigzag phase transition and then proceed to evaluate the correlation length for small chains with periodic boundary conditions. By evaluating the two point correlation function we uncover the finite size effects; these finite size effects should be considered when making KZ predictions that rely on the critical exponents that are valid strictly in thermodynamic limit. It is found that far away from the critical point the divergence of the correlation length has a mean field critical exponent (unless the correlation length is significantly smaller than the lattice spacing), but near the critical point the finite size effects dominate. We will see in the next chapter that the presence of these finite size effects does change the KZ scaling for very slow quenches but the KZ scaling still remains as predicted by the theory in thermodynamic limit for a wide range of quench rates.

2.1 Ginzburg-Landau theory for linear to zigzag phase transition

2.1.1 Ginzburg-Landau theory - a short introduction

Ginzburg-Landau (GL) approach for the study of critical phenomena was briefly discussed in the previous chapter. We will now recap the idea of GL theory and then apply it to the linear to zigzag ion chain. GL approach involves three main steps

1. Identifying an order parameter field $\mathbf{m}(\mathbf{x})$

2. Writing a Ginzburg-Landau free energy function, $\mathcal{F}[\mathbf{m}(\mathbf{x})]$ that describes the system near the critical point

3. Extracting thermodynamic properties of the system from the partition function $Z = \int \mathcal{D}\mathbf{m} \exp(-\beta \mathcal{F}[\mathbf{m}])$.

The order parameter field usually corresponds to a coarse grained quantity. For instance if we model a paramagnetic to ferromagnetic phase transition we may define $\mathbf{m}(\mathbf{x})$ as an average magnetization over some region of the material, rather than each individual atomic spin that gives rise to this magnetization. The GL free energy can be written as a series expansion in $\mathbf{m}(\mathbf{x})$

$$\beta \mathcal{F}[\mathbf{m}] = \int d\mathbf{x} \left[c_1 \mathbf{h} \cdot \mathbf{m} + c_2 \mathbf{m}^2 + c_3 \mathbf{m} \cdot \nabla \mathbf{m} + c_4 \mathbf{m}^3 + \ldots \right]. \tag{2.1}$$

Since $\mathbf{m}(\mathbf{x})$ is small in the vicinity of the critical point only a few lowest terms in (2.1) need to be considered to analyze critical behaviour. Also often it is possible to use symmetry arguments to set many of the terms in the series expansion (2.1) to zero. For instance, in the absence of external magnetic field the energy should be invariant under rotation of the order parameter i.e. $\mathcal{F}[\mathbf{m}] = \mathcal{F}[\mathbf{R}_n \mathbf{m}]$, where $\mathbf{R}_n$ is a rotation operator. Invariance under rotations implies that the $\mathcal{F}[\mathbf{m}]$ can only be a function of even powers of the order parameter. Once $\mathcal{F}[\mathbf{m}]$ is reduced to a simple form using the symmetry argument, one can analyze its partition function using a variety of techniques, such as mean field analysis, renormalization group and numerical methods [68].

2.1.2 Linear to zigzag phase transition - the order parameter and symmetry considerations

This phase transition was first studied numerically [116], where it was conjectured that it is a second order phase transition. Further numerical work showed that the ground state energy is characterized by a discontinuity in the second derivative with respect to the particle density [104]. In [51] it was shown analytically that the phase transition is of second order, and a Ginzburg-Landau free energy for this transition was derived. The proof was later generalized for the chains in confining potentials of the form r^α, where α is an integer and particle interaction of the form r^β, where β is an integer [54].

Before we quote the GL free energy obtained in [51] it is instructive to use physical arguments and symmetry considerations to anticipate the result. The system under consideration is an infinite chain of point charges confined to a line by a harmonic

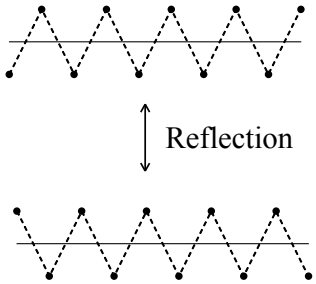

Figure 2.1: Two possible degenerate zigzag configurations.

potential. The minimum energy configuration of the chain can become a zigzag if the confining potential is reduced and/or the spacing between the charges is reduced. A natural order parameter is the transverse displacement of the ions. Suppose y_j is the transverse displacement of the jth ion, then let us define an infinite dimensional vector $\vec{\phi}$ with elements $\phi_j = (-1)^j y_j$. We define a scalar one dimensional order parameter field $\phi(x)$ such that $\phi(x_j) = \phi_j$, where x_j is the axial coordinate of the jth ion. The reason for inverting the sign of the transverse displacement of every odd ion in the definition of ϕ_j is to make the field $\phi(x)$ smooth and differentiable.

In the linear phase the order parameter is zero in the ground state i.e. $\phi(x) = \phi_0 = 0$. As the phase transition is crossed the order parameter gains a finite value i.e. $\phi_0 = \bar{\phi}$. For each given parameter set there are two possible degenerate zigzag configurations, $\phi_0 = \bar{\phi}$ and $\phi_0 = -\bar{\phi}$, which corresponds to a zigzag chain and its reflection about the chain axis (figure 2.1). The system is indeed invariant under the reflections of the order parameter about the chain axis i.e. $\mathcal{F}[\phi] = \mathcal{F}[-\phi]$. This automatically rules out the possibility of odd powers of ϕ in $\mathcal{F}[\phi]$, therefore the GL free energy has to be of the form

$$\begin{aligned} \beta\mathcal{F}[\phi] &= \int \left\{ U_0 + a\phi^2 + b\left(\partial_x\phi\right)^2 + c\phi\partial_x\phi + d\phi^3 \right. \\ &\quad \left. + e\phi^3\partial_x\phi + f\phi^2(\partial_x\phi)^2 + g\phi\left(\partial_x\phi\right)^3 + h\left(\partial_x\phi\right)^4 + \ldots \right\} dx. \end{aligned} \tag{2.2}$$

The linear to zigzag phase transition is a symmetry breaking phase transition for the following reason. Let $\phi(x) = \bar{\phi} + \psi(x)$ i.e. we express the order parameter field as a sum of its mean value and fluctuations about this value. In the linear phase, since $\bar{\phi} = 0$ we have $\mathcal{F}[\psi(x)] = \mathcal{F}[-\psi(x)]$ - an invariance under reflections of the fluctuations. The symmetry is broken in the zigzag phase since $\mathcal{F}[\bar{\phi}+\psi(x)] \neq \mathcal{F}[\bar{\phi}-\psi(x)]$. This symmetry breaking is reminiscent of the paramagnetic to ferromagnetic phase transition. In fact,

the linear to zigzag phase transition has exactly the same mathematical structure as the paramagnetic to ferromagnetic phase transition (assuming the axial motion of ions is negligible); this will become clear in the next section where we consider the GL Hamiltonian for the linear to zigzag phase transition.

2.1.3 Ginzburg-Landau free energy for linear to zigzag phase transition

Consider $N \to \infty$ interacting particles placed on an xy-plane. In the x-direction the particles do not experience an external potential and the systems is unbounded, but in the y-direction there is a harmonic confining potential. The potential energy of the systems is given by

$$V = V_{\text{external}} + V_{\text{int}} \tag{2.3}$$

$$V_{\text{external}} = \sum_{j}^{N} \frac{1}{2} m\omega_y^2 y_j^2. \tag{2.4}$$

$$V_{\text{int}} = \frac{1}{2} Q^2 \sum_{j}^{N} \sum_{i \neq j}^{N} \frac{1}{\sqrt{(x_j - x_i)^2 + (y_j - y_i)^2}}, \tag{2.5}$$

where $Q \equiv e^2/4\pi\epsilon_0$ is the Coulomb interaction factor. Equations (2.3)-(2.5) specify the microscopic structure of the system. In order to derive a GL free energy of the type (2.2) we must perform a Taylor expansion of (2.2) in $\phi_j = (-1)^j y_j$ around the linear chain configuration. Such calculation, carried out in the normal mode basis, is presented in [51, 30]. Here we simply quote the result

$$\mathcal{F}[\phi(x)] = \frac{1}{2}\frac{m}{a} \int \left\{ \delta\phi(x)^2 + h^2 \left(\frac{\partial\phi(x)}{\partial x} \right)^2 + \mathcal{A}\phi(x)^4 \right\} dx \tag{2.6}$$

where a is the spacing between ions when they are in the linear chain configuration, and the parameters h, δ and $\mathcal{A}$ are given by the following expressions

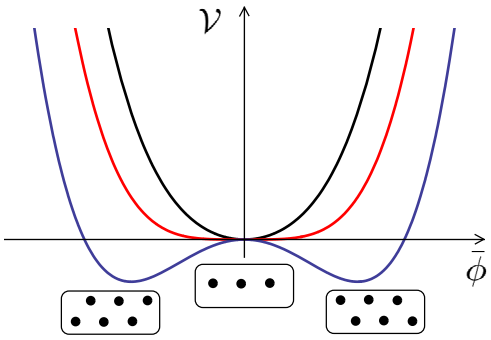

Figure 2.2: Energy density $\mathcal{V}$ as a function of average ion displacement $\bar{\phi}$ for three values of δ: $\delta > 0$ (black line), $\delta = 0$ (red line) and $\delta < 0$ (blue line).

$$h = \omega_0 a \sqrt{\log 2} \tag{2.7}$$

$$\delta = \omega_y^2 - \omega_c^2 \tag{2.8}$$

$$\mathcal{A} = \frac{93\zeta(5)}{32}\frac{\omega_0^2}{a^2} \tag{2.9}$$

$$\omega_c = \omega_0 \sqrt{\frac{7\zeta(3)}{2}} \tag{2.10}$$

where $\omega_0 = \sqrt{Q^2/ma^3}$. The free energy $\mathcal{F}[\phi]$ given by (2.6) is valid for a system in thermodynamic limit confined to an xy-plane. The derivation of the GL free energy is straightforwardly generalized for the case where the ions are allowed to move in the z-direction; in this case the order parameter becomes a two component vector field rather than a scalar field.

Now lets examine the GL potential energy given by (2.6). This potential corresponds to the classic ϕ^4 scalar field model. This model exhibits a textbook example of spontaneous symmetry breaking and is often introduced to explain the paramagnetic to ferromagnetic phase transition. If we set all of the spatial fluctuations to zero i.e. $\phi(x) = \bar{\phi}$, then the potential energy is given by

$$\mathcal{V} = \mathcal{V}_0 + \frac{1}{2}\frac{m}{a}\delta^2\bar{\phi}^2 + \frac{1}{2}\frac{m}{a}\mathcal{A}\bar{\phi}^4. \tag{2.11}$$

Equation (2.11) is the energy density in the zeroth order perturbation theory in the field fluctuations. The energy density is plotted for three different values of δ in figure 2.2. For $\delta > 0$ the energy function is a single well with only one minimum, which corresponds to the linear chain. For $\delta < 0$ the energy function is a double well with two

degenerate minima, which corresponds to the two possible zigzag configurations. Thus δ is the critical parameter the variation of which induces the linear to zigzag phase transition and when $\delta = 0$ the system is in the critical phase. Let's evaluate the value of the average transverse displacement of the ions within the zeroth order perturbation theory in fluctuations. Minimization of the energy given by (2.11) with respect to $\bar{\phi}$ gives

$$\frac{\partial \mathcal{V}}{\partial \bar{\phi}} = \frac{m}{a}\delta\bar{\phi} + \frac{2m}{a}\mathcal{A}\bar{\phi}^3 = 0. \tag{2.12}$$

Solving for $\bar{\phi}$ gives

$$\bar{\phi} = \begin{cases} 0 & \text{for } \delta \geq 0, \\ \pm\sqrt{\frac{-\delta}{2\mathcal{A}}}, 0 & \text{for } \delta < 0. \end{cases} \tag{2.13}$$

For $\delta < 0$ or by equation (2.8) $\omega_y > \omega_c$, the ground state of the system is a linear chain or by the analogy with magnetic systems, it is in the paramagnetic state. For $\delta > 0$ or $\omega_y < \omega_c$ the system is in a zigzag phase - it has acquired a net "magnetization" and is thus in ferromagnetic state. When $\delta = 0$ or $\omega_y = \omega_c$ the system is at the critical point. The frequency ω_c given by equation (2.10) is the critical frequency because if the secular frequency of the radially confining potential is lower than ω_c the minimum energy configuration of the system is the zigzag chain. Above the critical point $\delta > 0$ the order parameter growth as a power law of δ i.e. $\bar{\phi} \propto |\delta|^\beta$. Exponent β is one of the critical exponents of the phase transition and from equation (2.13) it is clear that $\beta = 1/2$, which corresponds to the exponent of the mean field universality class. Thus as expected neglecting the fluctuations of the order parameter corresponds to a mean field description with its characteristic exponents.

The exponent $\beta = 1/2$ can be verified numerically, by finding computationally the equilibrium configuration of ions for various values of δ. The equilibrium configuration of ions is given by a nonlinear algebraic system of equations

$$\begin{aligned} \partial_{q_1} V &= 0, \\ &\cdot \quad \cdot \quad \cdot \\ \partial_{q_{2N}} V &= 0, \end{aligned} \tag{2.14}$$

where $\mathbf{q} = (q_1, q_2 ... q_{2N}) \equiv (x_1, ..., x_N, y_1, ..., y_N)$ are all of the positional degrees of freedom of a chain of N ions in two dimension, and V is the potential energy given by equation (2.3). The system of equations (2.14) can be solved by initializing the ions around the zigzag configuration with some arbitrary small transverse displacement i.e. $x_j = \varepsilon(-1)^j$ and then solving dynamical problem of overdamped particle motion. The equations of motion are solved using Runge-Kutta 4th order method and the system evolves towards a steady state which is the equilibrium configuration for a given transverse confinement frequency and hence δ. The result of this numerical computation is shown in figure 2.3. The calculation was done for a system of 20 Ca^+ ions with 10 μm spacing and periodic boundary conditions. Calculations are carried out for various values of ω_y from which the critical parameter δ is calculated using the formula $\delta = \omega_y^2 - \omega_c^2$, where ω_c is given by equation (2.10). From the graph it is clear that the critical point is at $\delta \approx 0$. The accuracy of the linear fit of $\bar{\phi}^2$ vs $-\delta$ in the vicinity of the critical point confirms the validity of the mean field exponent $\beta = 1/2$. Note that for large $-\delta$ the linear fit is no longer accurate. The reason for this is that to derive $\beta = 1/2$ only the terms up to $O(\phi^4)$ where considered in the free energy, but higher order terms become important when the transverse displacement is large. If one wishes it is possible to calculate higher order corrections and predict the $\bar{\phi}$ further from the critical point. Finally, we should note since the calculation is done for 20 particles then one should see deviations from the case of thermodynamic limit where the number of particles is infinite. Indeed in the thermodynamic limit at the critical point of the second order phase transition the derivative $\partial\bar{\phi}/\partial\delta$ is discontinuous but as is evident from the inset in figure 2.3 this is not the case for the finite system. The discontinuity is smoothed out in the finite system and as the system becomes larger the discontinuity becomes sharper.

2.2 Fluctuations and divergence of the correlation length

In the previous section we have presented the GL free energy which is obtained by a series expansion of the microscopic energy function in transverse displacement. We have shown that the system undergoes a phase transition from a linear to a zigzag configuration if the transverse secular frequency is reduced below the critical value. This was done analytically by ignoring all possible fluctuations of the transverse displacement

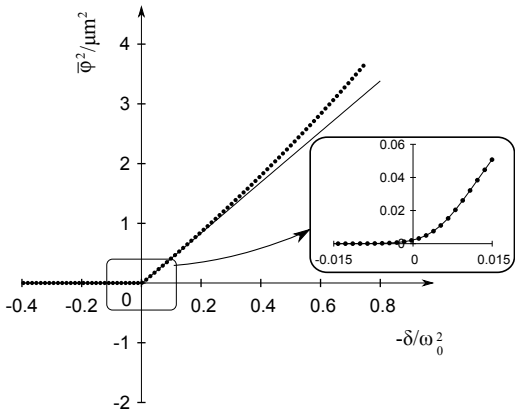

Figure 2.3: Square of the average transverse displacement vs the critical parameter $\delta = \omega_z^2 - \omega_c^2$ calculated numerically for 20 particles. ω_c is the critical transverse frequency for the system in thermodynamic limit of infinite number of particles, $\omega_0 \equiv \sqrt{Q^2/ma^3}$ is the characteristic frequency scale in the system and a is the lattice spacing. For $-\delta > 0$ the system is in the zigzag phase and $\bar{\phi}^2 \propto |\delta|$ as demonstrated by a linear fit. The inset shows that near the critical point the change from $\bar{\phi}^2 = 0$ to $\bar{\phi}^2 \propto |\delta|$ is smooth. The reason for the continuity of the derivative of $\bar{\phi}$ is the finite size of the system.

and minimizing the potential energy. Neglecting the fluctuations amounts to zeroth order mean field calculation and the resulting critical exponent of the average "magnetization" is found to be $\beta = 1/2$, which was also verified numerically. It is well known that fluctuations in the systems become large in the vicinity of the critical point. It is important to consider the effect of the fluctuations as they can modify the critical exponents and sometimes even the order of the phase transition [65]. In this section, we evaluate the two point correlation function for a linear chain in the vicinity of the critical point using second order perturbation theory in the fluctuations of the field.

Recall that all of the static properties of the system in thermal equilibrium can be obtained from the partition function

$$Z = \int \mathcal{D}\phi(x) e^{-\beta \mathcal{F}[\phi,\delta,h]}, \tag{2.15}$$

where $\beta \equiv 1/k_B T$. The functional (2.15) can be evaluated only if the potential is quadratic in ϕ. In our case the potential is not quadratic since it has the ϕ^4 term and for this reason we can only evaluate the functional perturbatively. The method works well when the fluctuations are small. Lets expand the field ϕ into a sum of the ground state value and the fluctuations

$$\phi(x) = \bar{\phi} + \psi(x). \tag{2.16}$$

The potential energy is given by

$$\mathcal{F} = \int_{-\infty}^{\infty} \left\{ \frac{1}{2} a\phi^2 + \frac{1}{2} c \left(\frac{\partial \phi}{\partial x} \right)^2 + \frac{1}{4} g\phi^4 \right\} dx, \tag{2.17}$$

where we have renamed the parameters appearing in (2.6) for notational simplicity. We would like to consider the effect of the fluctuations $\psi(x)$ to quadratic order in the system where $a > 0$ i.e. in the linear phase. Substituting (2.16) into (2.17) and keeping up to the quadratic order in $\psi(x)$ we get

$$\begin{aligned} \mathcal{V} &= \frac{1}{2} a \left(\bar{\phi} + \psi \right)^2 + \frac{1}{2} c \left(\frac{\partial \psi}{\partial x} \right)^2 + \frac{1}{4} g \left(\bar{\phi} + \psi \right)^4 \\ &= \mathcal{V}_0 + \frac{1}{2} a \bar{\phi} \psi + \frac{1}{2} a \psi^2 + \frac{1}{2} c \left(\frac{\partial \psi}{\partial x} \right)^2 + \frac{1}{4} g \left(4\bar{\phi}^3 \psi + 6\bar{\phi}^2 \psi^2 \right) + O(\psi^4) \quad (2.18) \\ &= \mathcal{V}_0 + \frac{1}{2} a \psi^2 + \frac{1}{2} c \left(\frac{\partial \psi}{\partial x} \right)^2 + O(\psi^4), \quad (2.19) \end{aligned}$$

where to go from the second to last line we have made use of the fact that $\bar{\phi} = 0$ for $a \geq 0$. Now the potential energy functional given by (2.18) is quadratic in field $\psi(x)$ i.e. it is of the form

$$\mathcal{F} = \frac{1}{2} \int dx \int dx' \psi(x) G^{-1}(x, x') \psi(x') + \frac{1}{2} \int dx q(x) \psi(x), \tag{2.20}$$

where $G^{-1}(x, x')$ is an operator kernel and the linear term $q(x)\phi(x)$ is included for generality. The two point correlation function is defined by

$$\langle \phi(x) \phi(x') \rangle = \left\langle \left(\bar{\phi} + \psi(x) \right) \left(\bar{\phi} + \psi(x') \right) \right\rangle, \tag{2.21}$$

where $\langle \ldots \rangle$ indicates ensemble average. If the system is in the symmetric phase (linear chain phase), then $\bar{\phi} = 0$ and the two point correlation function is $\langle \psi(x) \psi(x') \rangle$. The two point correlation function can be extracted from the partition function (2.14) using the cumulant expansion

$$\begin{aligned} \langle \psi(x) \psi(x') \rangle &= -\frac{\partial^2}{\partial q^2} \ln Z \Big|_{q=0} \\ &= G(x, x'), \end{aligned} \tag{2.22}$$

where $G(x,x')$ satisfies

$$\int dx' G^{-1}(x,x')G(x,x'') = \delta(x'-x''). \tag{2.23}$$

Thus in order to evaluate the two point correlation function we must first diagonalize the functional (2.18) to find $G^{-1}(x,x')$ and then we must invert $G^{-1}(x,x')$. The energy functional (2.18) is diagonal in the Fourier basis. The Fourier representation is given by

$$\begin{aligned} \psi(x) &= \int_{-\infty}^{\infty} \frac{dq}{2\pi} \tilde{\psi}(q) e^{-iqx}, & (2.24) \\ \tilde{\psi}(q) &= \int_{-\infty}^{\infty} dx \psi(x) e^{-iqx}. & (2.25) \end{aligned}$$

The orthogonality relations are given by

$$\begin{aligned} \int_{-\infty}^{\infty} dx e^{i(q+q')x} &= 2\pi\delta(q+q'), & (2.26) \\ \int_{-\infty}^{\infty} \frac{dq}{2\pi} e^{-i(q+q')x} &= \delta(x+x'). & (2.27) \end{aligned}$$

Substituting (2.24) into (2.18) and making use of (2.27) gives

$$\mathcal{F} = \int_{-\infty}^{\infty} \frac{dq}{2\pi} \left(\xi^{-2} + q^2\right) \tilde{\psi}(q)\tilde{\psi}(-q)dq \tag{2.28}$$

where $\xi^{-2} = a/c$. The expression for potential energy (2.28) is diagonal and the inverse of the two point correlation function is $G^{-1}(q) = \xi^{-2} + q^2$. The two point correlation function in Fourier space is thus $G(q) = 1/(\xi^{-2}+q^2)$. To find the two point correlation function in real space we perform the inverse Fourier transform

$$\begin{aligned} G(x,x') &= \int_{-\infty}^{\infty} dq G(q) e^{iq(x-x')} \\ &= \int_{-\infty}^{\infty} dq \frac{e^{iq(x-x')}}{\xi^{-2}+q^2} \\ &= \frac{1}{\delta\xi} e^{-|r|/\xi}, & (2.29) \end{aligned}$$

where $r = x - x'$. Thus the correlations decay exponentially with the characteristic length $\xi = \sqrt{c/a}$. In the vicinity of the critical point it is expected that the correlation length should diverge with a critical exponent ν i.e. $\xi \propto |a|^{-\nu}$. By accounting for the fluctuations to the second order we have shown that $\nu = 1/2$, which corresponds to the mean field universality class. Higher order corrections from the fluctuations will alter the value of the critical exponents. There are no known exact techniques of evaluating the critical exponents of the one dimensional ϕ^4 model, although there is a range of approximate methods [74]. Even though the true mean field critical exponents might differ from the mean field theory values, the Ginzburg criterion restores much of the credibility to the mean field theory. Ginzburg criterion states that mean field critical exponents are valid whenever one is sufficiently far from the critical point and always for system of dimensions $d \geq 4$. Thus for the case of linear to zigzag chain it may well be that Ginzburg region is difficult to resolve and instead one can take $\nu = 1/2$. We can check if this is the case by performing numerical simulations at realistic temperatures and extracting the correlation length from the correlation function. Since the ion chains are particularly small systems we are more likely to encounter the finite size effects on the correlation length than the higher order effects of the fluctuations.

Knowledge of the nature of the divergence of the correlation length near the critical point and the critical exponent ν is essential for the Kibble-Zurek theory. Since we are interested in ultimately testing KZ theory in a finite ion trap system in the next section we examine the finite size effect on the two point correlation function for the system in the vicinity of the critical point.

2.3 Finite size effects

If the system is of size L then the correlation length ξ can no longer diverge to infinity near the critical point since it is limited by the size of the system. Thus on the approach towards the critical point one may expect that $\xi \to L$. In general, the sharp features such as divergences of thermodynamic quantities and discontinuities that are characteristic of phase transitions in the thermodynamic limit will be smoothed out. Figure 1.1 in Chapter 1 shows a cartoon of how one might expect the correlation length to look like for different system sizes. It was mentioned in Chapter 1 that the finite size effects have to be accounted for when the critical properties of the system are evaluated using a computer or experiments in mesoscopic systems. To extrapolate the results obtained in finite size system to the thermodynamic limit one can make use of a set of results

collectively known as the finite size scaling theory [19]. Typically one has to measure the critical properties for systems of several different size L - the way the results change as the system size is varied is not arbitrary but depends on the critical exponents of the transition in the thermodynamic limit. In our case, we assume that the critical exponent is $\nu = 1/2$ but we would like to obtain an estimate of the finite size effect on the correlation length near the critical point of the linear to zigzag phase transition. It is important to get an idea of the magnitude of the finite size effects since later the KZ experiments will be carried out in small systems of 16 to 30 ions.

For periodic boundary conditions on a finite interval of size L, we can perform an exact mean field analysis of the ϕ^4 model. The potential energy of the ϕ^4 field for a system of size L is given by

$$\mathcal{F} = \int_0^L \left\{ \frac{1}{2}a\phi^2 + \frac{1}{2}c\left(\frac{\partial\phi}{\partial x}\right)^2 + \frac{1}{4}g\phi^4 \right\} dx \tag{2.30}$$

As before we express the field as a sum of its ground state and fluctuations, $\phi(x) = \bar{\phi} + \psi(x)$, and keep up to the quadratic order in the fluctuations in the expression for the potential energy. The mean field expression for the potential energy is

$$V = \int_0^L \left\{ \frac{1}{2}a\psi^2 + \frac{1}{2}c\left(\frac{\partial\psi}{\partial x}\right)^2 + \frac{1}{4}g\psi^4 \right\} dx \tag{2.31}$$

The potential energy given by (2.31) is diagonalized as before in the Fourier space. Since the systems is finite, this time we introduce the Fourier series instead of the Fourier transform

$$\psi(x) = \sum_q \tilde{\psi}_q e^{iqx} \tag{2.32}$$

$$\tilde{\psi}_q = \frac{1}{L}\int_0^L dx\psi(x)e^{-iqx}, \tag{2.33}$$

where the Fourier elements take values $q_i = 2\pi m/L$, where m is an integer and L is the

size of the system. In this representation we have

$$\mathcal{F}[\psi] = \int_0^L dx \left\{ \frac{a}{2}\psi^2 + \frac{c}{2}\left(\frac{\partial\psi}{\partial x}\right)^2 \right\} \tag{2.34}$$

$$= \int_0^L dx \sum_q \sum_{q'} \left[\frac{a}{2} e^{i(q+q')x} \psi_q \psi_{q'} - qq' \frac{c}{2} e^{i(q+q')x} \psi_q \psi_{q'} \right]. \tag{2.35}$$

Making use of the identity $\int_0^L dx e^{-i(q+q')x} = L\delta_{q,-q'}$ we have

$$\mathcal{F}[\psi] = L \sum_q \sum_{q'} \delta_{q,-q'} \left[\frac{a}{2}\psi_q\psi_{q'} - qq' \frac{c}{2}\psi_q\psi_{q'} \right] \tag{2.36}$$

$$= \frac{L}{2} a\xi^2 \sum_q \left[\xi^{-2} + q^2\right] |\psi|^2, \tag{2.37}$$

where $\xi^{-2} \equiv a/c$. Thus in Fourier space the propagator is given by $G(q) = \frac{1}{h}\left(\xi^{-2} + q^2\right)^{-1}$. In real space the correlation function is given by

$$G(x,x') \equiv \langle \psi(x)\psi(x') \rangle = \sum_q e^{iq(x-x')} G(q)$$

$$= \frac{1}{a\xi^2} \sum_q \frac{e^{iq(x-x')}}{\xi^{-2} + q^2}. \tag{2.38}$$

The sum in (2.38) can be evaluated analytically in terms of special functions. Figure 2.4 shows plots of $G(x,x')$ for several different values of a. Since the boundary conditions are periodic the two point correlation function must satisfy $G(r) = G(L-r)$, which is clear from the figure 2.4. If $\xi/L \ll 1$ then the two point correlation function closely matches the two point correlation function for the system in thermodynamic limit (figure 2.4). The finite size effects become important when ξ/L is of the order of unity.

From the two point correlation function we may extract the correlation length and investigate its behaviour near the critical point. Since the two point correlation function does not have the simple form of an exponential decay, we must first find an appropriate definition of the correlation length for finite size systems. A commonly used definition of the correlation length is [19]

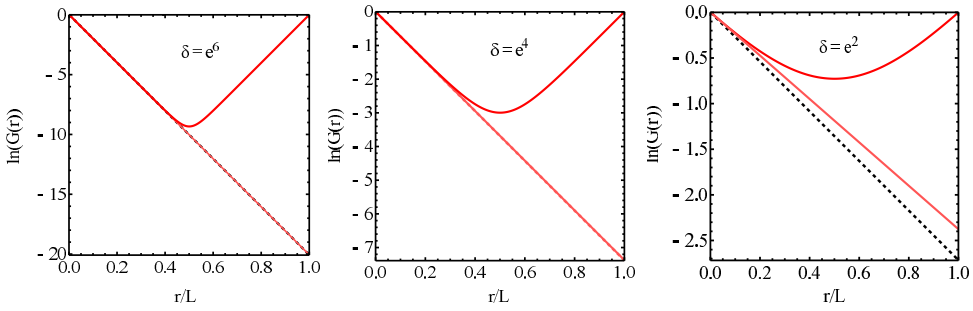

Figure 2.4: $G(x, x')$ for a finite size system for three different values of δ. Parameters chosen for the calculation were $L = 1$ and $h = 1$.

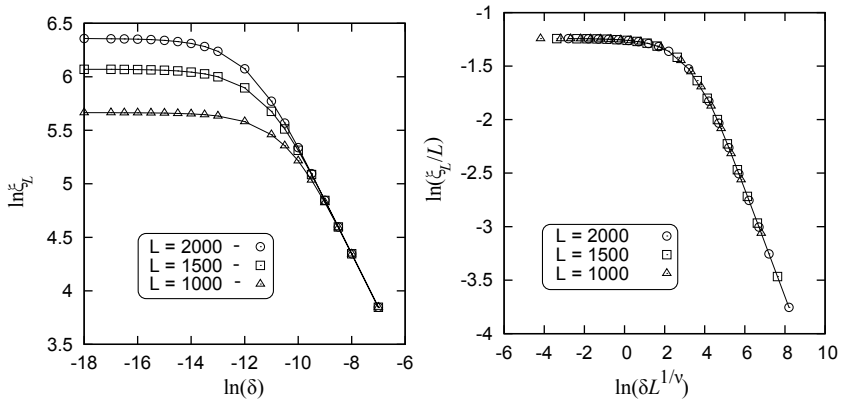

Figure 2.5: a) Finite size scaling of the correlation length for three different values of ξ. b) Collapse of the three curves when plotted in scaled units ξ_L/L vs $\delta L^{1/\nu}$ with $\nu = 1/2$.

$$\xi_L = \sqrt{\frac{\int_0^L r^2 G(r) dr}{\int_0^L G(r) dt}}. \tag{2.39}$$

It can be readily verified by inserting equation (2.29) into (2.39) that $\lim_{L\to\infty} \xi_L = \xi$. The plots of ξ_L as a function of δ are shown in figure 2.5a for several different values of L. For large δ, ξ scales with δ with a mean field exponent of 1/2. At small δ there are plateaus that arise because of the finite size of the system. It is interesting to note that according to the finite size scaling hypothesis

$$\frac{\xi_L}{L} = g_\xi(aL^{1/\nu}) \tag{2.40}$$

i.e. the correlation length is a homogeneous function of L. Thus if we plot ξ_L/L versus

$L^{1/\nu}$ for different values of L all graphs should align onto one universal function g_ξ. Figure 2.5b demonstrates this - the behaviour of ξ_L near the critical point in systems of various size L can be predicted from the knowledge of the function g_ξ. The result (2.40) is general for all finite size systems but the specific form of the function g_ξ is determined by the details of the system and the boundary conditions.

We have carried out an analytic calculation of the correlation length for a finite size periodic ϕ^4 model using the mean field approximation. This captures well the expected properties of the linear chain near the critical point. However, the GL free energy does not describe the ion chain system exactly and thus we will also evaluate numerically the two point correlation function for the ion chain system. Our calculation method is based on molecular dynamics simulations. The dynamics of N ions in contact with a heat bath of temperature T can be modelled using Langevin equations. For the jth ion the Langevin equation of motion reads

$$m\frac{d^2\mathbf{r}_j}{dt^2} = -\nabla_j V - \eta\frac{d\mathbf{r}_j}{dt} + \vec{\theta}_j(t) \tag{2.41}$$

where V is the potential energy of the system which includes the contribution from the harmonic confinement and the interaction between the ions; $-\eta\dot{\mathbf{r}}_j$ is the friction force and $\vec{\theta}_j(t) = (\theta_j^x, \theta_j^y, \theta_j^z)$ is the stochastic force having the following statistical properties

$$\begin{aligned} \langle\theta_j(t)\rangle &= 0 & (2.42)\\ \left\langle\theta_j^\alpha(t)\theta_k^\beta(t)\right\rangle &= 2\eta k_B T\delta_{jk}\delta(t-t'). & (2.43) \end{aligned}$$

The noise and friction forces are such that the fluctuation dissipation theorem is satisfied and hence the effect of those forces is to bring the system into a thermal equilibrium with a reservoir at temperature T. Performing Langevin dynamics simulations n times generates a sample of n configurations from a canonical ensemble. The statistical quantities such as two point correlation function can be estimated using the sample since $\langle\mathcal{O}\rangle = \lim_{n\to\infty}\langle\mathcal{O}\rangle_n$ where $\mathcal{O}$ denotes an observable quantity.

The two point correlation function for a system of N ions is given by a matrix with the following elements

$$G_{ij} = \langle x_i x_j\rangle\,, \tag{2.44}$$

where x_i and x_j are the transverse displacements of the ith and jth ion respectively.

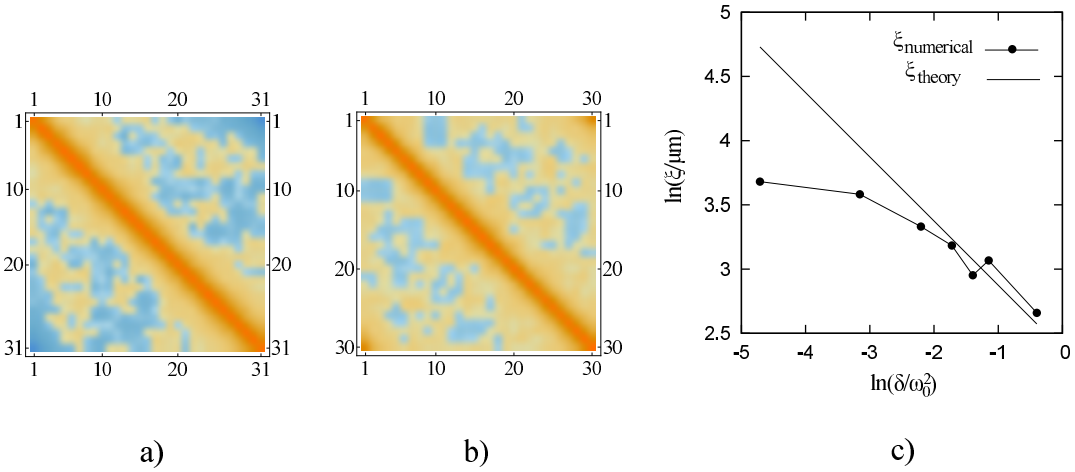

Figure 2.6: a) Numerically evaluated two point correlation function G_{ij} for a) 31 ions and b) 30 ions. c) Numerically evaluated correlation length as a function of critical parameter δ. Calculations were carried out by performing statistical averaging over approximately 2000 molecular dynamics simulations.

The numerically evaluated two point correlation function is shown in figure 2.6 for a system of 30 and 31 ions and periodic boundary conditions. The form of the two point correlation function is exponential decay. Thus even though there is a distinct length scale associates with the distances between the individual ions the important length scale near the critical point is indeed the correlation length. There is a qualitative difference between the two point correlation functions for chains with an odd number of ions and for chains with an even number of ions. In chains with an odd number of ions (e.g. in a chain with 31 ions shown in figure 2.6a) the distant regions are anticorrelated, whereas in chains with an even number of ions (e.g. in a chain with 30 ions shown in figure 2.6b) the distant regions have positive correlation. This observation can be accounted by the fact that chains with even and odd number of ions have effectively different boundary conditions. In terms of the field theory when the number of ions is even the boundary conditions are periodic $\phi(0) = \phi(L)$ and when the number of ions is odd the boundary conditions are twisted periodic $\phi(0) = -\phi(L)$. These different topologies imposed by the boundary conditions have an important consequence - in the zigzag phase the chain can have only an odd (even) number of topological defects if it consists of odd (even) number of ions. The topological defects will be considered in detail in the next chapter.

Figure 2.6c shows a plot of ξ_L for 30 ions evaluated numerically for several different values of δ. The correlation length ξ is obtained by fitting the evaluated two point

correlation function to $G(|j-k|a) \sim \exp(-|j-k|a/\xi)$. Far away from the critical point the divergence of the correlation length follows the mean field critical exponent of $\nu = 1/2$. In the vicinity of the critical point the correlation length saturates at a finite value because of the finite size of the system.

2.4 Chapter conclusions

In this chapter we have examined in detail the classical linear to zigzag structural phase transition of Coulomb crystals trapped in a harmonic potential. The Ginzburg-Landau theory for this transition in the thermodynamic limit was presented. The mean field analysis was reviewed and applied to the calculation of the exponent of the divergence of the correlation length. The finite size effects for this transition were considered by treating the continuum field theory on a finite interval using mean field approach and also numerically using an actual system of 30 and 31 ions.

The main points of this chapter are that mean field critical exponents are appropriate for the linear to zigzag phase transition if the system is relatively far away from the critical point. The finite size effects modify the critical behaviour when the systems is in close proximity of the critical point. This means that the theoretical predictions which make use of the critical exponents, in particular, the Kibble-Zurek theoretical predictions [138] should be treated with caution because of the presence of the significant finite size effects. In the next chapter, we will consider the process of generation of topological defects via a non-adiabatic quench from the linear to zigzag phase. We review the Kibble-Zurek theory and present a new approach consistent with KZ theory but which is also easily generalized to inhomogeneous system. It will be shown that the scaling of topological defects with the quench rate holds even for small systems consisting of 30 ions for a wide range of quench rates.

Chapter 3

Universality of the equations of motion

Traditionally the KZ scaling of topological defects with quench rate is derived using intuitive physical arguments of diverging correlation length and critical slowing down. This KZ argument was reviewed in Chapter 1. In this chapter, we show that in essence KZ theory identifies a time scale $\hat{t}$ and a length scale $\hat{\xi}$ such that if the equations of motion are written in these units the dynamics becomes quench independent and hence universal. In the KZ theory this time scale and this length scale are referred to as "freeze-out" time and "freezed-out" correlation length respectively. We will argue that instead of using the equilibrium calculation of divergence of correlation length and relaxation time to find $\hat{t}$ and $\hat{\xi}$ one can find this quantities by analyzing the equation of motion directly. The advantages of this approach is that first of all it may be considered a mathematical proof rather than a physical argument and secondly it can be used to derive finite size KZ scaling laws. The last point is particularly important since the linear to zigzag phase transition will be realized in small Coulomb crystals where one will measure the finite size KZ scaling. In this chapter, we derive the KZ scaling for model A and model B field theories as well as for the ion traps. The KZ scaling is tested numerically in the system of 30 ions with periodic boundary conditions and underdamped dynamics.

3.1 Topological defects

In general after the process of spontaneous symmetry breaking the vacuum state (ground state) is not unique but is a degenerate manifold. If in spatially separated regions the order parameter assumes different values from the vacuum manifold then topological defects may form. Topological defects are field configurations, such that their presence can be detected by looking at the values of the field far away from the defect. In other words, topological defects cannot be removed by local deformations of the field. As an

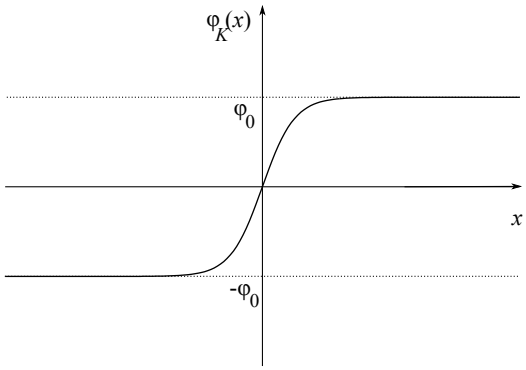

Figure 3.1: One dimensional ϕ^4 soliton.

example, lets consider the scalar one dimensional ϕ^4 field theory discussed in chapter 2. In the symmetry broken phase the mean field potential energy has a double well structure shown in figure 2.2 and the vacuum manifold is $\{-\phi_0, \phi_0\}$. The field configuration that interpolates between $\phi = -\phi_0$ and $\phi = \phi_0$ contains a Z_2 defects or kink. In the ϕ^4 theory the kink configuration $\phi_K(x)$ can be found analytically in terms of a hyperbolic tangent (see Chapter 5 for details of the solution). Figure 3.1 shows the form of the ϕ^4 kink. We can define the topological "charge" of the field by

$$Q = \int \partial_x \phi dx = \phi_K(x = -\infty) - \phi(x = +\infty). \tag{3.1}$$

The charge of a single Z_2 kink is either $+1$ or 1 depending on whether the field interpolates between $-\phi_0$ and ϕ_0 or between ϕ_0 and $-\phi_0$. Multiple kinks can be removed by bringing kinks of opposite charges next to one another. Field theories in higher dimensions and with vector order parameters can result in more complex defect structures. In general, the type of defect can be predicted from the dimensionality and the number of components of the order parameter vector field using homotopy theory [87]. In this chapter, we will be dealing with the scalar ϕ^4 theory since it is the simplest and describes the linear to zigzag phase transition but the results can easily be generalized to more complex field theories.

3.2 Equations of motion for the field - model A and model B dynamics

In Chapter 1 we have introduced the notion of local thermodynamic equilibrium (LTE) and phenomenological equations that can describe the dynamics of various systems in

LTE. There are a number of possible dynamical equations and they are labeled model A to J by Halperin and Hohenberg in [62]. Just as the Ginzburg-Landau free energy the various generators of dynamics should be regarded as phenomenological constructions motivated by physical arguments such as conservation laws. The dynamical equations must be constructed such that they accurately describe the dynamics of the order parameter in the vicinity of the critical point. Analysis of the linear response of these models allows one to calculate dynamic critical exponents for each model in the vicinity of second order phase transitions. We will use these phenomenological field equations to derive defect scaling laws. Making use of these equations for the purpose of studying defect formation is reasonable since often the defects form in the initial stages of the quench when higher order corrections to the free energy and dynamical generators are negligible.

We will focus on two commonly used dynamical models: model A and model B. Model A is constructed by postulating that the rate of change of the order parameter is proportional to the local thermodynamic force $\delta\mathcal{F}[\phi]/\delta\phi$. The equations of motion for model A are given by

$$\frac{\partial\phi(x,t)}{\partial t} = -\Gamma\frac{\delta\mathcal{F}[\phi]}{\delta\phi} + \theta(\mathbf{r},t), \tag{3.2}$$

where $\theta(x,t)$ is the stochastic white noise satisfying

$$\begin{aligned} \langle\theta(x,t)\rangle &= 0, & (3.3)\\ \langle\theta(\mathbf{r},t)\theta(\mathbf{r}',t')\rangle &= 2\Gamma k_B T\delta(\mathbf{r}-\mathbf{r}')\delta(t-t'). & (3.4) \end{aligned}$$

The system following the equations of motion given by (3.2) will flow along the energy gradient until it reaches a local minimum. The noise term simulates the equilibration of the system with a heat bath at temperature T. Real systems that are commonly described by model A dynamics include superconductors [82] and anisotropic alloys and magnets [62].

When the order parameter is locally conserved, such as in the process of separation of binary fluids the equations of motion of model B are employed [21]. In the case of conserved dynamics the order parameter obeys the continuity equation

$$\frac{\partial\phi}{\partial t} + \nabla\cdot\mathbf{j} = 0. \tag{3.5}$$

The current **j** is proportional to the gradient of the chemical potential, which is in turn proportional to the local thermodynamic force. Hence model B takes the form

$$\frac{\partial \phi}{\partial t} = -\Gamma \nabla^2 \frac{\delta \mathcal{F}[\phi]}{\delta \phi} + \theta(\mathbf{r}, t). \tag{3.6}$$

Equations (3.2) and (3.6) without the white noise term are known in the literature as the time dependent Ginzburg-Landau equation and the Cahn-Hillard equation respectively [21]. They can also be used to study the process of dynamic phase transitions and coarsening dynamics. The role of the white noise is mainly to provide random initial conditions; the noise itself does not significantly influence the coarsening process.

3.3 Rescaling and the universal equation

The principle idea of our approach of deriving the defect scaling laws is to show that one can find a linear transformation of variables in the equations of motion that eliminates their dependence on quench rate. This results in a quench independent and hence universal equations of motion - all of the spatial scaling information is contained within the coefficients of the linear transformation.

We will use a ϕ^4 GL free energy functional in equations of motion of model A and model B given by equations (3.2) and (3.6)

$$\mathcal{F}[\phi] = \int \left(\frac{1}{2}\delta\phi^2 + \frac{1}{2}c\left(\nabla_d \phi\right)^2 + \frac{1}{4}g\phi^4 \right) d^d\mathbf{r}, \tag{3.7}$$

where the order parameter ϕ is a scalar real field and d is the dimensionality of the system. We take the order parameter field to be real and scalar for simplicity - generalization to vector fields and complex field is trivial. As was discussed in detail in Chapter 2, for $\delta > 0$ the system is in the symmetric phase, for $\delta < 0$ the system is in the symmetry broken phase and for $\delta = 0$ the system is in the critical state. Now suppose that δ changes with time such that at some instance it crosses the critical value of $\delta = 0$. We take this quench function to be of power law form

$$\delta(t) = -\left(\frac{t}{\tau_Q}\right)^n \delta_0 \mathrm{sign}(t), \tag{3.8}$$

where, τ_Q is the quench timescale. The system crosses the critical point at $t = 0$; for $t < 0$ the system is in the symmetric phase and for $t > 0$ the system is in the symmetry broken phase. Any function $\delta(t)$ can be expanded as Taylor series near the critical point

$\delta = 0$ and usually in the experiments the linear term will have the greatest contribution. However, for generality we keep n to be an integer, which does not necessarily need to equal to one.

3.3.1 Model A dynamics

With GL free energy given by (3.7) and the quench function given by (3.8) the model A equation of motion is

$$\frac{\partial \phi}{\partial t} = -\left(\frac{t}{\tau_Q}\right)^n \text{sign}(t)\phi + \nabla_d^2 \phi + g\phi^3 + \sqrt{T}\theta(\mathbf{r}, t), \tag{3.9}$$

where now we have switched to natural units so that constants c, a_0 do not appear in the equation for notational simplicity and the nonlinear coupling strength g is dimensionless. The stochastic noise obeys the following statistical relationships

$$\langle \theta(t) \rangle = 0 \tag{3.10}$$

$$\langle \theta(\mathbf{r}, t)\theta(\mathbf{r}', t') \rangle = 2\Gamma k_B \delta^d(\mathbf{r} - \mathbf{r}')\delta(t - t'). \tag{3.11}$$

Quench can be terminated when the energy barrier between the two minima of the double well potential is much greater than $k_B T$ - this prevents spontaneous creation and annihilation of defects via thermal fluctuations. Now consider the following linear transformation of variables

$$\vec{\xi} = \beta \mathbf{r}, \quad \eta = \alpha t, \quad \varphi = \gamma \phi, \quad \tilde{T} = \sigma T, \tag{3.12}$$

with

$$\beta = \left(\frac{1}{\tau_Q}\right)^{\frac{n}{2(n+1)}}, \tag{3.13}$$

$$\alpha = \left(\frac{1}{\tau_Q}\right)^{\frac{n}{n+1}}, \tag{3.14}$$

$$\gamma = \tau_Q^{\frac{n}{2(n+1)}}, \tag{3.15}$$

$$\sigma = \beta^{d-4}. \tag{3.16}$$

Substituting equations (3.12)-(3.16) into the equations of motion (3.9)-(3.11) gives

$$\frac{\partial \varphi}{\partial \eta} = -\eta^n \mathrm{sign}(\eta)\varphi + \nabla_d^2 \varphi + g\varphi^3 + \sqrt{\tilde{T}}\theta(\vec{\xi}, \eta), \tag{3.17}$$

with

$$\langle \theta(t) \rangle = 0 \tag{3.18}$$

$$\left\langle \theta(\vec{\xi}, \eta)\theta(\vec{\xi}', \eta') \right\rangle = 2\Gamma k_B \delta^d(\vec{\xi} - \vec{\xi}')\delta(\eta - \eta'). \tag{3.19}$$

Equations (3.17)-(3.19) do not depend on τ_Q - all τ_Q dependence has been absorbed by the coefficients of the linear transformation given by (3.13)-(3.16). The linear transformation given by (3.12)-(3.16) transform the original equations of motion into the *universal* frame of reference where the dynamics does not depend on quench rate. Without solving this universal equations we can immediately say that in the original frame of reference all of the spatial properties of the system will scale with τ_Q according to equation (3.13). Thus, for instance, if topological defects form then we expect that the typical distance between them $\hat{\xi}$ must scale according to the equation (3.13)

$$\hat{\xi} \propto \left(\frac{1}{\tau_Q}\right)^{\frac{n}{2(n+1)}}. \tag{3.20}$$

Now let us compare the result (3.20) to the KZ "freeze-out" correlation length which was given by equation (1.13) in Chapter 1. Equation (1.13) stated that

$$\hat{\xi}_{KZ} \propto \left(\frac{1}{\tau_Q}\right)^{\frac{\nu}{1+\nu z}}. \tag{3.21}$$

If we take the linear quench $n = 1$ as was done in the KZ argument in Chapter 1, and use mean field critical exponents for the model A dynamics with the Landau free energy $z = 1$, $\nu = 1/2$ then both methods give the same result

$$\hat{\xi}_{MF} \propto \left(\frac{1}{\tau_Q}\right)^{\frac{1}{4}}, \tag{3.22}$$

where the subscript MF emphasizes the fact that the scaling is obtained using the mean field critical exponents.

The timescale given by equation (3.14) corresponds to the "freeze-out" time in the KZ argument

$$\hat{t} \propto \left(\frac{1}{\tau_Q}\right)^{\frac{n}{n+1}}. \tag{3.23}$$

For the linear quench $n = 1$ we have

$$\hat{t}_{MF} \propto \left(\frac{1}{\tau_Q}\right)^{\frac{1}{2}}, \tag{3.24}$$

where again the subscript MF emphasizes that the results is obtained using the mean field critical exponents.

Thus we have mathematically proven by transforming the equations of motion to a universal frame of reference that the distances between defects will scale as $(1/\tau_Q)^{1/4}$ as predicted by the mean field KZ argument. The reason why the transformation methods seems to only predict the mean field KZ scaling is connected to the fact that according to equations (3.12)-(3.16) one has to rescale the temperature in order to obtain the full universality. In the KZ scenario, however, only the quench rate is varied and not the temperature. The necessary temperature rescaling given by equations (3.12) and (3.16), $T \to T\beta^{d-4} = T\tau_Q^{2(n+1)(d-4)/n}$ affects the initial conditions and also changes the amount of thermal energy introduced into the system during the quench. When $d = 4$ the temperature dependence on quench rate disappears and equations (3.9)-(3.11) are completely universal. Now let us consider how the temperature affects quench dynamics for systems with $d \neq 4$. In order for the initial conditions to be completely independent of temperature and hence quench rate, the equations of motion must not contain a non-linear term. If the nonlinear term can be neglected then the order parameter field can simply be rescaled in such as way as to remove the temperature dependence. If the initial condition are independent of quench rate and we assume that the temperature is sufficiently low that the stochastic term in (3.17) can be neglected during the quench then the dynamics is universal and KZ scaling is $\hat{\xi} \propto (1/\tau_Q)^{1/4}$. From (3.17) the nonlinear term can be neglected if

$$|\eta_0^n \phi| \gg |g\phi^3|. \tag{3.25}$$

The magnitude of the order parameter field scales with $\sqrt{\tilde{T}}$ i.e. $|\phi| \sim \sqrt{\tilde{T}} = \sigma^{1/2} = \beta^{(d-4)/2}$, and substituting this expression in (3.25) gives

$$
\begin{aligned}
|\eta_0|^n &\gg |g\beta^{d-4}| \\
|\eta_0| &\gg A \qquad (3.26) \\
A &\equiv \left| g^{1/n} \left(\frac{1}{\tau_Q} \right)^{\frac{d-4}{n+1}} \right| \qquad (3.27)
\end{aligned}
$$

Thus as long as the condition (3.26) is valid the mean field KZ scaling $\hat{\xi} \propto (1/\tau_Q)^{1/4}$ holds. Let us consider in which cases the condition (3.26) is violated. Since KZ theory is concerned primarily with defect scaling at slow quenches we examine the slow quench limit. If the quench rate $1/\tau_Q$ is reduced then A decreases for $d > 4$ and increases for $d < 4$. Thus in the case $d \geq 4$ the condition (3.26) is always satisfied for slow quenches and the KZ scaling is always mean field $\hat{\xi} \propto (1/\tau_Q)^{1/4}$. In the case of $d < 4$ the condition (3.26) will eventually be violated and the fluctuations will start to influence the KZ scaling. By analogy with the equilibrium thermodynamics we may regard dimension $d = 4$ as an upper critical dimension above which KZ scaling always assumes the mean field form.

We have shown that it is possible to eliminate the τ_Q dependence from the equations of motion and the initial conditions for $d \geq 4$ and when conditions (3.26) holds. The method predicts the mean field KZ scaling. Using the simple linear transformation we were not able to eliminate τ_Q for all quench rates but had to impose an addition condition (3.26). When (3.26) does not hold the scaling is expected to alter from the mean field value. It seems that when the mean field approximations are not valid it may be much harder to predict the KZ scaling laws. In the case of equilibrium thermodynamics we encounter the same problem - it is much harder to characterize critical behaviour right at the critical point where thermal fluctuations dominate the dynamics of the system. It is an open question whether the non-mean field scaling limit suggested by KZ theory and given by equation (1.13) will hold. It is difficult to measure a non-mean field KZ scaling because of the finite size effects. For very slow quenches the correlation length will become very large during quench and may reach the order of the system size in finite size simulations. If this is the case, the boundaries will start to influence the scaling and can easily obscure any corrections to the mean field KZ scaling coming from the non-linear term in the GL free energy. We will look in more detail on how to deal with the finite size effect and inhomogeneities in the next section but first, to illustrate the power of the our technique let us apply it to model B

dynamics.

3.3.2 Model B dynamics

With GL free energy given by (2.3) and the quench function given by (3.8) the model B equation of motion is

$$\frac{\partial\phi}{\partial t} = -\left(\frac{t}{\tau_Q}\right)^n \mathrm{sign}(t)\nabla_d^2\phi + \nabla_d^4\phi + g\nabla_d^2\phi^3 + \sqrt{T}\theta(\mathbf{r},t), \tag{3.28}$$

where now we have switched to natural units so that constants c, a_0 do not appear in the equation of motion for notational simplicity and the nonlinear coupling g is dimensionless. The stochastic noise obeys the statistical relationship given by (3.10)-(3.11).

To eliminate the dependence of the equation (3.28) on τ_Q we can use the following linear transformation

$$\vec{\xi} = \beta\mathbf{r}, \quad \eta = \alpha t, \quad \varphi = \gamma\phi, \quad \tilde{T} = \sigma T, \tag{3.29}$$

with

$$\beta = \left(\frac{1}{\tau_Q}\right)^{\frac{2n}{1+2n}}, \tag{3.30}$$

$$\alpha = \left(\frac{1}{\tau_Q}\right)^{\frac{2n}{4(1+2n)}}, \tag{3.31}$$

$$\gamma = \tau_Q^{\frac{2n}{4(1+2n)}}, \tag{3.32}$$

$$\sigma = \beta^{(d-6)/4}. \tag{3.33}$$

Substituting equations (3.29)-(3.33) into the equation of motion (3.28) gives

$$\frac{\partial\varphi}{\partial\eta} = -\eta^n\mathrm{sign}(\eta)\nabla_d^2\varphi + \nabla_d^4\varphi + g\nabla_d^2\varphi^3 + \sqrt{\tilde{T}}\theta(\vec{\xi},\eta), \tag{3.34}$$

with

$$\langle\theta(t)\rangle = 0 \tag{3.35}$$

$$\left\langle\theta(\vec{\xi},\eta)\theta(\vec{\xi}',\eta')\right\rangle = 2\Gamma k_B\delta^d(\vec{\xi}-\vec{\xi}')\delta(\eta-\eta'). \tag{3.36}$$

Equations (3.34)-(3.36) are τ_Q independent and hence universal. For model B the scaling of the typical distance $\hat{\xi}$ between topological defects is given by equation (3.30)

$$\hat{\xi} \propto \left(\frac{1}{\tau_Q}\right)^{\frac{2n}{1+2n}}. \tag{3.37}$$

For linear quench $n = 1$ we have

$$\hat{\xi} \propto \left(\frac{1}{\tau_Q}\right)^{\frac{2}{3}}. \tag{3.38}$$

By the same argument as was given for model A equation (3.37) gives the mean field KZ scaling, that is always valid above the upper critical dimension which in this case is $d_u = 6$. The mean field scaling is also valid for sufficiently large $1/\tau_Q$.

We have derived the expected scaling of the number of topological defects with quench rate to illustrate the general applicability of our method. In exactly the same way we can analyze other dynamical models. To the best of our knowledge the scaling law given by (3.30) was not verified in computer simulations.

3.4 Scaling of topological defects in finite size and inhomogeneous systems

In the previous section, we have shown that τ_Q can be eliminated from the equations of motions for spatially unbounded fields. If we consider the same equations of motions in a bounded region of space then the transformations do not completely eliminate the τ_Q dependence from the equations of motion. The reason for this is that τ_Q will enter in the boundary conditions.

For concreteness lets consider a field following model A dynamics with periodic boundary conditions in a cell of dimensions $\underbrace{L \times ... \times L}_{d \text{ times}}$

$$\frac{\partial \phi}{\partial t} = -\left(\frac{t}{\tau_Q}\right)^n \text{sign}(t)\phi + \nabla_d^2 \phi + g\phi^3 + \sqrt{T}\theta(\mathbf{r}, t), \tag{3.39}$$

with

$$\begin{aligned}
\phi(L/2,0,...,0) &= \phi(-L/2,0,...,0), && (3.40)\\
\phi(0,L/2,...,0) &= \phi(0,-L/2,...,0), && (3.41)\\
. \quad . \quad . & && \\
\phi(0,0,...,L/2) &= \phi(0,0,...,-L/2). && (3.42)
\end{aligned}$$

If we carry out the linear transformation given by (3.12)-(3.16) then the equation of motion becomes τ_Q independent

$$\frac{\partial\varphi}{\partial\eta} = -\eta^n \mathrm{sign}(\eta)\varphi + \nabla_d^2\varphi + g\varphi^3 + \sqrt{\tilde{T}}\theta(\vec{\xi},\eta), \tag{3.43}$$

but the boundary conditions now depend on τ_Q

$$\begin{aligned}
\phi(\beta L/2,0,...,0) &= \phi(-\beta L/2,0,...,0), && (3.44)\\
\phi(0,\beta L/2,...,0) &= \phi(0,-\beta L/2,...,0), && (3.45)\\
. \quad . \quad . & && \\
\phi(0,0,...,\beta L/2) &= \phi(0,0,...,-\beta L/2), && (3.46)\\
\beta &= \left(\frac{1}{\tau_Q}\right)^{\frac{n}{2(n+1)}}. && (3.47)
\end{aligned}$$

In order to eliminate τ_Q from the boundary conditions (3.44)-(3.47) we have to rescale the size of the system according to

$$\begin{aligned}
\tilde{L} &= \chi L, && (3.48)\\
\chi &= \beta. && (3.49)
\end{aligned}$$

The meaning of the rescaling (3.48)-(3.49) is the following. If we perform a measurement of KZ scaling on a finite system then strictly speaking we have to vary the size of the system. The factor by which we have to vary the size of the system depends on τ_Q as given by equation (3.49). Thus for $n = 1$ if we change the quench rate by a factor of q then we have to change L by a factor of $q^{1/4}$ in order to get a universal scaling. This parallels the equilibrium finite size scaling theory which tells us how to extract scaling

laws in thermodynamic limit from measurements on finite size systems. Naturally if the size of the system is large $L \to \infty$ then varying the system size will not affect the defect density significantly. It is only when the maximum correlation length is of the order of L then we have to start worrying about the finite size effects.

Now let us consider model A dynamics for a field in an external potential. An external potential, which could be for example harmonic trapping as in the case of trapped BECs, results in an inhomogeneous field. Similar to the case of finite homogeneous system, the transformation (3.12)-(3.16) will not remove the τ_Q dependence from the equations of motion completely. The equation of motion for a field with model A dynamics in an external potential is given by

$$\frac{\partial \phi}{\partial t} = -\left(\frac{t}{\tau_Q}\right)^n \text{sign}(t)\phi + V_{ext}(\mathbf{r}, L)\phi + \nabla_d^2 \phi + g\phi^3 + \sqrt{T}\theta(\mathbf{r}, t), \tag{3.50}$$

where we have assumed that only the quadratic part of GL free energy is spatially dependent. The parameter L was introduced in the spatial dependence and it can play a role for instance of the length scale associated with the external potential. For concreteness let us consider the following external potential

$$V(\mathbf{r}, L) = -\left|\frac{\mathbf{r}}{L}\right|^m. \tag{3.51}$$

Then the rescaled equations of motion are given by

$$\frac{\partial \varphi}{\partial \eta} = -\left(\eta^n \text{sign}(\eta) + \frac{1}{\alpha}\left|\frac{\vec{\xi}}{\beta L}\right|^m\right)\varphi + \nabla_d^2 \varphi + g\varphi^3 + \sqrt{\tilde{T}}\theta(\vec{\xi}, \eta). \tag{3.52}$$

Equation (3.52) is independent of τ_Q provided we add an additional rescaling

$$\tilde{L} = \chi L, \tag{3.53}$$

$$\chi = \beta \alpha^{1/m}. \tag{3.54}$$

Thus to obtain a KZ scaling in an experiment in a trapped system we must vary the trapping parameter L according to equations (3.53)-(3.54). This is similar to the case of finite size homogeneous system; in fact we can view the external potential as a way to alter the boundary conditions of the system. We have considered the power law confining potential as it is a particularly simple and physically realistic potential. However, it can be shown that as long as $V(\mathbf{r}, L)$ is invertible it is possible

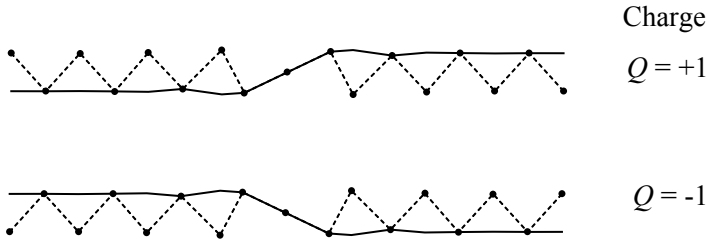

Figure 3.2: Kink and an antikink in the zigzag chain of 17 particles with periodic boundary conditions.

to find a transformation that eliminates τ_Q from the equations of motion, though this transformation may in general be non-linear.

3.5 Linear to zigzag phase transition and topological defects

Having considered defect scaling in abstract field theories we will now apply the same ideas to the linear to zigzag structural phase transition. If we induce a non-adiabatic quench from a linear to zigzag configuration by reducing the strength of transverse confinement at a finite rate $1/\tau_Q$ then there is a finite probability of defect creation. The defect in the zigzag chain has a structure of Z_2 kink as shown in figure 3.2. We are interested in predicting the scaling of the average number of kinks with quench rate $1/\tau_Q$.

The scaling of defects in zigzag chains was studied theoretically in [37, 30]. A critical review of these papers is necessary before we proceed with our derivation. In [37] the authors consider the problem of defect scaling in a chain of 50 ions trapped in a 3 dimensional harmonic potential. In order to derive the scaling it is argued that the critical exponents are known by virtue of the mapping to the GL theory [51] and KZ theory can be applied. Since the system considered in [37] is in a harmonic trapping potential the system is inhomogeneous and direct KZ theory is not applicable. Nevertheless, by considering an interplay between the speed of sound and the front velocity a modified scaling limit is derived (the argument parallels exactly the case of soliton creation in BEC [140]). The numerical molecular dynamics simulations in [37] provide additional quantification of the scaling law for the linear to zigzag phase transition. A related paper [30] repeats the same arguments but also adds an additional numerical result of defect scaling in a homogeneous chain with overdamped dynamics. The

theoretically predicted scalings in [37, 30] are: for the inhomogeneous chain 4/3 (underdamped), 1 (overdamped) and for the homogeneous chain 1/3 (underdamped), 1/4 (overdamped). Even though the authors claim that there is an agreement between the numerical simulations and theoretical prediction, a more detailed examination indicates that the agreement is not at all clear. The reason for this is the following. The scaling plots in [37, 30] display $\ln\langle n_{\rm defects}\rangle$ vs $\ln(1/\tau_Q)$. For a chain with open boundary conditions the number of domains relates to the number of defects via

$$n_{\rm domains} = n_{\rm defects} + 1. \tag{3.55}$$

Thus if $n_{\rm defects} \gg 1$ then $n_{\rm domains} = n_{\rm defects}$ and for the purpose of measuring the KZ scaling both plots $\ln\langle n_{\rm defects}\rangle$ vs $\ln(1/\tau_Q)$ and $\ln\langle n_{\rm domains}\rangle$ vs $\ln(1/\tau_Q)$ will give the same results. However if $n_{\rm defects} \lesssim 1$ then since $\ln(x+1) \neq \ln x$ there will be a big difference between plotting the logarithms of defects vs quench rate and the logarithms of domains vs quench rate. Clearly as $1/\tau_Q \to 0$, $n_{\rm defects} \to 0$ and $\ln(n_{\rm defects}) \to -\infty$ and the graph $\ln\langle n_{\rm domains}\rangle$ vs $\ln(1/\tau_Q)$ is a curve that becomes ever steeper on the approach to 0. Since KZ theory predicts a characteristic length scale $\hat{\xi}$ which is related to the number of domains, $n_{\rm domains} \propto 1/\hat{\xi}$, then one should plot the number of domains vs the quench rate rather than the number of defects as was done in [37, 30]. In [37, 30] the authors extracted the scaling from the wrong plot but found it consistent with the prediction only because the fit was done in a selected region of the curve that gives the expected result. We will now perform an independent analysis of the scaling in a periodic chain with underdamped dynamics - a regime which was not studied numerically in [37, 30].

In the previous chapter we have introduced the GL theory for the linear to zigzag phase transition. The dynamics of the system near the critical point of the phase transition is well described by the following field theoretical equations

$$\frac{\partial^2\phi}{\partial t^2} = \delta(t)\phi + h\frac{\partial^2\phi}{\partial x^2} + \mathcal{A}\phi^3, \tag{3.56}$$

where $\phi(ja) = (-1)^j z_j$, h, $\mathcal{A}$ are parameters that depend on the spacing between the ions a and $\delta(t)$ is the critical parameter given by

$$\delta = \omega_z^2(t) - \omega_c^2. \tag{3.57}$$

Equation (3.56) describes underdamped dynamics where the frictional force that is linear in particle velocity and stochastic force have been neglected. The other case is

the overdamped limit where the frictional force dominates and the inertial force can be neglected. We will focus on the underdamped case since it is experimentally relevant for trapped ions. Now suppose that the system undergoes a linear quench and the equations of motions are

$$\frac{\partial^2\phi}{\partial t^2} = -\frac{t}{\tau_Q}\text{sign}(t)\phi + h\frac{\partial^2\phi}{\partial x^2} + \mathcal{A}\phi^3. \tag{3.58}$$

In order to eliminate the τ_Q dependence from the equation (3.58) we use the following linear transformation

$$\xi = \beta x, \quad \eta = \alpha t, \quad \varphi = \gamma\phi, \tag{3.59}$$

with

$$\beta = \left(\frac{1}{\tau_Q}\right)^{\frac{1}{3}}, \tag{3.60}$$

$$\alpha = \left(\frac{1}{\tau_Q}\right)^{\frac{1}{3}}, \tag{3.61}$$

$$\gamma = \left(\frac{1}{\tau_Q}\right)^{\frac{1}{3}}. \tag{3.62}$$

Substituting equations (3.59)-(3.62) in (3.58) gives

$$\frac{\partial^2\varphi}{\partial\eta^2} = -\eta\text{sign}(\eta)\varphi + h\frac{\partial^2\varphi}{\partial\xi^2} + \mathcal{A}\varphi^3. \tag{3.63}$$

Equation (3.63) is τ_Q independent and hence universal. The universal length scale and hence the scaling of the domains size $\hat{\xi}$ with quench rate is obtained from equation (3.60)

$$\hat{\xi} \propto \left(\frac{1}{\tau_Q}\right)^{\frac{1}{3}}. \tag{3.64}$$

The 1/3 KZ scaling for fields in the underdamped regime was first predicted and verified numerically in [77]. For the case of linear to zigzag phase transition the result was derived (but not numerically verified) using KZ theory in [37, 30].

Now we would like to verify equation (3.64) using molecular dynamics simulations. The potential energy of the system is given by

$$
\begin{aligned}
V &= V_h + V_c, && (3.65)\\
V_h &= \frac{1}{2} m \sum_{j=1}^{N} \omega_x^2 x_j^2, && (3.66)\\
V_c &= \frac{Q^2}{2} \sum_j \sum_{k \neq j} \left(\frac{1}{r_{jk}^{(1)}} + \frac{1}{r_{jk}^{(2)}} \right), && (3.67)\\
r_{jk}^{(1)} &= \sqrt{(x_j - x_k)^2 + (z_j - z_k)^2}, && (3.68)\\
r_{jk}^{(2)} &= \begin{cases} \sqrt{(x_j - x_k)^2 + (-2L + z_j - z_k)^2} & , \quad \text{for } j < k \\ \sqrt{(x_j - x_k)^2 + (2L + z_j - z_k)^2}, & \text{for } j > k \end{cases} && (3.69)
\end{aligned}
$$

where z_j is the axial coordinate of the jth ion, x_j is the transverse coordinate of the jth ion, ω_x is the transverse confinement frequency, $Q \equiv e^2/4\pi\epsilon_0$ and L is the size of the simulation cell. The term $Q^2 \sum_j \sum_{j \neq k} 1/r_{jk}^{(2)}$ is needed to create periodic boundary conditions in the z-direction. According to Newton's laws the dynamics of the system having potential energy (3.65)-(3.69) is given by the following equations of motion

$$
\begin{aligned}
\frac{\partial^2 x_j}{\partial t^2} &= -\omega_x^2(t) x_j + \frac{Q^2}{m} \frac{\partial}{\partial x_j} V_c, && (3.70)\\
\frac{\partial^2 z_j}{\partial t^2} &= \frac{Q^2}{m} \frac{\partial}{\partial z_j} V_c. && (3.71)
\end{aligned}
$$

We take the $\omega_x(t)$ to be a linear function of t

$$
\omega_x(t) = \begin{cases} -\frac{\omega_i - \omega_f}{\tau_Q} t + \omega_i & \text{for } 0 \leq t < \tau_Q \\ \omega_f & \text{for } t \geq \tau_Q. \end{cases} \qquad (3.72)
$$

The linear time dependence of the radial frequency does not result in strictly linear time dependence in the critical parameter $\delta(t)$ in the GL theory. However, if one Taylor expands the resulting $\delta(t)$ around the instance of the transition then one finds that the linear term has the greatest contribution. For this reason we assume that equation (3.72) produces a linear quench with a quench rate proportional to $1/\tau_Q$. The reason for taking the linear variation in $\omega_x(t)$ is that it is more realistic to produce such quench in the experiment. It is possible to induce non-linear quenches and if the quench is a power law in t then the KZ scaling law can be predicted. However, if the quench

function is some polynomial in t then it is not known how to predict a precise KZ scaling law. For this reason we assume that near the critical point the quench function is almost linear and any corrections to the scaling law due to a small non-linearity of the quench function are neglected.

To measure the average number of defects produced after a quench with a given quench rate $1/\tau_Q$, we simply numerically evaluate the equations of motion many times, each time starting with random initial conditions. The initial conditions must correspond to a system configuration taken from the canonical ensemble. In order to produce such initial conditions we may evolve the system using Langevin stochastic dynamics given by the following equations

$$m\frac{\partial^2 x_j}{\partial t^2} = -m\omega_x^2(t)x_j + Q^2\frac{\partial}{\partial x_j}V_c + \Gamma\frac{\partial x_j}{\partial t} + \theta_x(t), \tag{3.73}$$

$$m\frac{\partial^2 z_j}{\partial t^2} = Q^2\frac{\partial}{\partial z_j}V_c + \Gamma\frac{\partial x_j}{\partial t} + \theta_z(t), \tag{3.74}$$

with

$$\langle\theta_\alpha(t)\rangle = 0, \tag{3.75}$$

$$\langle\theta_\alpha(t)\theta_\beta(t')\rangle = 2\Gamma k_B T\delta_{\alpha\beta}\delta(t-t'). \tag{3.76}$$

There are a number of numerical algorithms that can be used to evaluate equations (3.73)-(3.76). We use Langevin impulse method [120]. The system is initialized in a linear chain configuration and then evolved for a time t_0 during which the chain thermalizes with a reservoir at temperature T. In the thermalized system equipartition theorem is satisfied $1/2m\langle v^2\rangle = 3/2k_BT$ and the two point correlation function assumes the equilibrium form. Once the system is equilibrated we simulate the quench dynamics. In order to simulate the system in the underdamped regime one can either use the Langevin equations of motion (3.73)-(3.76) with small Γ or the Newton's laws (3.70)-(3.71). In our simulations we evaluate the whole quench dynamics using the Langevin-Impulse integrator. We use a simple algorithm to count the number of kinks. If two adjacent ions have the same sign of the transverse displacement, $x_j x_{j+1} > 0$ then we assume that there is a kink around the location j. The total number of "kinks" counted using this method is denoted by n_{defects}. Strictly speaking this does not always

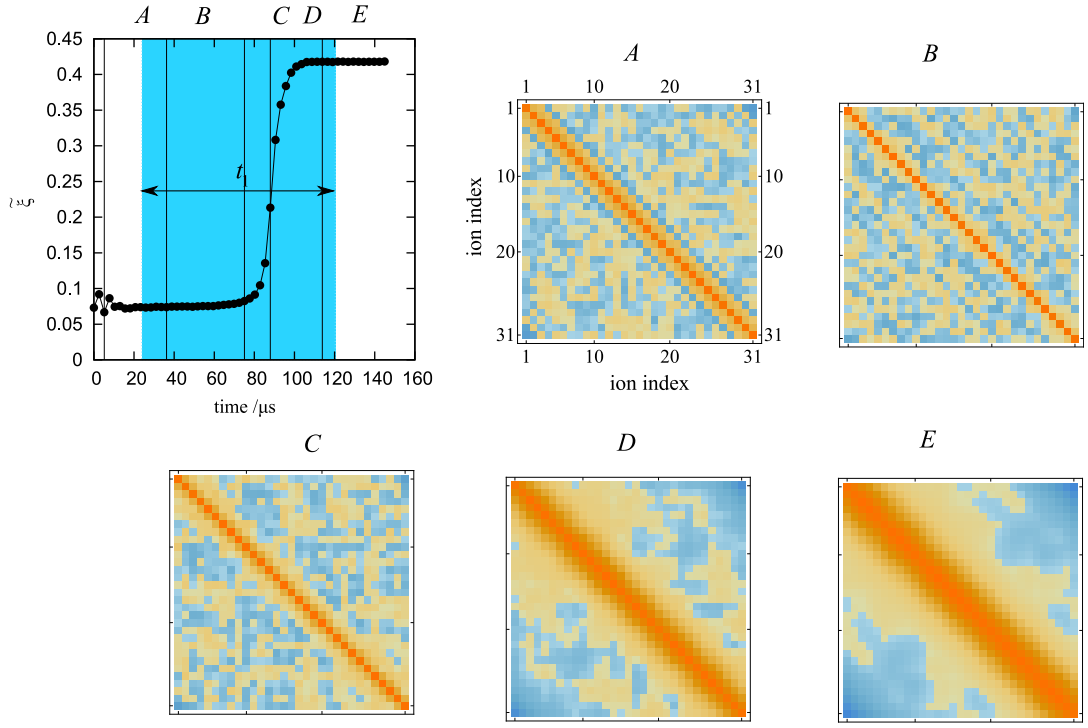

Figure 3.3: Quench experiment in the linear to zigzag phase transition and two point correlation functions at various instances during quench. (Top left) The characteristic length scale $\tilde{\xi}$ as a function of time. $(A-E)$ Two point correlation functions at instances $A-E$, which are marked at the top left graph. The data was calculated by averaging the results of ~ 2000 simulation runs. Simulation was done for 31 Yb^+ ions with $a = 12.9$ μm, $\omega_i/(2\pi) = 500$ kHz and $\omega_f/(2\pi) = 140$ kHz. The time of the quench is $t_1 = 96$ μs.

correspond to the true number of topological defects because this method does not remove the influence of thermal fluctuations. However, at the later stages of evolution when the system is in the zigzag phase, the thermal fluctuations are unlikely to move an ion vertically from one row to the other and in this case n_{defects} does correspond to the number of kinks in the chain. We carry out the simulation in the system with periodic boundary conditions and 31 ions. In such system the number of kinks is equal to the number of domains i.e. $n_{\text{domains}} = n_{\text{defects}}$. From the number of domains we evaluate the characteristic length scale in the system $\tilde{\xi} = L/n_{\text{domains}}$.

Figure 3.3 shows the non-equilibrium correlations extracted from the molecular dynamics simulations at one particular quench rate. The top left of the figure shows the calculated $\tilde{\xi}$ as a function of time. The region filled in blue, t_1, indicates the time interval when the ω_x was reduced linearly from its initial value ω_i to its final value. During the initial stages of the evolution $0 < t \lesssim 10$ μs one can see that $\tilde{\xi}$ fluctuates. The reason for these initial fluctuations is that during this time the system thermalizes.

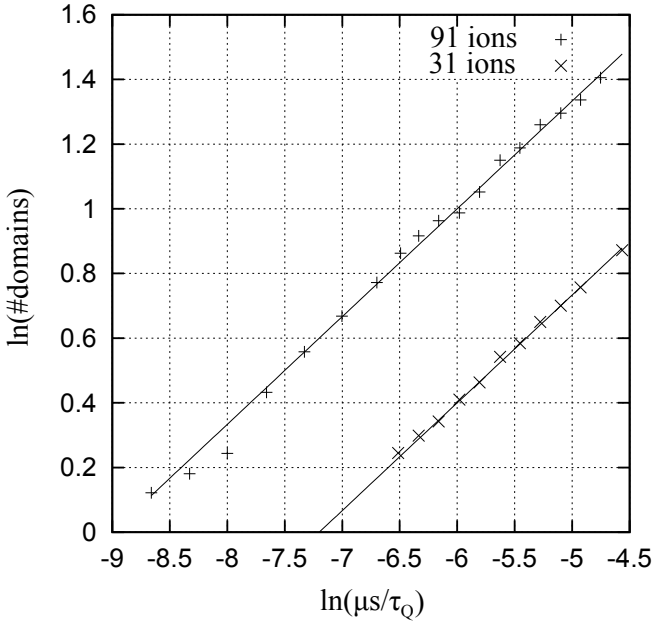

Figure 3.4: KZ scaling measured for the homogeneous linear to zigzag structural phase transition in the system with 31 and 91 ions. The two lines have slope of 1/3 and are drawn to visualize how closely the measured scaling matches the theoretical prediction of 1/3.

Once the system have thermalized, $\tilde{\xi}$ changes only slowly, adapting to the changing ω_x. Snapshot A shows the two point correlation function during the initial stages of the quench when the system still adjusts to its equilibrium state. Between $80 \lesssim t \lesssim 100$ the system crosses the critical point, falls out of the equilibrium and assumes a domain structure. Note that initially the correlation length starts to diverge with a critical exponent of $\nu = 1/2$ (cf figure 1.2), but eventually the system can no longer adjust to its equilibrium state and topological defects can form. At time instances D and E in figure 3.3 the system is out of equilibrium.

To measure the KZ scaling we perform ~ 2000 simulations for different quench rates $1/\tau_Q$ and measure the average number of kinks in the end of the evolution. To check that the measured scaling is not influenced by finite size effects we perform two sets of simulations: simulations for chains with 31 ions and for chains with 91 ions. The parameters of the simulations are as follows: separation between ions in linear chain configuration, $a = 12.9$ μm, $\omega_i/(2\pi) = 500$ kHz, $\omega_f/(2\pi) = 140$ kHz, $T = 5$ mK, $\Gamma = 1.5 \times 10^{-20}$ kg s^{-1} and ions mass is $m = 172$ a.m.u., which corresponds to Yb^+ ions. The above parameters were chosen since they approximate well the physically realistic Yb^+ traps (apart from the fact that the chain in physical experiments would normally have

open boundary conditions). Figure 3.4 shows the results of the simulations. Both graphs have approximately linear form with similar slopes. The two lines that have slopes of 1/3 and are drawn to check how well the data matches the theoretical prediction. As we can see there is a good agreement between the computer experiment and the theory. To be more quantitative, the linear regression analysis of the results of simulations with 31 ions gives a line of slope 0.3267 with regression coefficient of 0.9988. The linear regression analysis of the results of simulations with 91 ions gives slope of 0.3417 with regression coefficient of 0.9957. Both results give a scaling within 2.5 % of the theoretically predicted value.

We believe that figure 3.4 provides a strong evidence for the existence of mean field KZ scaling with an exponent of 1/3. One should note that these simulations have a significant difference to the previous numerical tests of KZ theory. Here, we simulate the microscopic equations of motion and extract numerically the KZ scaling exponents. The theoretical prediction is made using an analytic mapping to the field theory followed by a transformation that eliminates τ_Q from the field theoretic equations of motion. These approaches are very different but give the same scaling of 1/3. On the other hand in many works (e.g. [76, 77]), both the theoretical analysis and the numerical analysis is carried out on the same field theoretic equations of motion.

3.6 Chapter conclusions

In this chapter, we have presented an alternative method of deriving the scaling of the average number of topological defects formed in non-adiabatic phase transition as a function of quench rate. Whereas KZ theory relies on the knowledge of the equilibrium critical exponents of the phase transition and an intuitive physical argument, the presented method does not use equilibrium critical exponents and is mathematically rigorous. We use this method to derive the defect scaling law for a field obeying model A equations of motion and find it in agreement with existing predictions that are based on KZ theory. To demonstrate the general applicability of our approach we also derive the defects scaling for the field theory obeying model B equations of motion. We also show that using our method it is possible to naturally generalize the scaling laws to finite size systems. Finally, we apply the theory to linear to zigzag phase transition and obtain the scaling exponent of 1/3 for the underdamped dynamics. This prediction is confirmed using molecular dynamics simulations.

Chapter 4

Experimental generation of kinks

This chapter focuses on experimental measurement of KZ scaling using structural linear to zigzag transition in the trapped ion system. The experiments were done in Physikalisch-Technische Bundesanstalt (PTB, Germany) using Yb^+ ions [108] and in the University of Mainz (Germany) using Ca^+ ions [129]. The experimental results agree very well with the results of molecular dynamics simulations and quantify precisely the defects scaling in small inhomogeneous crystals. More data will be needed to extrapolate these finite size scaling measurements to the thermodynamic limit.

4.1 General experimental considerations

Ideally for the measurement of the KZ scaling we should impose periodic boundary conditions (PBC) onto the ion crystal. We have seen in the previous chapter that with PBC the KZ scaling in a small system consisting of just 31 ions was identical to the scaling expected in the thermodynamic limit. In principle, periodic boundary conditions could be realized using ion storage rings [131, 13] or octupole traps. To the best of our knowledge, at the moment there are no groups working with ion crystals in storage rings. Laser cooling and structural organization in octupole traps has been observed only recently [66] and is currently under investigation [86]. For this reason, we have to resort to studying KZ mechanism in inhomogeneous crystals produced in linear Paul traps. The inhomogeneity of the phase transition will affect the measured scaling. To extrapolate the measurements to the homogeneous thermodynamic limit one would have to vary the size of the system as described in Chapter 3, but in this thesis we will only measure finite size inhomogeneous scaling leaving this extrapolation for future work.

From a practical point of view creating kinks via a structural phase transition in small inhomogeneous chains poses a problem of kink losses at the boundaries of the chain. In order to minimize kink losses one either has to dissipate energy quickly via laser cooling, use longer chains or find a parameter regime where kinks are attracted

to the centre of the chain rather then the edges of the chain. The rate of dissipation is limited by the available laser power. The number of trapped ions in a crystal is often limited by the fact that to trap many ions in a linear chain necessitates the use of low axial secular frequencies at which it is difficult to maintain low ion temperatures. The trap in PTB can easily hold 30 Yb^+ ions but longer chains become increasingly difficult to obtain. The trap in Mainz could easily hold 16 Ca^+ ions and with difficulty up to 22 Ca^+ ions. On the other hand the numerical simulations in the theoretical proposal paper [37] were done for 50 Ca^+ ions. Thus it is important to determine whether it is at all possible to measure defect scaling in chains of as little as 16 ions or will the kink losses be too great. Using molecular dynamics (MD) simulations we have observed that the two dimensional kinks used in the original proposal are always lost in chains of 16 ions. To stabilize the kinks one has use a small radial asymmetry of the trap ($\omega_x/\omega_y \lesssim 1.1$), such that the kink can transform into a quasi 3-dimensional structure. The quasi 3-dimensional kinks are lowest in energy when they are in the centre of the chain [89] and thus they move to the centre where they stabilize. For a chain of 30 ions used in PTB experiments, the MD simulations indicate that it is possible to obtain two dimensional Z_2 kinks (cf Chapter 3) and use them to measure defect scaling with the quench rate. However, if the quench is performed sufficiently deeply then as was first noted in [81] these kinks are transformed into "extended" kink structures where one row of the zigzag has an excess of one ion. Similarly to the quasi 3-dimensional kinks, these extended kinks are attracted to the centre of the chain. Kinks can be regarded as collective particles moving in an effective potential known as the Peierls-Nabarro potential. The technique for calculating the PN potential and hence predicting the stable locations of the kinks will be presented in Chapter 5.

4.2 Molecular dynamics simulations

Molecular dynamic simulations are important both in the design stage of the experiments and for the interpretation of the experimental results. During the experimental design MD simulations help to choose the optimal experimental parameters. For the analysis of the results the MD simulations provide information about the dynamics of the system during the quench - due to the long camera exposure time the experimental results only provide kink statistics in the end of the dynamical evolution.

We have tried to keep the simulation model as simple as possible whilst capturing the essential features of the dynamics. In particular, we ignore trap micromotion, the

non-linear nature of the laser cooling force and we approximate the time dependence of the trap frequencies. We take the potential energy of N ions to be given by

$$\begin{aligned} V(t) &= V_h(t) + V_c, \\ V_h &= \sum_{j=1}^{N} \frac{1}{2} m \left(\omega_x^2(t) x_j^2 + \omega_y^2(t) y_j^2 + \omega_z^2(t) z_j^2 \right) \\ V_c &= \frac{Q^2}{2} \sum_{i \neq k}^{N} \sum_{j=1}^{N} \frac{1}{\sqrt{(x_i - x_j)^2 + (y_i - y_j)^2 + (z_i - z_j)^2}} \end{aligned}$$

where the secular frequencies ω_x, ω_y and ω_z have a possible time dependence that induces the structural transition of the ion chain from a linear to zigzag configuration. The dynamics of the system is modeled by the Langevin equation. The equations of motion for the jth ions are given by

$$\frac{d^2 x_j}{dt^2} + \omega_x^2(t) x_j + \eta \frac{dx_j}{dt} + \frac{\partial}{\partial x_j} V_c = \xi_{xj}(t) \tag{4.1}$$

$$\langle \xi_{xj}(t) \rangle = 0 \tag{4.2}$$

$$\langle \xi_{\alpha j}(t) \xi_{\beta k}(t') \rangle = 2\eta k_{\mathrm{B}} T \delta_{\alpha\beta} \delta_{jk} \delta(t - t'), \tag{4.3}$$

where $\alpha, \beta = x, y$ or z. Equations for the y an z degrees of freedom are of the same form as equations (4.1)-(4.3). By the fluctuation dissipation theorem the effect of the frictional force $F_\eta = -\eta \dot{x}$ and the stochastic force $\xi_j(t)$ is to thermalize the ions at a temperature T.

4.2.1 Validity of modelling approximations

The simulation model outlined above contains several approximations and free parameters. The first approximation is the ponderomotive or pseudopotential approximation, which approximates the time varying potential of the Paul trap by a time independent harmonic confining potential. Secondly, the model uses the Langevin dynamics approximation, which simplifies the description of atom-laser interaction. Finally, there are two parameters in the model, whose true experimental values are only approximately

known. These are the values of the friction coefficient and the temperature.

It is important to make sure that the KZ scaling law is not sensitive to the free parameters and the modelling assumptions at least for some range of parameters. If a small change in parameters affects the measured scaling then it is not possible to claim that a universal scaling law has been measured. Moreover, to have a meaningful comparison of simulation results and experimental data one has to make sure that the choice of the parameters and the modelling simplifications do not significantly influence the simulation results. We now individually consider the effect of each modelling assumption.

Pseudopotential approximation and micromotion

The use of pseudopotential theory (PPT) significantly reduces the computational difficulty of the simulations. The reason for this is that the the integration time step in the PPT simulations can be much greater than the integration time step in the time dependent trap model. In this section we briefly review linear Paul trapping theory and PPT. Then we discuss the limitations of PPT and argue why it is nevertheless appropriate for modelling defect creation in linear to zigzag phase transition.

The equations of motion of a jth ion in a Paul trap are given by

$$\frac{d^2x_j}{d\xi^2} = -\left(a - 2q\cos\left(2\xi\right)\right)x_j - \frac{e^2}{4\pi\epsilon_0}\frac{d}{dx_j}\sum_{j<k}\frac{1}{|\mathbf{r}_j - \mathbf{r}_k|} \tag{4.4}$$

$$\frac{d^2z_j}{d\xi^2} = -\left(\frac{2\omega_z}{\Omega}\right)^2 z_j - \frac{e^2}{4\pi\epsilon_0}\frac{d}{dx_j}\sum_{j<k}\frac{1}{|\mathbf{r}_j - \mathbf{r}_k|}, \tag{4.5}$$

where $a = 4eU/m\Omega^2 r_0^2$, $q = 2eV/m\Omega^2 r_0^2$, U and V are static and dynamic voltage magnitudes on the electrodes, Ω is rf driving frequency on the trapping electrode, r_0 is the distance between the centre of the trap and the electrodes, $\xi \equiv t\Omega/2$ and $\mathbf{r}_j = (x_j, z_j)$ denotes the coordinate of the jth ion. Here for simplicity we consider the motion of the ion in the xz-plane, ignoring the motion in the radial y-direction. If the cloud of ions is very dilute then the Coulomb interaction term in equations (4.4) and (4.5) can be neglected since the ions are unlikely to be close enough to each other to experience significant mutual repulsion. In this case, the equations of motions for a transverse coordinates of each ion are simply Mathieu equations. For small Mathieu parameters $|a| \ll 1$ and $|q| \ll 1$ the system is stable and the cloud will

remain indefinitely confined to a finite region of space. In this non-interacting limit, the ion coordinates in the transverse direction obey

$$x_j(t) = x_0 \cos\left(\omega_x t + \phi_x\right)\left(1 - \frac{q}{2}\cos\left(\Omega t\right)\right) + O\left(\frac{q^2}{4}\right), \tag{4.6}$$

where $\omega_x = \frac{1}{2}\Omega\sqrt{\frac{q^2}{2} + a}$ is the secular transverse frequency. In equation (4.6) the term $x_0\cos(\omega_x t + \phi_x)$ is the secular motion of the ion and the term $\frac{q}{2}\cos(\Omega t)$ describes the small amplitude rapid modulation of the secular motion, which is known as the micromotion.

At low temperatures the ions have less kinetic energy and the density of the clouds reduces. Consequently, the ions start to interact and eventually crystallize. The ion crystal is not a static structure but is a periodic solution with ions oscillating at the rf frequency Ω, about a well-defined average locations. The ion coordinates in the transverse direction obey

$$x_j(t) = \bar{x}_j\left(1 - \frac{q}{2}\cos(\Omega t)\right) + O\left(\frac{q^2}{4}\right). \tag{4.7}$$

The pseudopotential (PPT) or ponderomotive approximation replaces the time-dependent trapping potential in the transverse direction with the harmonic potential at secular frequency ω_x. This approximation accurately reproduces the secular motion of non-interacting ions but looses the micromotion and can lead to inaccuracies in the dynamics of interacting particles. The full time dependent theory of trapped interacting particles and the PPT can potentially disagree on 1) the equilibrium positions of ions in the crystal and 2) the normal modes of the crystal [80]. Both of these points are relevant for the KZ experiments, since the theory of the linear to zigzag structural phase transition and hence the KZ critical exponents were derived using PPT.

The equilibrium positions of the ions in a crystal are found in PPT by initializing the ions approximately near their expected equilibrium locations and solving numerically the overdamped equations of motion. The ions move along the energy gradient until they reach a configuration that minimizes the potential energy. In order to obtain the periodic crystal solution in the time dependent trap, one solves the equations of motion with friction and then slowly the friction is turned off giving numerically the oscillating solution. It was verified in many works that the linear crystal with its axis of symmetry along the z-direction has essentially the same structure in PPT and full time dependent trap (see, for example, [89] and [70]). In [89] it was shown that the structures of zigzag

chains of 20-60 trapped Mg^+ ions (possibly containing kinks) are essentially identical with and without micromotion. Similarly, the agreement has been found between the equilibrium positions found using PPT and time dependent trap calculations for zigzag crystals composed of 6 to 17 trapped Ca^+ ions. These results encourage the use of the PPT for modelling the linear to zigzag phase transition but do not fully justify its use, since it is also necessary to determine the effect of micromotion on the normal modes of the crystal. One should note that it is not immediately obvious that PPT would accurately predict the equilibrium positions, and in fact counter examples have been found - crystals whose shape cannot be obtain using the PPT and, which, for this reason, have been named "peculiar" crystals [80].

In order to fully justify the use of the PPT as a starting point for the derivation of the Ginzburg-Landau theory of the linear to zigzag phase transition and hence also KZ scaling, it must also be shown that the transverse modes of the crystal and their frequencies are identical within the PPT and the full time dependent theory. In [80] it is shown analytically that if the crystal is in linear chain configuration and lies along the axis of symmetry (the z-axis) then the PPT transverse modes and their frequencies are indeed identical to the full time dependent solutions. A good agreement has also been found between the location of the critical point in the PPT calculations and full time dependent calculations [70]. On the other hand, in the zigzag configuration the true modes and their frequencies may significantly deviate from the PPT calculations, as was demonstrated in [70] using Floquent-Lyapunov theory calculations [79] and experimental measurements. The Ginzburg-Landau theory is only applicable in the vicinity of the linear to zigzag phase transition and thus the partial failure of the PPT in describing the crystal dynamics deep within the zigzag regime has no bearing on the critical properties of the phase transition and hence on the Kibble-Zurek mechanism.

The combined evidence provided by the works [80], [70] and [89] suggest that indeed the PPT is a justified approximation in describing the dynamics in the vicinity of linear to zigzag phase transition, since the crystal structure, the mode spectrum and the location of the critical point are shown to be accurately described by the PPT. One may, however, still suspect that the micromotion oscillations directly influence the defect creation mechanism or the stability of the resulting defects. This would be surprising since micromotion is a driven synchronous motion, which takes place on the timescale which is at least an order of magnitude faster than quench rate. Nevertheless, in order to make sure that the micromotion has no effect on statistics of defect formation, we have carried out simulations to test KZ mechanism using PPT and the full time

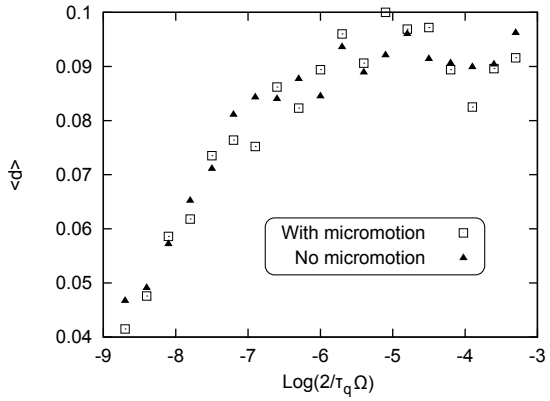

Figure 4.1: Average density of defects $\langle d \rangle$ vs the logarithm of quench rate $\log(1/\tau_Q)$. The data was averaged over 178 runs. The simulations were done with and without micromotion.

dependent equations of motion. The simulation were done for crystals of 40 Ca^+ ions. Trap parameters were taken to be $U = 0$, $\Omega/2\pi = 12$ MHz and $\omega_z/2\pi = 55$ kHz. The Mathieu parameters were $a = 0$ and q was varied linearly from $q = 0.13$ to 0.05. These values of q correspond to voltages V of the order of 100 V. In the pseudopotential approximation this corresponds to quench from the secular frequency $\omega_x/2\pi = 551$ kHz to 212 kHz. The friction coefficient was taken to be the optimal for the laser cooling $4S_{1/2} - 4P_{1/2}$ transition. The results of these simulations are shown in figure 4.1. The results do not indicate any significant statistical difference between simulations with and without micromotion. These simulations provide further empirical evidence for the validity of PPT for modelling dynamic linear to zigzag phase transition and defect formation.

Langevin dynamics

The simulation model utilizes stochastic Langevin equation for emulating the interaction of the ions with a heat bath. Particles undergoing Langevin dynamics will execute a random walk around their equilibrium positions; the mean squared displacement of the walk and the mean squared velocity are related to the temperature and the friction coefficient via the fluctuation dissipation theorem. Previous numerical work on KZ mechanism in linear to zigzag phase transition have also used Langevin thermostat model [30, 37]. What is the justification for this modelling approach and when does it fail to describe accurately the dynamics of ions undergoing Doppler cooling?

During Doppler cooling ions in the electronic ground state absorb photons from the

laser beam with red detuning and the excited ions emit photons in random directions. The rate of photon absorption is given by a Lorentzian function in the velocity of the ions

$$R_s = \frac{\Gamma}{2} \frac{\Omega^2/2}{(\omega - \omega_0 + \mathbf{k} \cdot \mathbf{v})^2 + \Omega^2/2 + \Gamma^2/4}, \tag{4.8}$$

where Γ is the rate of spontaneous emission for the electronic transition, ω is the frequency of the laser, ω_0 is the frequency of the transition, Ω is the Rabi frequency, $\mathbf{k} = (k_x, k_y, k_z)$ is the wavevector of the laser beam and $\mathbf{v} = (v_x, v_y, v_z)$ is the velocity of the ion. The laser beam is typically oriented at 45° to the trap axis so that an ion can experience radiative pressure and ultimately cooling in all three directions. When an ion moves towards the laser beam it is more likely to absorb a photon since due to the Doppler effect the ion comes closer to resonance with the beam. Conversely, when the ion moves away from an ion beam it is less likely to absorb a photon. An ion confined in a trap undergoes oscillatory motion, reversing its direction of motion in every period of the oscillation, thus the ion will experience a net slowing down force from the laser. If velocity $\mathbf{v}$ is small, then by Taylor expanding equation (4.8), it can be shown that the rate of photon absorption in one oscillation cycle is approximately linearly proportional to $\mathbf{v}$ and thus the frictional force is inversely proportional to $\mathbf{v}$ as in the Langevin dynamics. The stochastic force on the ion arises due to the spontaneous emission of photons in a random direction. Thus when the velocity of ions is small the ions undergo approximately Langevin dynamics.

Simulation of laser cooling using the Lorentzian distribution (4.8) for describing ion-laser interaction have shown that the cloud of ions can crystallize and reach thermodynamic equilibrium [24]. In the state of thermodynamic equilibrium and at low temperatures, the dynamics is essentially Langevin. Since in the KZ experiments the ion crystal is close to the thermodynamic equilibrium and Doppler cooling limit, we are justified to use the Langevin dynamics model. Note that at high quench rates the system is driven far from the thermodynamic equilibrium and in this regime the Langevin dynamics model is likely to fail. However, at high quench rate, KZ mechanism breaks down due to non-universal defect losses and thus this regime is of little interest to the investigations of KZ mechanism.

Friction coefficient

The dynamics of the trapped ions interacting with the cooling laser contains both the inertial and the friction forces. Recall from previous chapters or reference [30] that the time dependent Ginzburg-Landau model for the linear to zigzag phase transition in the homogeneous chain is given by

$$\partial_{tt}\phi - h^2\partial_{xx}\phi + \eta\partial_t\phi + \delta(t)\phi + 2\mathcal{A}\phi^3 = \theta(x,t), \tag{4.9}$$

where $h = \omega_0 a\sqrt{\log 2}$, $\mathcal{A} = 93\zeta(5)\omega_0^2/(32a^2)$, $\omega_0 = \sqrt{Q^2/ma^2}$, a is the spacing between the ions, $\delta(t)$ is the quench function, η is the friction coefficient, $\theta(x,t)$ is the stochastic white noise and $\phi(x = aj) = (-1)^j y_j$ is the order parameter with y_j being the transverse displacement of the jth ion. $\theta(x,t)$ obeys the following statistical relations

$$\langle\theta(x,t)\rangle = 0 \tag{4.10}$$

$$\langle\theta(x,t)\theta(x,t')\rangle = 2\eta k_B T\delta(t-t')\delta(x-x'). \tag{4.11}$$

Since equation (4.9) contains both the second and the first time derivatives of the order parameter there are two different time scales associated with equation (4.9). Thus, there are two dynamic universal exponents associated with equation (4.9): $z = 1$ corresponding to the overdamped dynamics and $z = 2$ corresponding to the underdamped dynamics. KZ scaling laws can be derived by neglecting either the friction or inertial term. Neglecting the inertial term results in the overdamped KZ scaling and neglecting the friction term results in the underdamped KZ scaling. The formation of defects and KZ mechanism in a system with the dynamics given by equation (4.9) was analyzed in [77]. In [77] it was shown using qualitative KZ arguments that in the overdamped limit the domain length scale is $\hat{\xi} \propto (\tau_Q/\eta)^{1/4}$ and in the underdamped limit $\hat{\xi} \propto \tau_Q^{1/3}$. There are two notable features of the results presented in [77]: 1) that the KZ scaling is different in the overdamped and underdamped regimes and 2) that in the overdamped regime the number of domains depends on the friction coefficient whereas in the underdamped regime it is independent of the friction coefficient. These two predictions were corroborated in [77] using numerical simulations. The numerical simulations involved measuring the KZ scaling for a range of different values of η. It was observed that at low η the number of defects produced at a given quench rate looses its sensitivity on the friction coefficient η. The fact, that when the friction is small the density of defects

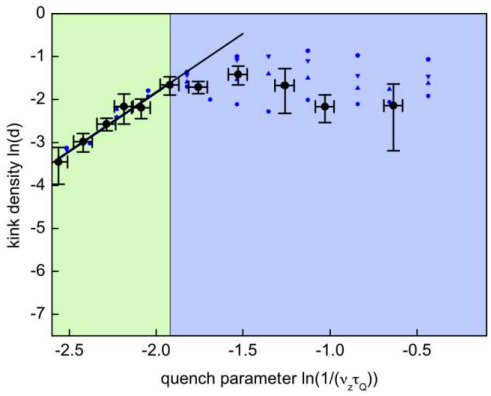

Figure 4.2: Defect formation vs. quench rate. The blue markers correspond to $\eta = 2.5 \times 10^{-21}$ kg s^{-1} (circles), $\eta = 3.0 \times 10^{-21}$ kg s^{-1} (triangles), $\eta = 4.0 \times 10^{-21}$ kg s^{-1} (inverted triangles) and $\eta = 6.0 \times 10^{-21}$ kg s^{-1} (pentagons). The black markers correspond to the experimental results. The black line gives the measured scaling and was fitted only in the green region which is free of losses.

is independent of η, is very convenient for the KZ experiments in ion traps, since in the ion trap system it is only known that the frictional force is small compared to the inertial force and the precise value of η is unknown. This implies that η is not a fitting parameter when it comes to comparing the results of the simulations and experiments.

To verify that the simulations in the underdamped regime are not sensitive to the friction coefficient η we have performed simulations with η ranging from 2.5×10^{-21} kg s^{-1} to 6.0×10^{-21} kg s^{-1}. The simulations were done for crystals of 30 Yb^+ ions with a linear quench in radial secular frequency with the following parameters, $\omega_x^{(i)}/(2\pi) = 500$ kHz, $\omega_x^{(f)}/(2\pi) = 140$ kHz, $\omega_y^{(i)}/(2\pi) = 517$ kHz, $\omega_y^{(f)}/(2\pi) = 206$ kHz and $\omega_z/(2\pi) = 24.6$ kHz. The temperature in the simulations was set to $T = 5$ mK. The results of the simulations are shown in figure 4.2. The figure also contains experimental data taken in the PTB group; the details of the experiment will be described in the later parts of the chapter. The simulation results for the four different friction coefficients and the experimental results closely match for quench rates $\ln(1/(\nu_z \tau_Q)) \lesssim -1.9$. At faster quench rates there is a plateau in the KZ scaling and a high sensitivity on the friction coefficient. This behaviour was also observed in previous work, for example, in [76, 77]. The reason for this is that when the quench rate is fast the system gains a large amount of kinetic energy, which does not have time to dissipate. This kinetic energy results in high mobility of kinks and consequently large kink losses due to annihilation of kinks and losses at the boundaries of the chain. Kink motion and annihilation processes are not universal and result in the deviations from the KZ scaling law. We

may expect poor agreement between the simulation results and the experimental results at high quench rates due to the sensitivity of the results to the friction coefficient in this regime. However, in the regime of slow quenches, which is the important regime for the observation of KZ mechanism, there should be a good agreement between the results of the simulations and experiments since there the results are independent of the friction coefficient. This is corroborated by the simulations results shown in figure 4.2.

Temperature

The magnitude of the stochastic force in the Langevin dynamics simulations is related by the fluctuation dissipation to the friction coefficient η and the temperature T. The temperature of the trapped ion crystal is only approximately known and therefore it is important to make sure that the KZ scaling is not sensitive to temperature.

The primary role of the stochastic force in the KZ simulations is to randomize the system and to simulate the interaction of the system with a heat bath. The correlations in the system are determined by the internal structure of the system and not on the magnitude of the temperature. For this reason, it is plausible that the "freeze-out" correlation length, that dictates the size of the domains, should not depend on the temperature magnitude. Of course, the stochastic force should be a white noise, as coloured noise would affect the correlations in the system and potentially the KZ scaling. Numerous simulations at different temperatures confirm the KZ scaling thereby providing empirical evidence for the lack of sensitivity of KZ scaling on the temperature. However, it is also observed that at sufficiently high temperatures the scaling can be disrupted. One reason for this is that the thermal fluctuations may be large enough to flip a domain thereby destroying the defects. Thermal noise can also induce diffusion of defects, which can results in their mutual annihilation. The process of defect annihilation is not universal since KZ mechanism only describes the creation of defects. Motion of the defects (domain walls) is less energetically demanding than a sudden flip of the whole domain and for this reason it is likely to be the dominant mechanism for the loss of defects. In order for a defect to move by one lattice site along the chain it needs to overcome an energetic barrier known as the Peierls-Nabarro (PN) barrier E_{PN} (see Chapter 5 for detail discussion of the PN barrier and its calculations). If the thermal kinetic energy has a similar value to E_{PN} or is greater than E_{PN}, then a high defect diffusion rate is expected.

As long as the temperature is low enough to strongly suppress kink diffusion the

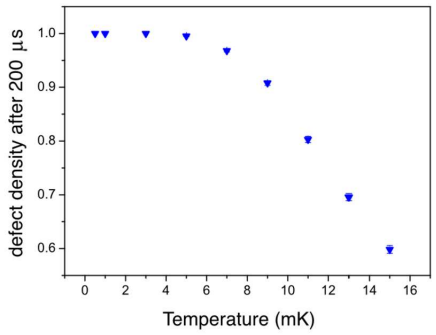

Figure 4.3: Probability that a reared extended kink remains in the crystal after 200 μs with increasing temperature.

effect of temperature on the final density of defects should be negligible. In the PTB experiments, Yb^+ ions are laser cooled on the $^2S_{1/2} -^2 P_{1/2}$ transition and for realistic trap parameters the estimate of the Doppler cooling temperature is 0.5 mK. Typically in such ion trap experiments the temperature may be an order of magnitude higher than the Doppler cooling limit. In order to test whether the thermal fluctuations can induce kink motion and cause loss of kinks from the trap, we conducted the following simulations. A chain was initialized in an extended kink configuration (see next section for the definition of extended kink). This configuration was chosen to closely match the parameters of the trap in the end of quench that was ultimately used in the PTB experiment. The system was then evolved for 200 μs using Langevin-Impulse method at different temperatures and the temperatures ranged from 1 mK to 15 mK. In the end of each simulation the number of kinks present in the chain was evaluated. The simulations were repeated a number of times in order to measure the probability of kink being lost from the chain in 200 μs. The plot of kink loss probability versus temperature of the crystal is shown in figure 4.3. We can see that below $\sim$ 7 mK kink losses are strongly suppressed. For temperatures $T \gtrsim 7$ mK the kink losses are considerable. Extended kink is stable in the centre of the chain and its loss is caused by the thermal fluctuations that excite the motion of the kink, enabling it to reach the edge of the crystal. The potential energy that the simulated kink must overcome in order to reach the edge of the crystal is around 20 mK/k_B as will be shown in calculations in Chapter 5. The results shown in figure 4.3 are qualitatively consistent with this calculation.

The results shown in figure 4.3 provide a level of confidence that the scaling measured in PTB experiment would not be influenced by post quench losses of kinks induced by the thermal fluctuations. The post quench time is given by the camera exposure times, which in the PTB experiments ranged from 50 to 200 ms. Nevertheless, since the

temperature in the crystal is likely to be smaller than 7 mK the probability of the loss of kink due to the action of the stochastic thermal forces is small. The kinks are more likely to escape from the crystal not because of thermal effects but rather because of the kinetic energy that they gain during the quench and the rare collision events with the molecules of the residual gas in the vacuum chamber.

4.3 PTB experiments

The trap used in PTB is a microfabricated trap designed for metrological application. The apparatus is dedicated to the trapping of Yb^+ ions. The details of the operation and construction of the trap can be found in [109]. Using preliminary MD simulations we have identified

- that ~ 30 ions is a sufficient number of ions for generation of kinks in the trap with an experimentally realistic secular frequencies,
- the size of the asymmetry factor ω_x/ω_y that confines the kink structure to two dimensions is ~ 1.3,
- the range of quench times for which a KZ scaling can be observed is from about 40 μs to 400 μs.

Kinks were generated using the radial quench as was suggested in the theoretical proposal [37].

4.3.1 Numerical simulations

Quench is achieved experimentally by the modulation of the radio frequency (rf) driving signal. The signal itself can be precisely measured and the secular frequencies can be calculated as a function of time. In general, the quench of the secular frequencies is not a linear function in time. Nevertheless to simplify the modelling we will take the quench function to vary linearly between the initial and final values of the secular frequencies

$$\omega_x(t) = \begin{cases} \omega_x^{(i)} & \text{for } t < 0 \\ -\frac{t}{\tau_Q}\left(\omega_x^{(i)} - \omega_x^{(f)}\right) + \omega_x^{(i)} & \text{for } 0 \le t \le \tau_Q \\ \omega_x^{(f)} & \text{for } t > \tau_Q, \end{cases} \tag{4.12}$$

where $\omega_x^{(i)}$ is the initial secular frequency, $\omega_x^{(f)}$ is the final secular frequency and τ_Q is the time of the quench. The quench in the radial y direction has the same form as given by equation (4.12) only with different values of $\omega_y^{(i)}$ and $\omega_y^{(f)}$. We assume that it is the rate of change of the secular frequency in the vicinity of the critical point that is important for the production of defects. The experimental quench function is approximately linear near the critical point of the linear to zigzag phase transition. For this reason in the simulations we use a linear quench function with the slope corresponding to the slope of the experimental quench near the critical point.

The optimal parameters were found to be $\omega_x^{(i)}/(2\pi) = 500$ kHz, $\omega_x^{(f)}/(2\pi) = 140$ kHz, $\omega_y^{(i)}/(2\pi) = 517$ kHz, $\omega_y^{(f)}/(2\pi) = 206$ kHz, $\omega_z^{(i)}/(2\pi) = 24.6$ kHz and $\omega_z^{(f)}/(2\pi) = 24.6$ kHz. Setting the trap asymmetry $\omega_x/\omega_y \sim 1.3$ squeezes the configuration to the zx plane. The temperature of the crystal in the trap is not easy to measure and was not possible at the time of the experiment. The temperature can, however, be estimated. Yb^+ ions are laser cooled on the ${}^2S_{1/2} - {}^2P_{1/2}$ transition at a wavelength of 370 nm. The Doppler cooling limit for this transition is 0.5 mK. The temperature of a the crystal of 30 ions is likely to be somewhat higher - in the simulation we use 5 mK.

For the laser cooling of the ions a single traveling wave leads to the following greatest possible coefficient of the optical cooling force [88]

$$\eta = \frac{2s}{(2+s)^2}\hbar k^2, \tag{4.13}$$

where s is the saturation of the cooling transition, k is the wave vector of the cooling laser. Equation (4.13) gives the friction coefficient when the laser detuning is $\Delta = -\Gamma/2$, where Γ is the linewidth of the transition. The transverse beam profile is focused down to horizontal and vertical waist sizes of 8.8 mm and 80 μm. For a laser power of 630 μW this results in an estimated experimental friction coefficient of $\eta = 4 \times 10^{-21}$ kg s^{-1}, along a single axis. In reality the friction coefficient is smaller and we performed simulations for a range of different η, applying the same friction coefficient in all three directions. We expect to find that as long as the system is underdamped and the inertial term dominates the dynamics there should be no influence of the friction coefficient on the scaling of defects. Friction coefficient can influence the observed number of defects at fast quench rates, since in the regime of slow rate of energy dissipation resulting kinks can have high kinetic energy and escape the chain at the boundaries.

Figure 4.4 shows snapshots of simulated dynamics illustrating the creation and trapping of a defect. As the radial confinement is weakened the linear chain undergoes

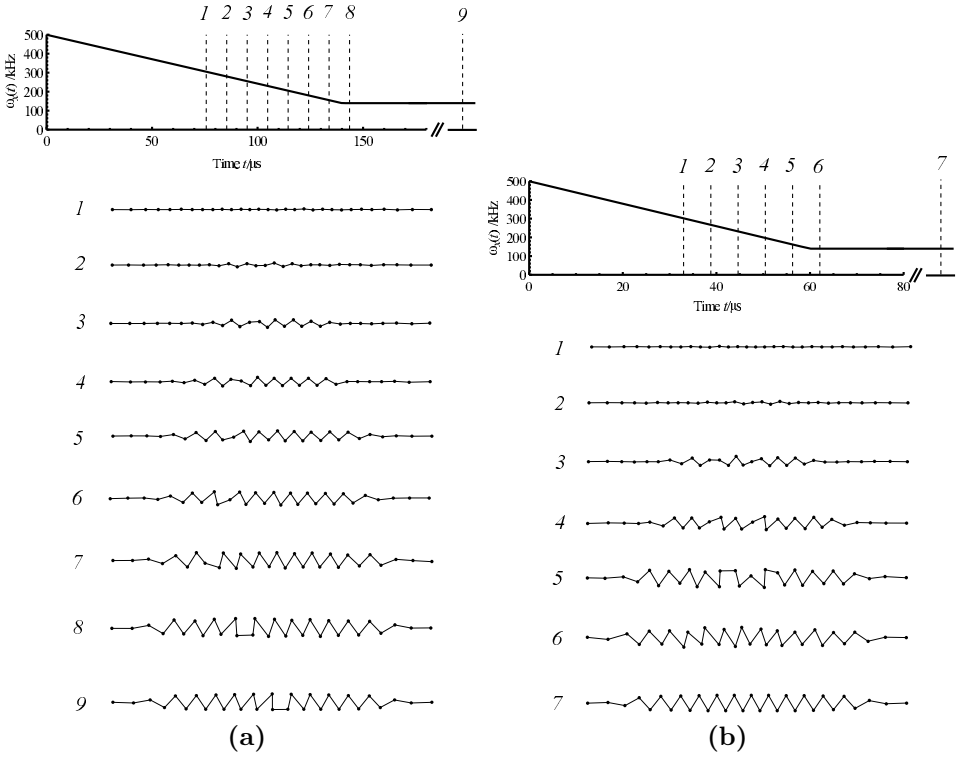

Figure 4.4: a) Creation of one kink and its stabilization via the transition into extended kink structure. The trap parameters were be $\omega_x^{(i)}/(2\pi) = 500$ kHz, $\omega_x^{(f)}/(2\pi) = 140$ kHz, $\omega_y^{(i)}/(2\pi) = 517$ kHz, $\omega_y^{(f)}/(2\pi) = 206$ kHz, $\omega_z^{(i)}/(2\pi) = 24.6$ kHz, $\omega_z^{(f)}/(2\pi) = 24.6$ kHz and $\tau_Q = 140$ μs. b) Formation of two defects during quench and their ultimate annihilation. The trap parameters are the same as in a) except $\tau_Q = 60$ μs.

a structural phase transition. The phase transition is inhomogeneous - first it occurs in the centre of the chain and the zigzag phase continuously grows as the quench progresses. Since the quench is rapid there is a possibility of kink creation; a nascent kink is visible in figure 4.4a2. This type of kink is similar to the soliton of the ϕ^4 model and was used in the previous chapter in the study of KZ mechanism for linear to zigzag transition with periodic boundary conditions. This type of kink propagates along the chain by the transverse movement of ions. Since the system gains the kinetic energy from the quench, the kink moves and its motion is typically directed towards the edges of the chain (figure 4.4a3-a7). If the kink continues its progress towards the edge of the zigzag region, it will be eventually lost from the chain. However, at some critical value of ω_x the kink undergoes a structural transition into an extended kink. The structure of this kink is such that the top or bottom row has an excess of ion. The motion of this type of kink is via the axial movement of ions. This type of kink is attracted to the centre of the chain as will be discussed in detail in Chapter 5. After a brief oscillation the kink settles in the centre. The kink stabilization mechanism via structural transition to the extended structure is useful since it increases the chance of a kink being observed in the experiment.

Figure 4.4b shows a simulation where two kinks are created. After the kinks are created they move towards the opposite edges and eventually transform into extended structures. The extended kinks then annihilate one another (figure 4.4b5-b6). In principle, it is possible to create chains with multiple extended kinks, but this would require the use of more ions, specifically engineered trapping potentials or addition of ions of different mass. In our set up the chains in the end of the evolution will always have either no kinks or one kink.

Figure 4.5 shows the results of simulations for the number of defects produced as a function of quench rates for several different values of friction coefficients. The number of defects can be calculated at all times during the quench. This provides the information about the kink losses that can come from the annihilation of defects or losses at the edges of the zigzag. In figure 4.5 the open markers indicate the domains counted shortly after the system underwent the structural transition. The filled markers indicate the number of domains after some time has elapsed after quench. One can see that for $\ln(1/\omega_x\tau_q) \gtrsim -2.1$ the number of created defects is significantly larger than the number of surviving defects. There are two reasons for this: firstly, at fast quench rates the system acquires more kinetic energy and the defects have a higher chance to escape the chain at the edges, and secondly at high quench rates there is a higher

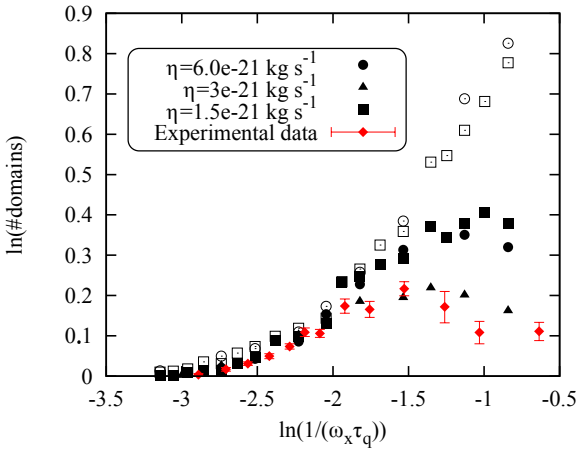

Figure 4.5: Scaling of the average number of domains in the zigzag phase as a function of quench rate in an inhomogeneous crystal of 30 ions. The trap parameters were $\omega_x^{(i)}/(2\pi) =$ 500 kHz, $\omega_x^{(f)}/(2\pi) = 140$ kHz, $\omega_y^{(i)}/(2\pi) = 517$ kHz, $\omega_y^{(f)}/(2\pi) = 206$ kHz, $\omega_z^{(i)}/(2\pi) =$ 24.6 kHz, $\omega_z^{(f)}/(2\pi) = 24.6$ kHz Open markers indicate the number of defects shortly after quench. Filled markers indicate the final number of defects. Red diamond markers are experimental results.

chance of creating a pair of defects that would annihilate one another. Note also that the structure of the observed plateau at high quench rates is sensitive to the friction coefficient. This is because the rate of energy dissipation influences the amount of kinetic energy in the system remaining after quench and hence the probability of kink loss. For $-2.4 \lesssim \ln(1/\omega_x\tau_q) \lesssim 2.1$ the number of created defects is very close to the number of surviving defects. For this quench range the probability of formation of two defects is very small and thus there are very few annihilation events. The quench is also slow and the amount of kinetic energy in the system in the end of the quench is small and hence few defects are lost at the edges. The dependence on the friction coefficient η is weak in this quench range. For low quench rate $\ln(1/\omega_x\tau_q) \lesssim -2.4$ the number of created defects is visibly larger than the number of surviving defects. The reason for this is that for very slow quenches the kinks can move faster than the phase transition front and thus can escape the chain before they have a chance to transform to extended structures.

4.3.2 Experimental results

The details of the experimental implementation can be found in [108] and Appendix A.

Figure 4.6 shows experimental images of odd and extended kinks obtained by a

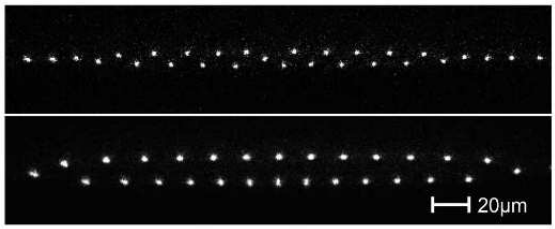

Figure 4.6: Pictures of experimentally realized kink configurations. Top: Odd kink, dominant for shallow quenches ($\nu_t/2\pi = 500$ kHz to 204 kHz). Bottom: Extended kink, dominant for deep quenches in radial frequency from $\nu_t/2\pi = 500$ kHz to 140 kHz. Exposure times are 50 ms and 200 ms, respectively. The Coulomb crystals consist of 29 ± 2 ions and the phase transition sets in at $\nu_t^{(c)}/2\pi \approx 275$ kHz. For the statistics measurements, we use the extended kink configuration to preserve and stabilize the created localized odd kinks. [The picture was taken from [108].]

non-adiabatic quench from linear configuration to zigzag configuration. These kink were obtained by performing a radial quench from $\omega_x/2\pi = 500$ kHz to 204 kHz in the case of odd kink and $\nu_t/2\pi = 500$ kHz to 140 kHz in the case of extended kinks. An ellipticity of 30% was induced to confine the ions to a plane i.e. $\omega_y = 1.3\omega_x$.

The experimental results are shown in figure 4.5 (red diamond markers). Each point is obtained by averaging around 2000 experimental images. There is a good agreement between the experimental results and the simulations. These data constitute an accurate quantification of the KZ scaling in a finite system. In order to extrapolate the scaling to the thermodynamic limit more experiments would be needed. In particular, as was explained in Chapter 3, one should make the same measurement for chains in traps at different values of axial confining frequency ω_z. However, this is beyond the scope of the present work.

4.4 Mainz experiments

The Mainz experiment differs from the PTB experiment in several aspects

- chains of 16 Ca^+ ions are used,
- linear to zigzag phase transition is induced via axial compression rather than the radial relaxation,
- quasi 3d-kinks are produced rather than extended kinks.

The outcomes of the Mainz experiment are similar to the outcomes of the PTB experiment: both experiments produce for the first time kinks via structural transition; the results of both experiments agree with molecular dynamics simulations and both experiments quantify finite size KZ scaling.

In the remaining part of the chapter we present the details of Mainz experiment, which is based on [129].

4.4.1 Numerical simulations

Numerical simulations were essential for the design of the experiment and the interpretation of the experimental results. The molecular dynamics simulation method was the same as for the PTB experiment, namely, the pondermotive approximation was used and the Langevin-Impulse integrator was used to evaluate the dynamics of the ions. The transition is induced by increasing the axial confining frequency. Recall that from the Ginzburg-Landau analysis (Chapter 2) the critical parameter for the linear to zigzag is

$$\delta = \omega_x^2 - \omega_c^2 \tag{4.14}$$

where ω_x is the radially confining frequency and ω_c is the critical frequency of the transition. According to [96, 95], for finite number of ions the critical transition frequency is given by

$$\omega_c \approx \frac{3N\omega_z}{4\sqrt{\log N}}. \tag{4.15}$$

where ω_z is the axially confining frequency. The system is at a critical point when $\delta = 0$ or in other words when $\omega_x = \omega_c$. Since $\omega_c \propto \omega_z$ it is possible to induce the phase transition by axial trapping frequency ω_z rather than the radial confining frequency ω_x. The axial trapping frequency is determined by the voltage amplitudes on the end cap electrodes of the rf Paul trap. It is possible to measure the axial frequency as a function of the applied endcap voltage (figure 4.7) and the endcap voltage can be measured accurately using an oscilloscope. Thus the functional form of the time dependence of the axial frequency is known to a high degree of accuracy. This quench function is used in the molecular dynamics simulations and the radial frequencies are kept at constant values. Care had to be taken to make sure that the endcap voltage variation (figure 4.7) is a smooth function. Sharp features in the quench function can excite breathing modes of the chain and even result in melting of the crystal. For example, a constant-linear-

constant quench function used in modelling the PTB experiments results in melting of the crystal. Figure 4.7 (bottom) shows the simulated axial trajectories of the ions during the quench with a smooth sigmoid function. We can see that during the phase transition the chain undergoes a smooth compression and the breathing mode is only excited at the late stages of the dynamics, when the chain is already in zigzag phase.

The radial aspect ratio used in the simulations and experiments was ω_x/ω_y between 1.03 and 1.07. This aspect ratio is much smaller than 1.3 - the aspect ratio used in the PTB experiment. The radial confinement is almost symmetric but the small asymmetry is enough to confine the zigzag configuration without kink to the zx-plane. The kinks in such a system assume a 3 dimensional structure - the ions in the kink region will move in y-direction to minimize the energy of the system. Such kink structures were studied in detail in [89], where they were spontaneously created in chains of Ca^+ ions by chance collisions of the zigzag chain with the background gas. In [89] the authors have shown that quasi 3-dimensional kink structures have the lowest energy when the kink is in the centre of the chain. So just as the extended kinks, quasi 3-d kinks have a global minimum in the Peierls-Nabarro potential which is located at the centre. In the Mainz experiment, quasi 3-d kinks are used in order to stabilize the kinks in the chain. Indeed, numerical simulations have indicated that restricting the 16 Ca^+ system to a single plane results in total loss of the kinks during the quench (for the given temperature and final values of secular frequencies).

4.4.2 Experimental results

The details of the experimental implementation can be found in [129] and Appendix A.

Figure 4.8 shows experimental photographs of the linear, zigzag and quasi 3-dimensional kink configurations. These kinks were obtained via axial quench as explained in the previous section. The numerical and experimental results for the scaling of the average number of kinks versus the quench rate are shown in figure 4.9. The constant offset visible at lower ramping rates stems from background gas collisions at a base pressure of 1×10^{-9} mbar. The scaling was measured at two trap anisotropies: at $\omega_x/\omega_y = 1.03$ and at $\omega_x/\omega_y = 1.05$. At higher anisotropy, more defects are lost but the scaling remains the same. These higher losses can be explained by the fact that kinks have a larger energy density at higher trap anistropies and hence are more likely to escape the crystal. There is a good agreement between the experimental results and the results of the simulation indicating that the molecular dynamics simulations accurately describe

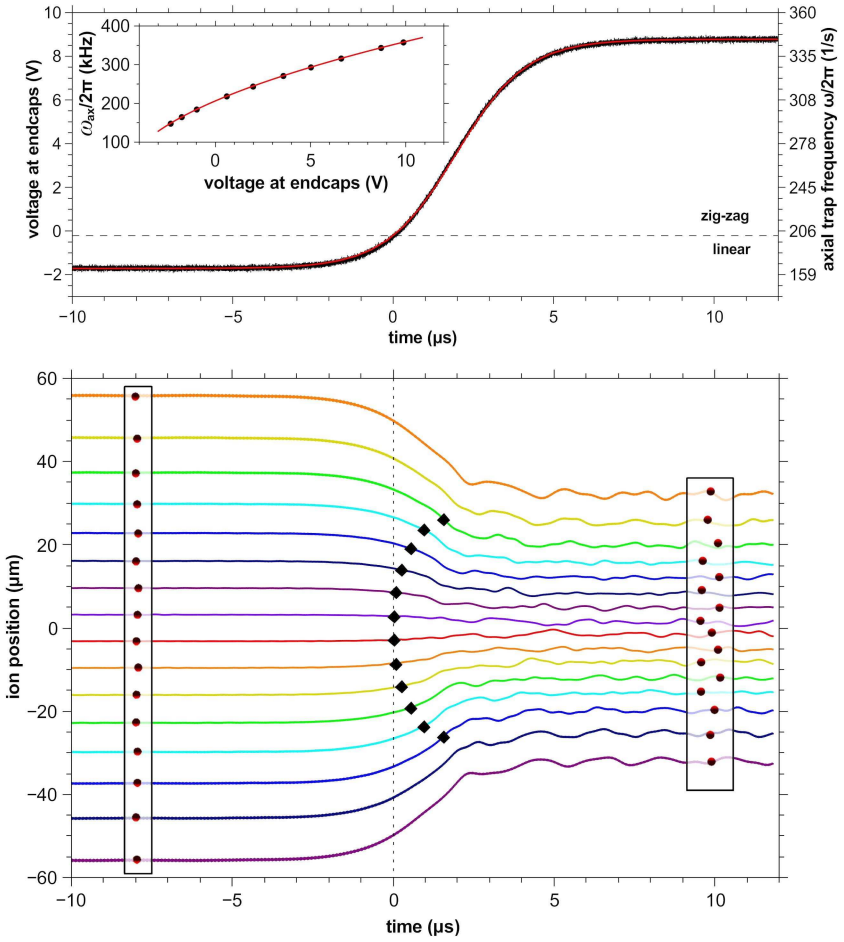

Figure 4.7: a) Measured voltage (left y-axis) applied to the end-caps (black line). The dashed line shows the separation between the two structural phases at an axial trap frequency of $\omega_{\mathrm{ax}}/(2\pi) = 201.7$ kHz and a radial trap frequency of $\omega_{\mathrm{rad}}/(2\pi) = 1394.1$ kHz. Inset: dependence of the trap frequency $\omega_{\mathrm{ax}}/(2\pi)$ on the applied end-cap voltage. (b) Axial positions of the 16 ions during the ramp as extracted from simulation results. Diamonds indicate the onset, if any, of the local phase transition for each ion, which are reached at different times because of the inhomogeneous charge density. The dashed line indicates the time when the middle ions reach the critical point. The corresponding crystal configuration is shown before and after the ramp. [The diagrams were take from [129].]

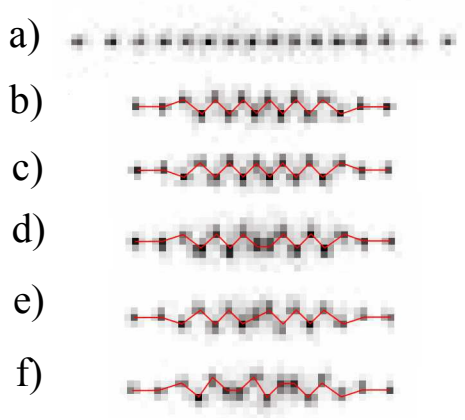

Figure 4.8: Fluorescence images of a 16 ion crystal. a) Linear ion crystal before ramping the axial potential; b) and c) zigzag configuration after the ramp; d) and e) single quasi-3d defects; and f) double defect configuration. The line clarifies the configuration of the crystals. The width of one pixel corresponds to 1.7 μm. [The picture was taken from [129].]

the system. The measured scaling is the finite size KZ scaling and an extrapolation to the thermodynamic limit requires more measurements.

4.5 Chapter conclusions

In this chapter we have presented two ion trap experiments [108, 129] that generate structural defects and investigate KZ mechanism. These experiments were the first to produce kinks in the zigzag chains via spontaneous symmetry breaking. For the successful generation of kinks in small Coulomb crystals, it was necessary to understand kink dynamics at realistic experimental parameters. This was done using extensive molecular dynamics simulations. The dependence of the average number of defects on the quench rate was quantified experimentally and in numerical simulations. The experiments provide an important step towards accurate verification of KZ theory. Nevertheless, in order to extrapolate the KZ scaling measured in small inhomogeneous crystals to thermodynamic limit more experiments are needed, in particular, one should also measure the scaling in crystals of various sizes.

After the experiments were carried out, a group in Simon Fraser University performed an experiment, which confirmed the findings of the PTB experiment [49].

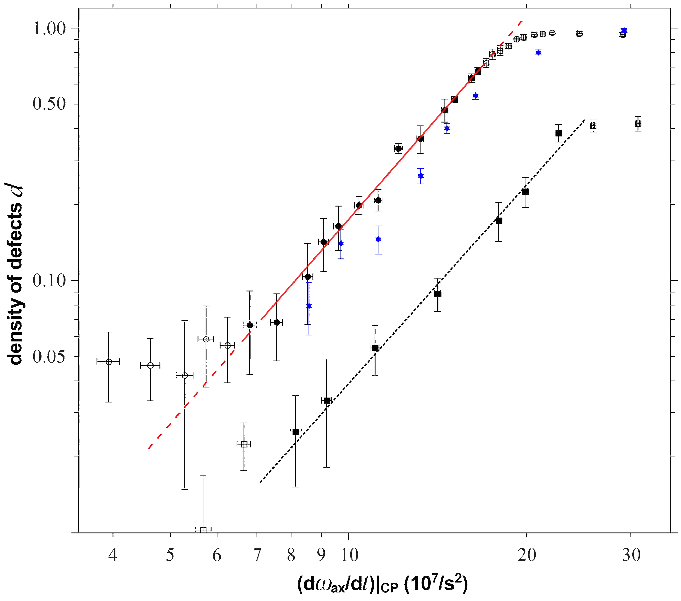

Figure 4.9: Double-logarithmic plot of the measured density of defects d versus the rate of change γ of the axial trap frequency at the critical point. The fitted function of the form $d \propto \gamma^d$ (red line) gives an exponent of $\beta = 2.68 \pm 0.06$. Square markers represent the rate of defects measured with a higher trap anisotropy of 1.05, showing a reduced number of defects but a similar fitted exponent of $\beta = 2.62 \pm 0.15$ (dotted line). Solid data points are used for the fits. The uncertainty in γ is deduced from the scatter of repeated recordings of voltage ramps, whereas the uncertainty in d is the s.d. of the measurements. The blue stars depict the result of MD simulations. [The graph was taken from [129].]

Chapter 5

Kinks as discrete solitons

Previous chapters were focused on non-equilibrium phase transitions and the Kibble-Zurek scenario. The stable topological defects are produced in phase transition because of the non-linear term in the GL free energy. In one dimensional ϕ^4 theory defects can be identified as soliton waves, which are localized packets produced by the interactions of dispersive and non-linear effects. Kinks in the zigzag chains are examples of discrete solitons. Discrete solitons occur in many other physical systems, for example, in solids, non-linear optics and polymer molecules [69]. Discrete solitons exhibit rich nonlinear dynamics and are extensively studied [20]. In this chapter we will focus on some dynamical features of kinks in the zigzag chain. In particular, we will present a method for calculating the Peierls-Nabarro (PN) potential - the potential in which the kink moves. The method will be used to calculate the PN potential for the kinks in the PTB experiment and thereby demonstrate how the stability of the kink is influenced by the radial confining frequency. We also show that the heavy molecular ions, which can spontaneously form by chemical reactions with the background gas, produce a dip in the PN potential and therefore can act as kink "traps". A method for moving kinks using heavy ions and applied electric field is suggested. Finally we sketch out a way the equations of motion can be derived for the kink using the collective variable formalism.

5.1 Solitons and discrete kinks

As was discussed in Chapter 2 when the transverse extent of the zigzag is small compared to the inter-ion spacing, the system can be described by the following Hamiltonian

$$H = \int \left[\frac{m}{2} \left(\partial_t \phi\right)^2 + \frac{\delta}{2}\phi^2 + \frac{h}{2} \left(\partial_x \phi\right)^2 + \frac{g}{4}\phi^4 \right] dx. \tag{5.1}$$

The equation of motion for the field is

$$m\partial_{tt}\phi - \delta\phi - h\partial_{xx}\phi + g\phi^3 = 0. \tag{5.2}$$

Changing units to $t' = t/\sqrt{m}$, $x' = x/\sqrt{h}$ and dropping primes for notational simplicity gives

$$\partial_{tt}\phi - \partial_{xx}\phi + \lambda(\phi^2 - \eta^2)\phi = 0, \tag{5.3}$$

where $\lambda = 1/g$ and $\eta = \sqrt{\delta/g}$. The solutions $\phi(x,t) = \eta$ and $\phi(x,t) = -\eta$ have vanishing energy density and are the trivial vacua solutions. There exist also solutions with non-vanishing energy density that satisfy $\phi(t,-\infty) = -\eta$ and $\phi(t,\infty) = \eta$. By continuity there must be a point x_0 such that $\phi(t,x_0) = 0$, and in vicinity of this point the energy density is not zero. Such solution is known as the Z_2 kink. It is possible to show that the Z_2 static kink solutions have the following form

$$\phi_K(x) = \pm\eta \tanh\left(\sqrt{\frac{\lambda}{2}}\eta x\right). \tag{5.4}$$

One can Lorentz boost this solution to get a solution describing the kink propagating at a constant velocity

$$\phi_K(t,x) = \pm\eta \tanh\left(\sqrt{\frac{\lambda}{2}}\eta \frac{x - X}{\sqrt{1-v^2}}\right), \tag{5.5}$$

where $X = vt$ is the centre of the kink and v is the velocity of the kink.

It is easy to show that translation of the kink does not affect the energy of the system. Moreover, one has a Lorentz invariance in the system i.e. there exist soliton solutions traveling with constant velocity. Such traveling kinks do not excite the phonon modes of the system i.e. they do not radiate and hence the energy always remains localized at the soliton - one of the defining features of the soliton systems. The soliton solution (5.5) exactly satisfies the equations of motion of the field (5.3). However, if one wishes to solve the partial differential equation (5.3) numerically one must discretize in space. The discretized version of equation (5.3) is given by

$$\ddot{\phi}_n = \frac{\phi_{n+1} - 2\phi_n + \phi_{n-1}}{a^2} + f(\phi_{n-1}, \phi_n, \phi_{n+1}). \tag{5.6}$$

Equation (5.6) no longer has translational and Lorentz invariance and in general we should not expect traveling dissipationless kinks to exist (although in special instances this may be possible [99]). There are several different ways to discretize the non-linearity $f(\phi_{n-1}, \phi_n, \phi_{n+1})$. Most commonly a one-site discretization is used

$$f(\phi_{n-1}, \phi_n, \phi_{n+1}) = \frac{1}{2}\phi_n(1 - \phi_n^2). \tag{5.7}$$

It is known that equations (5.6) and (5.7) with boundary conditions

$$\lim_{n\to-\infty} \phi_n(t) = -1, \qquad \lim_{n\to+\infty} \phi_n(t) = +1, \tag{5.8}$$

admit only a countable set of stationary kink solutions. Physically, this implies that the kinks are located in an effective Peierls-Nabarro potential which is a periodic potential with the period given by the lattice spacing. Half of the stationary kinks are centred on the maxima of the PN potential - these are metastable kinks; half of the stationary kinks are centred on the minima of the PN potential - these are stable kinks. The height of the PN potential is the Peierls-Nabarro barrier, which is physically the minimum amount of energy that is needed to move a kink by one lattice site. In some very special types of discretization it is possible to have translationally invariant kinks and moreover it can be proven that there can also exist kink solutions that travel without radiation, but this can only be true for special values of kink velocity [99].

In vast majority of cases the discretization of the soliton leads to the PN potential with a finite PN barrier and also to the coupling of the motion of the kink and the phonon modes of the system. For this reason, whenever one has a traveling discrete kink one should expect it to gradually lose its kinetic energy and eventually be trapped in one of the PN potential wells. Much of the interest in the field of discrete soliton physics is to analyze the phenomena of kink motion, phonon radiation and kink trapping (see [20] for a comprehensive review). Many papers focus their analysis on discrete kink arising in idealized mathematical models, for example, in ϕ^4 model and in Sine-Gordon model. In the next section we develop a general technique for evaluating the PN potential, which can be applied to any type of kink including the kinks in zigzag ion chains.

5.2 Method for calculating the PN potential

Let the vector $\mathbf{u} = \{u_1, u_2, u_3 \dots u_N\}$ describe the state of a system with N degrees of freedom. This can for instance describe the state of the field of the discrete ϕ^4 model, in which case $N \to \infty$. Suppose that there is a kink in the system that is in state $\mathbf{u}$. The kink can be in different locations and we can introduce a variable $X \in \mathbb{R}$ that will denote the position of the kink. To calculate X we must define some function $g : \mathbf{u} \to \mathbb{R}$ such that $X = g(\mathbf{u})$. The definition of $g(\mathbf{u})$ has to be physically motivated. Let $V[\mathbf{u}]$

be the function denoting the potential energy of the system. We can now define the PN potential as a solution to the following optimization problem

$$U_{\mathrm{PN}}(X) = \min_{\mathbf{u}} V[\mathbf{u}] \quad \text{subject to } g(\mathbf{u}) = X. \tag{5.9}$$

This optimization problem can be solved using the method of Lagrange multipliers. The problem (5.9) is equivalent to

$$U_{\mathrm{PN}}(X) = \min_{\mathbf{u},\lambda} \left(V[\mathbf{u}] + \lambda \left(g(\mathbf{u}) - X \right) \right). \tag{5.10}$$

The minimization (5.10) can be done by solving the following set of simultaneous algebraic equations

$$\begin{aligned} \partial_{u_1} \left\{ V[\mathbf{u}] + \lambda \left(g(\mathbf{u}) - X \right) \right\} &= 0, && (5.11) \\ &\cdot \quad \cdot \quad \cdot \\ \partial_{u_N} \left\{ V[\mathbf{u}] + \lambda \left(g(\mathbf{u}) - X \right) \right\} &= 0, && (5.12) \\ \partial_{\lambda} \left\{ V[\mathbf{u}] + \lambda \left(g(\mathbf{u}) - X \right) \right\} &= 0. && (5.13) \end{aligned}$$

If we know approximately the solution of these equations then using the gradient descent numerical algorithms it is easy to find an accurate solution for $\mathbf{u}$ and hence the Peierls-Nabarro potential.

5.3 PN potential for kinks in the zigzag ion chains

5.3.1 Types of kinks and definition of kink centre

In order to calculate the PN potential for kinks in zigzag ion chains we must first understand the structure of the kink and assign the function $g(\mathbf{u})$ which represents the kink centre. Consider a chain of N ions in 3 dimensional space. The location of jth ion is specified by a coordinate (z_j, x_j, y_j) and the state of the whole system is specified by a vector $\mathbf{u} = (z_1, \ldots z_N, x_1 \ldots x_N, y_1 \ldots y_N)$. Let z-axis be the axis along which lies the crystal and x and y-axes lie in radial directions. The labeling of the ions is ordered such that $z_1 \leq z_2 \ldots z_N$. Figure 5.1a shows the chain that is in the linear configuration. The weakening of the harmonic confining potential below the critical value leads to a phase transition into a zigzag and a possibility of kink creation; this is shown in figure 5.1b.

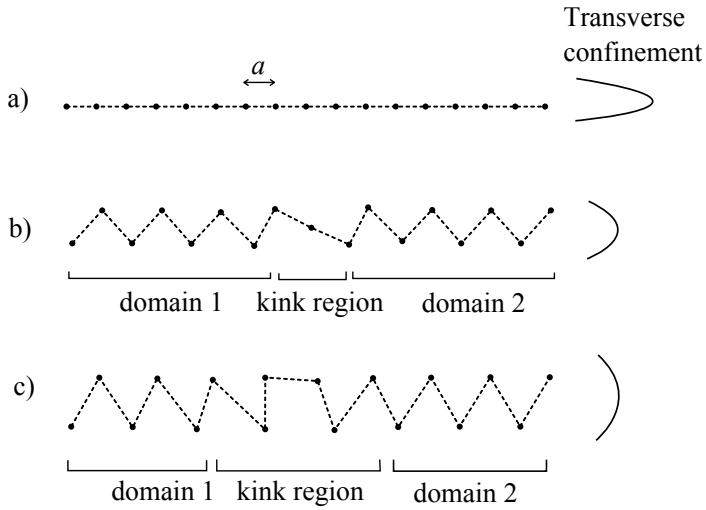

Figure 5.1: a) Linear chain configuration. b) "Odd" kink configuration. c) "Extended" kink configuration. Structural transitions from a) to b) to c) are induced by reducing the strength of the harmonic confining potential relative to the strength of the Coulomb repulsion in the system.

Just below the critical point the system can be well described by the discrete ϕ^4 model. The kink divides the system into two domains - in one domain the coordinate of each ion is given by $\mathbf{r}_n = (na, (-1)^n b)$ and in the other domain it is given by $\mathbf{r}_n = (na, -(-1)^n b)$ where b is the radial distance of the ion from the z-axis and a is the spacing between ions. The kink centre should be located somewhere in the region where one domain interpolates into the other domain. If the transverse confining potential is reduced further the domains themselves do not change their structure but the kink will change. As the confining potential is reduced and the ratio a/b decreases, the propagation of the kink increasingly involves the axial motion of the ions. In other words the coupling between the radial and axial motions becomes more and more significant. At some point, the axial motion of ions is so great that the ions start to swap places i.e. the z-ordering of the ions is disrupted. We identify three types of kinks on the basis of the disruption of the z-ordering during their propagation

Odd kink z-ordering is not disrupted; movement of kink is due to the radial motion of the ion.

Extended kink z-ordering changes whenever a kink moves by one lattice site; movement of kink is due to the axial motion of the ions.

Intermediate kink z-ordering changes once when a kink moves by two lattice sites; movement of kink is due to the radial and axial motions of the ions.

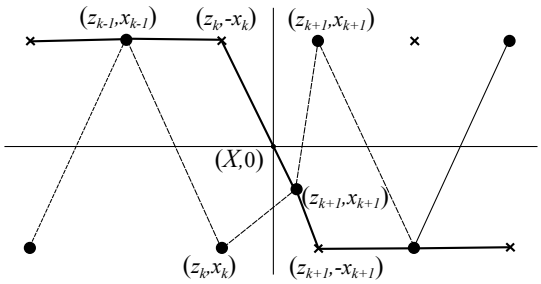

Figure 5.2: Graphical meaning of the kink centre X. The point $(X, 0)$ is an intersection of the line connecting points $(z_k, -x_k)$ and (z_{k+1}, x_{k+1}) where $x_k x_{k+1} > 1$.

The terms "odd" and "extended" kink is taken from the nomenclature introduced in [81]. In the extended kink the two rows of the zigzag have a different number of ions. The extended kink is shown in figure 5.1c. The intermediate kink looks like an odd kink at the local minima of the PN potential and like extended kink at the local maxima of the PN potential (see next section for more detailed description).

One of the reason for identifying the three type of kinks is that all three may require different definition of the kink centre $g(\mathbf{u})$. Lets consider the odd kink first. Odd kink arises as ϕ^4 kink and we can use the analogy between the two kinks to suggest a function $g(\mathbf{u})$. In the case of ϕ^4 soliton the kink centre is normally taken to be the point where the field is zero i.e. $\phi_K(X) = 0$. In the case of the odd kink, we know that there must be two adjacent ions in the chain that are both either above the z-axis or below, that is $\exists x_k : \quad x_k x_{k+1} \geq 0$. The kink centre should be somewhere between those ions i.e. $X \in [z_k, z_{k+1}]$ and by analogy with the ϕ^4 model we can take it to be the point where the line connecting points $(z_k, -x_k)$ and (z_k, x_{k+1}) intersects the z-axis. Graphically the meaning of the kink centre is shown in figure 5.2. A simple exercise in elementary geometry gives

$$g(\mathbf{u}) = \frac{x_{k+1} z_k + x_k z_{k+1}}{x_k + x_{k+1}}, \tag{5.14}$$

$$x_k x_{k+1} \geq 0 \tag{5.15}$$

The reason for a possible equality in the condition (5.15) is that it is possible for an ion that is involved in kink structure to lie exactly on the z-axis.

It is not hard to see that the definition of kink centre given by (5.14) and (5.15) is such that it parametrizes the location of the odd kink continuously - as one moves a kink from one end of the chain to the other, $X = g(\mathbf{u})$ varies continuously. If, however,

one tries to apply the same definition to extended kinks then one will find that X will no longer be a continuous function. The reason for this is due to the fact that the ordering of ions swaps which would require their relabeling and the relabeling will introduce the discontinuities. To define the centre of the extended kink we will make use of the following observation: an extended kink structure involves an extra ion either at the top row or the bottom row of the zigzag and hence a local increase of charge density. Let us denote the spacing between the ions by the following function $\psi(\bar{z}_j) = z_{j+1} - z_j$, where $\bar{z}_j \equiv (z_{j+1} + z_j)/2$. We know that if the chain is homogeneous than inside the domain $\psi(\bar{z})$ is constant but it varies in the region where the two domains interpolate into one another. We define the centre of the kink as the weighted average of the function characterizing the spacing between ions

$$g(\mathbf{Q}) = \frac{\sum_j^{N-1} \bar{z} \left[\psi(\bar{z}_j) - \psi^{(0)}(\bar{z}_j^{(0)})\right]^2}{\sum_j^{N-1} \left[\psi(\bar{z}_j) - \psi^{(0)}(\bar{z}_j^{0})\right]^2}, \tag{5.16}$$

where $\psi^{(0)}(\bar{z}^{(0)})$ denotes the ion spacing function when no kink is present in the chain. The function $\psi^{(0)}(\bar{z}^{(0)})$ is introduced in order to remove any contribution to the variation of the spacing between ions that arises from the inhomogeneity of the crystal rather than the presence of the kink.

The motion of the intermediate kink involves changes of z-ordering and we define the centre of the intermediate kink in the same way as for the extended kink using equation (5.16).

5.3.2 PN potential for kinks in chains trapped in a harmonic potential

We now consider the case of finite chains trapped by a harmonic potential in all three directions. We will focus first on the 2 dimensional case that is relevant when the ratio ω_y/ω_x is sufficiently large to confine ions to the xz-plane. The potential energy of the system is given by

$$V(\mathbf{u}) = \sum_{j=1}^{N} \frac{1}{2} m \left(\omega_x^2 x_j^2 + \omega_z^2 z_j^2\right) + Q^2 \sum_{i<j}^{N} \frac{1}{\sqrt{(x_i - x_j)^2 + (z_i - z_j)^2}}. \tag{5.17}$$

The structure of the kink in potential (5.17) depends only on one parameter, namely

the ratio $\alpha \equiv \omega_x/\omega_z$. This can be seen by putting the equation (5.17) into dimensionless units. Setting $x_j = l\tilde{x}_j$ and $z_j = l\tilde{z}_j$, where $l = \left(Q^2/m\omega_z\right)^{1/3}$ we get

$$\tilde{V}(\mathbf{u}) = \sum_{j=1}^{N} \frac{1}{2}\left(\alpha^2\tilde{x}_j^2 + \tilde{z}_j^2\right) + \sum_{i<j}^{N} \frac{1}{\sqrt{\left(\tilde{x}_i - \tilde{x}_j\right)^2 + \left(\tilde{z}_i - \tilde{z}_k\right)}}, \tag{5.18}$$

where $\alpha \equiv \omega_x/\omega_z$ and $\tilde{V}(\mathbf{u}) = V(\mathbf{u})/\left(ma^2\omega_z^2\right)$. Figure 5.3 shows the PN potential for kinks corresponding to several different values of α. We performed the calculations for a system of 30 Yb^+ ions in a trap with experimentally realistic parameters.

The PN potential for the odd kinks is shown in figure 5.3. One can see that for odd kinks the PN potential is lower at the edges of the chain. Thus odd kinks have a tendency to move from the centre toward the edges where they can be lost. In addition there is a periodic variation of the potential which comes from the discreteness of the lattice. The local minima in the potential that arise because of the discreteness of the system allow for a stable trapping of the odd kinks. Thermal fluctuations can move a kink from one local minimum of the PN potential to the adjacent minimum inducing kink diffusion. The stable trapping of odd kinks is achieved when $T < E_a/k_B$ i.e. the thermal energy has to be less than the height of the barrier separating the two adjacent minima (the Peierls-Nabarro barrier). The PN barrier increases when the radially confining potential is reduced. For $\omega_t/(2\pi) = 336$ kH the PN barrier is less than 1 mK/k_B and for these trapping parameters the kinks would not be stable in practice since in the experiments the temperature of the chains is around 5 mK. For $\omega_t/(2\pi) = 204$ kHz the PN barrier between the two adjacent local minima in the centre of the chain is around 10 mK. In this case, the kinks would be stable with respect to physically realistic thermal fluctuations; the experimentally obtained image in figure 4.6 corresponds to $\omega_t/(2\pi) = 204$ kHz. Traces of the adiabatic trajectory of the kink are shown on the right side of figure 5.3. We can see that odd kink propagates via the transverse motion of ions as we have already discussed. Note that the motion is not purely transverse but involves an axial component. The reason for this is that the transverse and axial modes are coupled by the Coulomb interaction and the axial translational symmetry is broken by the harmonic confinement. The axial component of motion increases with decreasing ω_t and eventually this leads to a different type of kink transport exhibited by "intermediate" and "extended" kinks, where adjacent ions can swap and alter the z-ordering.

The PN potential for the extended kinks is shown in figure 5.3b. For extended kinks

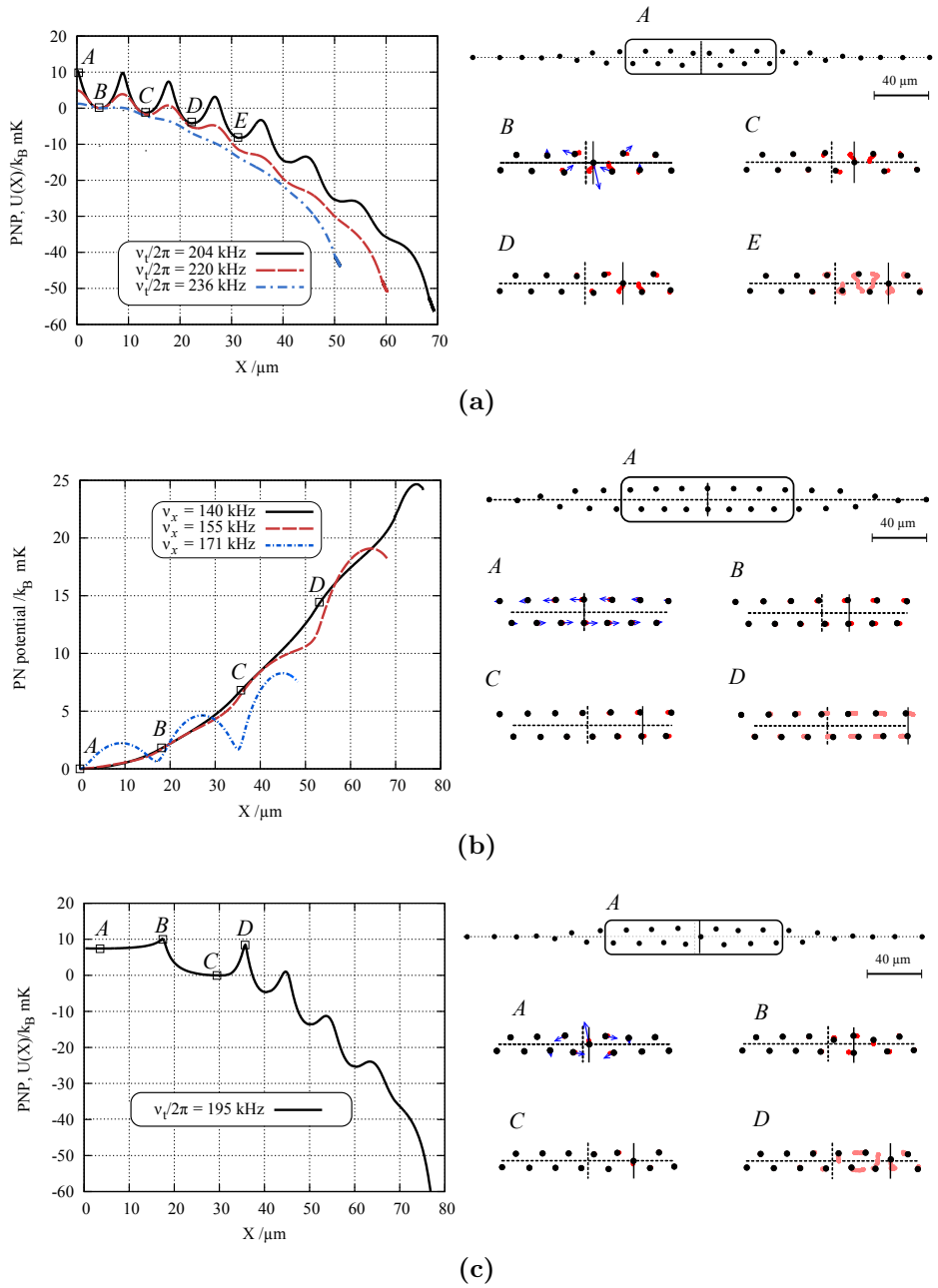

Figure 5.3: PN potentials and adiabatic trajectories for several kinks in a chain of 30 ions in a harmonic confining potential. PN potential is shown for a) odd kinks b) extended kinks c) intermediate kinks. The diagrams on the right show the kink structures corresponding for several different values of X. The red traces indicate the movement of the ions as kink moves from current point to the next point e.g. from A to B. The pink trace indicate the motion of the ions as kink moves from point A to D. The blue arrows indicate the lowest frequency mode that is localized at the kink.

the PN potential increases towards the edges of the chain and the global minimum is in the centre of the chain. Thus the extended kinks are attracted towards the centre of the chain and are easier to stabilize and observe in the experiment. For this reason, extended kinks were used to measure the KZ scalings in the PTB experiment [108] (see Chapter 4). There is also a visible periodic variation of the PN potential which comes from the discreteness of the lattice. The height of the barrier between adjacent local minima decreases with increasing radial confining frequency ω_x. For $\omega_x/(2\pi) = 171$ kHz the kink can be located at distinct local minima but already for $\omega_x/(2\pi) = 155$ kHz the PN barrier is zero and the kink will always slide towards the centre of the chain. The depth of the PN well for the extended kinks with $\omega_x/(2\pi) = 140$ kHz is around 25 mK/k_B which is more than enough for experimental trapping of the kink. The experimental image of extended kink shown in figure 4.6 corresponds to the radial trapping frequency of $\omega_x/(2\pi) = 140$ kHz. From the traces of the adiabatic trajectory on the right of figure 5.3, it is clear that the extended kinks propagate via the longitudinal motion of the ions, which does not conserve the z-ordering.

The transition from an odd kink that propagates via the transverse motion of ions to an extended kink that propagates via the longitudinal motion of ions happens via the intermediate kink configuration. The PN potential and the adiabatic trajectory traces of an intermediate kink is shown in figure 5.3c. It is clear that for the propagation of intermediate kink both the transverse and longitudinal motions of ions are equally important. Intermediate kinks were experimentally observed in [49].

The calculated adiabatic trajectory for the kinks and the Peierls-Nabarro potential are consistent with the observation obtained by numerical simulations and experimental data. The PN potential predicts correctly for which trap parameters we may expect stable kink confinement. The mode of kink propagation is consistent with results of MD simulations and the blurring of experimental images.

5.3.3 Effect of heavy ions on PN potential

Usually the trapped ion crystal consists of ions of the same type. Mixed species crystals are also of interest and are used for example for sympathetic cooling [83]. Mixed species ion crystals can be created either by deliberately loading different ions or by chance *in situ* chemical reactions of the ions with the background gas. We will refer to an ion with a mass which is different from the rest of the ions in the chain as a mass defect. A mass defect in the pondermotive potential of a Paul trap experiences a different radial

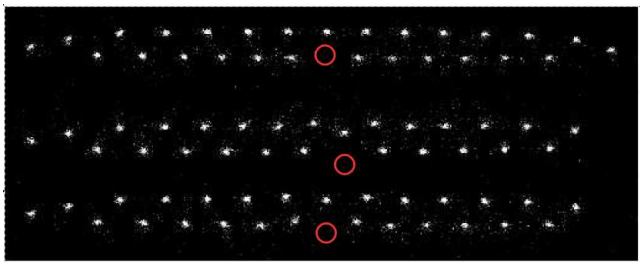

Figure 5.4: Experimental images of kinks with molecules (indicated by the red circles). (Top) Extended kink with a light molecule ($m \approx 188$). (Middle) Extended kink with a heavy molecule ($m \approx 220$) located at the kink. (Bottom) Extended kink with the heavy molecule moved by one lattice site. Comparing the distortion of the crystal with numerical simulations allows us to distinguish between light and heavy molecules. [The photograph was taken from [100].]

confinement than the rest of the ions, since the secular frequency $\omega_x \propto 1/m$ where m is the mass of the ion. Because of this, the mass defect changes the configuration of the crystal and deforms the PN potential, consequently affecting the dynamics of the kinks. This modification of the PN potential depends on the location and the mass of the impurity species and the type of kink.

In the PTB experiments the $^{172}Yb^+$ ions occasionally react with the background gas forming heavier molecular ions. In a fluorescence image of the chain, a molecular mass defect appears as a dark ion. The $^{172}Yb^+$ ions can react with water to produce YbO^+, $Yb(OH)^+$ and other molecules [125, 126, 112]. By performing parametric excitation of two to four ions including a mass defect, the ions have been measured primarily as YbO^+ or $Yb(OH)^+$; the addition of hydrogen was not resolvable by this method. Since these heavy masses distort the crystal as well as the kink configurations, the amount of distortion can be used as an alternative method of estimating the mass of the molecule by comparing the experimental images with crystal configurations inferred from molecular dynamics simulations. This analysis indicates the presence of even heavier molecules with one to three oxygen atoms involved. In the simulations, we investigate mass defects with representative masses $m = 188$ (YbO^+) and 220 (YbO_3^+), consistent with the observations in the experimental system (figure 5.4).

Experimental measurement of the KZ scaling indicates that the mass defects modify the dynamics and the stability of the kink. Figure 5.5 shows a measured scaling for chains with no mass defects, one mass defect and two mass defects. The mass defects are randomly distributed in the chain. As we can see, at low quench rates, a higher kink density is observed when mass defects are present. Thus the mass defects must

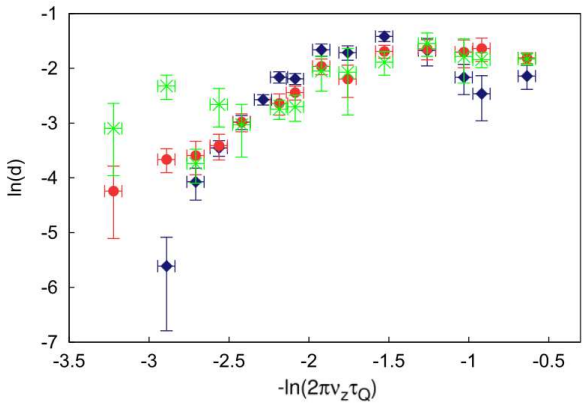

Figure 5.5: Scaling of measured kink density with the quench parameter τ_Q, with no molecules (blue), one molecule (red) and two molecules (green) present in the crystal. The vertical error bars include the s.e.m. as well as the statistical uncertainty assuming a binomial distribution. Horizontal error bars indicate uncertainty in the axial trapping frequency and a nonlinear distortion of the applied ramp. [The graph was taken from [100].]

influence either the defect creation probability, defect surviving probability or both.

In order to understand the effect that the heavy mass defects have on the dynamics of the kinks we evaluate the Peierls-Nabarro potential for kinks in chains with mass defects. Figure 5.6a shows the results of the calculation for the extended kink with $m = 220$ mass defect at various positions of the chain. We can see that the PN potential is lowered in the vicinity of the mass defect. The well created by the mass defects acts as a kink trap that can stabilize the defects. Note, however, that when the mass defects are located near the edge of the chain, such as at positions 5 and 7, they lower the PN barrier created by the inhomogeneity of the chain. In these cases we would expect that the kinks would be more easily lost from the chain and this prediction is confirmed by the molecular dynamics simulations and experimental observations [100]. If there are two mass defects placed on both sides of the chain centre (e.g. positions 11 and 19) then it is possible to fit two extended kinks into a 30 ion chain as shown in figure 5.6b. A two kink configuration in chain with two mass defects was observed experimentally in [100]. Such kink configurations may be of interest as they may allow an investigation of kink-kink interactions. Figure 5.6c shows a PN potential for an odd kink in a chain with a mass defect at position 11. The depth of the potential well created by the mass defect is around 20 mK/k_B. This potential well can act as kink trap that reduces kink losses that can come from kink motion towards the left edge of the chain.

In experiments the camera exposure time is of the order of milliseconds whereas

kinks are generated in quenches lasting dozens of microseconds (see Chapter 4). This means that the camera does not provide information about the kink dynamics during the quench - it only provides information about the final configuration of the chain. In order to obtain information about kink dynamics during quenches we had to resort to molecular dynamics simulations. In particular, the PN potential calculation provides qualitative predictions of the effect of mass defects on kink dynamics, which can be verified using molecular dynamics simulations.

First, we consider the case of the created kinks in figure 5.7a. For fast quenches the molecule has no effect on kink creation, but for slow quenches, the kink density exhibits a strong position dependence. When the molecule is in the centre (e.g. positions 13 or 15), kink formation is suppressed for slow radial quenches. Because the molecule is less bound radially than the rest of the crystal, it breaks out of the linear chain earlier and initiates the phase transition sooner than in a pure crystal. This leads to a prolonged time period in which the phase transition spreads out, suppressing defect formation for sufficiently slow quenches [37, 30]. At intermediate sites (e.g. positions 9 and 11), the kink density is enhanced. Here, in addition to the quench induced phase transition, which always begins at the crystal centre due to its inhomogeneity, a second phase transition is initiated at the molecule's position. This occurs because of the lower radial confinement of the mass defect and the higher charge density close to the centre pushing the molecule out of the chain. These two phase transitions take place independently, bringing about an enhanced probability of kink formation due to the possible conflict when the phase fronts meet. With the molecule at the edges of the chain (positions 1-7), the kink density is unaffected by the presence of the molecule. In the outer parts of the crystal the molecule does not experience a sufficient repulsion in this region of lower charge density to initiate an independent phase transition. The influence of molecule position on kink creation behaviour is reduced at faster ramp times and eventually has no effect (i.e. for $\tau_Q < 30$ μs). In this regime the system behaves as a homogeneous system (the phase front is faster than the speed of sound), and this characteristic dominates the kink creation dynamics.

The case of experimentally accessible kinks is shown in figure 5.7b. The density of kinks remaining after 400 μs is mainly governed by the altered rate of kink creation shown in figure 5.7a and not by a modified loss rate, with two exceptions. Firstly, in positions 9–11, the losses from the crystal are strongly reduced for slower ramps. For these intermediate positions, the PN potential at the molecule provides a very strong confinement that traps kinks formed at the centre as they start to move out of the

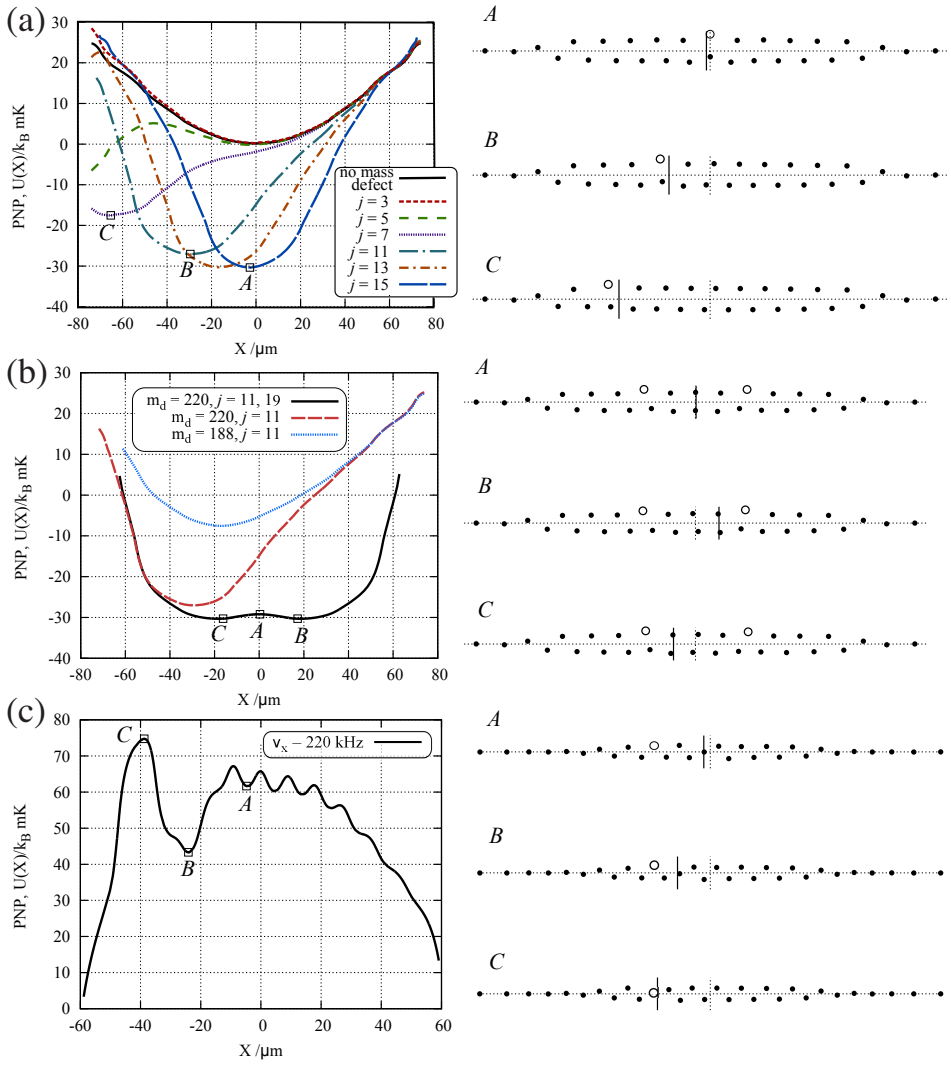

Figure 5.6: Kink-confining PN potentials for crystals with mass defects. (a) PN potential calculated for the extended kink case with a molecule of mass $m = 220$ located at different positions in the crystal ($\omega_z = 24.6$ kHz and $\omega_x = 140$ kHz). (b) Comparison of PN potentials with mass defects of $m = 220$ and 188. The depth of the PN potential increases with the mass of the defect. Also shown is the case of two heavy molecules located at positions 11 and 19 (black line) creating a double well potential. (c) PN potential for an odd kink with transverse trapping frequency $\omega_x = 220$ kHz ($\omega_z = 24.6$ kHz) and a molecule with $m = 220$ at position 11. The open squares on the left correspond to the vertical lines indicating the kink centre in the configurations on the right.

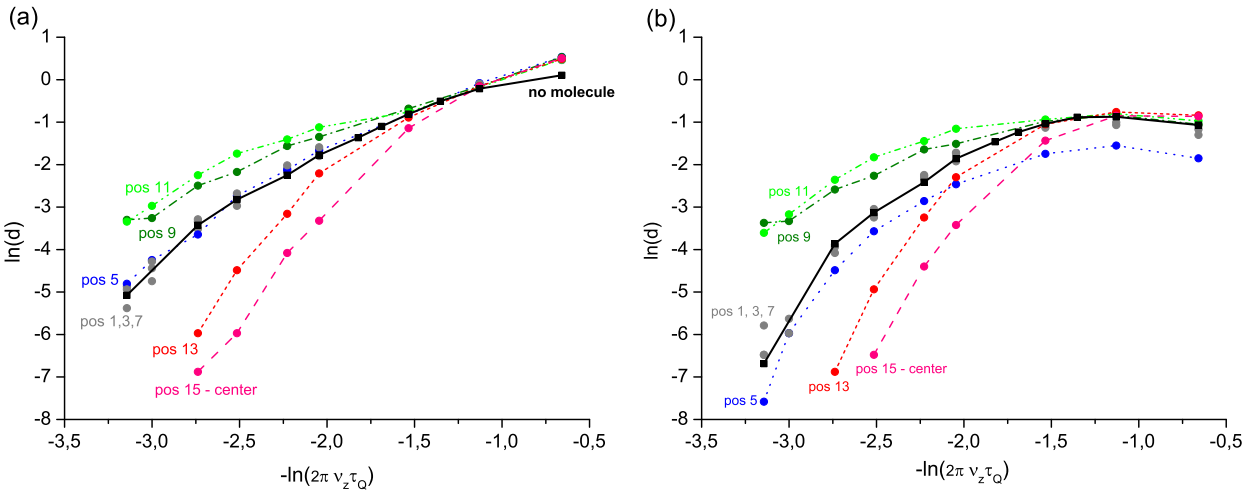

Figure 5.7: Simulated kink density scaling with ramp time for a molecule of mass $m = 220$ at various positions in a chain of 30 ions. (a) Density of kinks created during the ramp. (b) Density of kinks still present 400 μs after the ramp started and energy is dissipated (experimentally accessible kinks). [The graphs were taken from [100].]

crystal, reducing losses. Secondly, at position 5, high losses occur. When the molecule is around position 5, it is easy for the kink to be lost due to the reduced barrier of the PN potential caused by the molecule, as seen in figure 5.6a.

Heavy mass defects experience a weaker radial confinement than the main ions in the chain. This means that the dynamics of the system can be influenced by the application of static electric field. When a static electric field is applied in the transverse direction the heavier ions will experience a greater transverse displacement than the lighter ions. Effectively the "mass" of the heavy ion can be tuned by the application of electric field and in turn the depth of the PN well induced by the mass defect can be controlled. Thus when the chain has mass defects the dynamics of kinks can be controlled using static electric fields. In [100], several examples of kink manipulations using elective fields were presented, namely, deterministic creation of one kink, deterministic creation of two kinks, displacement of a kink and displacement of a mass defect.

Figure 5.8 shows an example of the experimental sequence with a molecule of $m \approx 188$. After a quench of length τ_Q, a series of pictures is taken with exposure times of 20 ms, with 20 ms between exposures. After a kink has been created by the ramp (figure 5.8i), the electric field is increased linearly over 60 ms (figure 5.8ii). In figure 5.8iii the entire ion chain is heated by reducing the detuning of the cooling laser by a few MHz. This causes the kink to oscillate in the confining PN potential, until it reaches the position of the molecule. As the kink gets trapped at the molecule it pushes the

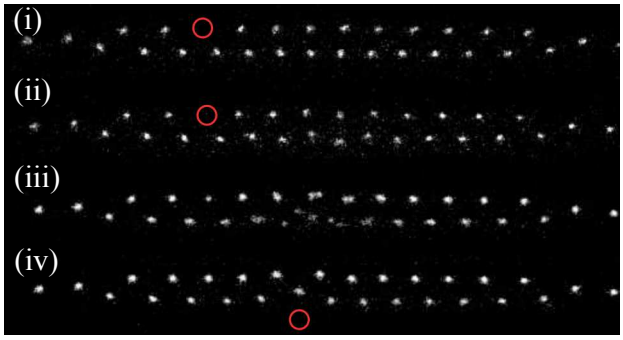

Figure 5.8: Time series demonstrating control of a kink and molecule using an electric field (20 ms exposures). Image (i) shows a kink in the centre of the crystal after the radial quench. Image (ii) shows the crystal after the adiabatic application of an electric field in the plane of the zigzag (downward in the image). In (iii) the laser cooling light is shifted a few MHz closer to resonance, heating the Coulomb crystal and providing the kink with motional energy. In this image, motion during the exposure is visible when the kink begins to oscillate in the PN potential, gets trapped by the mass defect, and returns to the centre with the molecule. The kink and molecule then stabilize (iv). [The pictures were taken from [100].]

molecule further out of the crystal where it is free to move to the centre of the axial potential. When the molecule changes its position, the PN potential minimum and the kink trapped therein moves along with it. The kink and molecule finally stabilize at the centre of the crystal (figure 5.8iv). We have verified that for the parameters used, the molecule does not move in the crystal without the presence of a kink.

5.4 Equations of motion for the kink

The PN potential predicts some qualitative features of kink dynamics, such as trapping and losses of kinks at the boundaries. By itself the PN potential does not provide quantitative dynamical information such as the frequency with which a kink oscillates around a local minimum of the PN potential. To obtain such dynamic information it is necessary to derive the effective equation of motion for the kink centre. This can be done, for example, using the collective variable formalism developed in [128, 15, 17, 16]. The equations of motion of all particles are known - they simply follow Newton's equations of motion. However, *a priori* it is not clear how the motion of the particles generates an effective motion of the kink centre. The idea of the collective variable formalism is to clarify this by making a change in canonical coordinates that preserves the Hamiltonian equations of motion $(\mathbf{Q}, \mathbf{P}, t) \rightarrow (X, \Pi, \mathbf{q}, \mathbf{p}, t)$, where $\mathbf{Q}$ and

$\mathbf{P}$ are vectors containing the particle position degrees of freedom and their canonical momenta, X and Π are the variables denoting kink centre, and its canonical momentum and $\mathbf{q}$ and $\mathbf{p}$ are the variables denoting the fluctuations of the system around the kink configuration. The introduction of the two dynamical degrees of freedom, X and Π, requires an addition of two constraints, which are normally chosen to minimize the fluctuations around the kink. The canonical transformation is an exact procedure - the dynamics of the system in the new coordinates is equivalent to the dynamics of the system in the old coordinates. The solution of the resulting equations of motion may be even more demanding numerically than the original equations of motion. The virtue of performing the transformation is that in principle it allows one to perform physically motivated approximations and extract information of interest such as effective masses, momentum and kinetic energy of kinks. In the future it is possible to extend our work in this direction.

5.5 Chapter conclusions

In this chapter we have shown that methods developed in the field of discrete soliton physics can be used to study the dynamics of kinks in the zigzag ion chains. We have shown how to calculate the PN potential for various types of kinks and predict their stability. This type of calculations may prove useful when designing novel ion trap experiments with kinks. The effect of mass defects on kink dynamics was examined using a combination of the PN potential calculation, experimental results and numerical simulations.

In the future it may be possible to study in ion traps various discrete soliton phenomena such as kink-kink and kink-phonon interactions.

Chapter 6

Conclusions and further work

In the thesis a number of interrelated ideas are developed with an underlying theme, namely, the use of linear to zigzag phase transition in ion crystals to study non-equilibrium dynamics. The main focus is on the possibility to accurately measure the Kibble-Zurek (KZ) scaling law - the scaling law that predicts the dependence of the average number of defects produced in non-adiabatic phase transition on the quench rate. One can summarize the achievements of the work as follows

1. We show that the KZ scaling can be derived by finding a transformation that eliminates the quench rate from the equations of motion. Using this method, we generalize KZ scaling law to finite size systems (Chapter 3).

2. We predict and verify numerically the KZ scaling for the linear to zigzag phase transition in homogeneous crystals with periodic boundary conditions (Chapter 3).

3. In collaboration with experimental groups, structural defects are for the first time produced using non-adiabatic phase transition. The KZ scaling is measured in small ion crystals. The experimental results agree very well with extensive molecular dynamics simulations (Chapter 4).

4. A technique for evaluating the Peierls-Nabarro potential for the kinks is developed and used to evaluate the stability of several experimentally realistic kinks (Chapter 5).

One can view ion crystals as rough analogues of solid state lattices and thus certain physical phenomena that are relevant to condensed matter systems can be studied in ion traps. In contrast to atoms in solids, the ions interact via Coulomb interaction. For this reason the distances between particles in ion crystals are very large, of the order of several micrometers, and thus the whole crystal can be imaged using an optical microscope. The structural organization of ion crystal is very much influenced by the trapping potentials and thus can be easily controlled in the experiment. These two

points, ease of imaging and control of crystal structure, make ion trap system very attractive for studies of physics of equilibrium and non-equilibrium phase transitions, heat transport, dislocation dynamics, friction and other phenomena.

The experiment that uses linear to zigzag phase transition to study KZ mechanism is an excellent illustration of this fact - a one row crystal lattice is transformed by a precise control of trap parameters into a two row crystal lattice whilst being directly imaged to measure the probability of the creation of structural defect. The experimental measurements presented in the thesis can be regarded as one of the most accurate quantifications of KZ scaling to date. The results of these experiments, however, come with a caveat: the measurements were carried out on small inhomogeneous ion crystals. We show that in such small crystals the correlation length is affected by the finite size effects and KZ theory has to be modified. In order to find a way of extrapolating the scaling measured in finite inhomogeneous systems to the thermodynamic limit, we develop a technique for deriving the KZ scaling by directly analyzing the equations of motion. Our analysis indicates that in the ion trap experiments additional measurements are needed in order to verify the KZ scaling in the thermodynamic limit. This is one of the open problems raised in the thesis. In future theoretical and experimental investigations it will be also desirable to explore quantitatively the effect of the molecular dynamics modelling approximations that were used in the thesis, in particular, the effect of pseudopotential approximation on the linear to zigzag structural phase transition. Even though it was argued in Chapter 4 that the statistics of produced defects is not affected by micromotion, it is likely that the dynamics of the produced defects is affected by micromotion since it modulates periodically the Coulomb interaction between the ions in the chain. This is a subject for future investigations.

The structural defects or kinks in the Coulomb crystal lattice are examples of discrete soliton systems. In the thesis, we establish a connection between the fields of ion trapping and the field of discrete soliton physics. This connection is important since there is a considerable gap between theoretical and experimental studies of discrete soliton physics with theory leading. Coulomb crystal in ion trap could potentially be used to explore the unintuitive dynamics of discrete solitons. We have provided a starting point for such investigations by numerically evaluating the potential in which such collective the structures move - the Peierls-Nabarro potential.

A unique feature of ion trap crystals, which drastically differentiate them from colloidal Coulomb crystals or dusty plasmas, is that ion crystals can be cooled to a point where quantum mechanics is important for the dynamics of the system. Various

quantum optical techniques make it possible to reach ultralow temperatures, where discrete levels associated with the motional and electronic degrees of freedom of the crystal are spectroscopically resolved. This means that, in the future, one may study non-linear and non-equilibrium physics in quantum dynamical regimes. Quantum linear to zigzag phase transition has already been studied theoretically in a number of works [4, 5, 118, 119]. The fact that it is possible to control the electronic degrees of freedom of the ions implies the possibility of a whole range of fascinating ion crystal experiments that are not explored in the thesis. For example, one direction in this area that is pursued by several groups is to study quantum spin chains using ion crystals [64, 52].

In the world of technology there is clear trend of miniaturization of devices. Machines with nanoscale gears and nanoscale wires may exist in the near future but for this to become reality much basic science still remains to be done. Our understanding of physics at the nanoscale is far from complete, for example, many well studied phenomena such as friction, thermal and electrical conductivity will require a new theoretical description at the nanoscale. Coulomb crystals in ion traps provides a convenient model system where many theoretical ideas can be tested. Nano-friction and thermal conductivity in ion crystal has already been explored theoretically in several recent works [10, 107, 12, 97, 111]. In the future, one may look forward to more ion trap experiments clarifying physical theories that will be ultimately applied in nanoscale engineering.

Bibliography

[1] Als-Nielsen J J and Birgeneau R J. Mean field theory, the Ginzburg criterion, and marginal dimensionality of phase transitions. *American J. Phys.*, 45, 554 (1977)

[2] Andrei E Y, Deville G, Glattli D C, Williams F I B, Paris E and Etienne B. Observation of a magnetically induced Wigner solid. *Phys. Rev. Lett.*, 60, 2765 (1988)

[3] Bagatskii M I, Voronel' A V and Gusak V G. Measurement of the specific heat C_v of argon in the immediate vicinity of the critical point. *JETP*, 517, 16 (1963).

[4] Baltrusch J D, Cormick C, De Chiara G, Calarco T and Morigi G. Quantum superpositions of crystalline structures. *Phys. Rev. A*, 84, 063821 (2011)

[5] Baltrusch J D, Cormick C and Morigi G. Quantum quenches of ion coulomb crystals across structural instabilities. *Phys. Rev. A*, 86, 032104 (2012)

[6] Bauerle C, Bunkov Yu M, Fisher S N, Godfrin H and Pickett G R. Laboratory simulation of cosmic string formation in the early universe using superfluid ^{3}He. *Nature*, 382, 332 (1996)

[7] Baxter R J. *Exactly solved models in statistical mechanics.* Academic Press (1989)

[8] Beatus T, Bar-Ziv R and Tlusty T. Anomalous microfluidic phonons induced by the interplay of hydrodynamic screening and incompressibility. *Phys. Rev. Lett.*, 99, 124502 (2007)

[9] Beatus T, Tlusty T and Bar-Ziv R. Phonons in a one-dimensional microfluidic crystal. *Nat. Phys.*, 2, 743 (2006)

[10] Benassi A, Vanossi A and Tosatti E. Nanofriction in cold ion traps. *Nat. Commun.*, 2, 236 (2011)

[11] Bermudez A, Almeida J, Ott K, Kaufmann H, Ulm S, Poschinger U, Schmidt-Kaler F, Retzker A and Plenio M B. Quantum magnetism of spin-ladder compounds with trapped-ion crystals. *New J. Phys.*, 14, 093042 (2012)

[12] Bermudez A, Bruderer M and Plenio M B. Controlling and measuring quantum transport of heat in trapped-ion crystals. *Phys. Rev. Lett.*, 111, 040601 (2013)

[13] Birkl G, Kassner S and Walther H. Multiple-shell structures of laser-cooled 24mg+ ions in a quadrupole storage ring. *Nature*, 357, 310 (1992)

[14] Bloch I, Dalibard J and Zwerger W. Many-body physics with ultracold gases. *Rev. Mod. Phys.*, 80, 885 (2008)

[15] Boesch R, Stancioff P and Willis C R. Hamiltonian equations for multiple-collective-variable theories of nonlinear Klein-Gordon equations: A projection-operator approach. *Phys. Rev. B*, 38, 6713 (1988)

[16] Boesch R and Willis C R. Exact determination of the Peierls-Nabarro frequency. *Phys. Rev. B*, 39, 361 (1989)

[17] Boesch R, Willis C R and El-Batanouny M. Spontaneous emission of radiation from a discrete Sine-Gordon kink. *Phys. Rev. B*, 40, 2284 (1989)

[18] Bowick M J, Chandar L, Schiff E A and Srivastava A M. The cosmological Kibble mechanism in the laboratory: String formation in liquid crystals. *Science*, 263, 943 (1994)

[19] Brankov J G. *Introduction to Finite-Size Scaling*. Leuven University Press (1996)

[20] Braun O M and Kivshar Y S. *The Frenkel-Kontorova Model: Concepts, Methods, and Applications*. Springer (2004)

[21] Bray A J. Theory of phase-ordering kinetics. *Advances in Physics*, 43, 357 (1994)

[22] Campostrini M and Vicari E. Critical behavior and scaling in trapped systems. *Phys. Rev. Lett.*, 102, 240601 (2009)

[23] Cardy J. *Scaling and Renormalisation in Statistical Physics*. Cambridge University Press, Lecture Notes in Physics (1996)

[24] Casdorff R and Blatt R Ordered Structures and Statistical Properties of Ion Clouds Stored in a Paul Trap. *Appl. Phys. B*, 45, 175 (1988)

[25] Ceccarelli G and Torrero C. Scaling behavior of trapped bosonic particles in two dimensions at finite temperature. *Phys. Rev. A*, 85, 053637 (2012)

[26] Ceccarelli G, Torrero C and Vicari E. Critical parameters from trap-size scaling in systems of trapped particles. *Phys. Rev. B*, 87, 024513 (2013)

[27] Chae S C, Lee N, Horibe Y, Tanimura M, Mori S, Gao B, Carr S and Cheong S W. Direct observation of the proliferation of ferroelectric loop domains and vortex-antivortex pairs. *Phys. Rev. Lett.*, 108, 167603 (2012)

[28] Chandran A, Erez A, Gubser S S and Sondhi S L. Kibble-Zurek problem: Universality and the scaling limit. *Phys. Rev. B*, 86, 064304 (2012)

[29] Chashkin Yu R, Voronel' A V, Gorbunova V G and Shchekochikhina V V. Specific heat of nitrogen near the critical point. *JETP*, 23, 597 (1966)

[30] De Chiara G, del Campo A, Morigi G, Plenio M B and Retzker A. Spontaneous nucleation of structural defects in inhomogeneous ion chains. *New J. Phys.*, 12, 115003 (2010)

[31] Chuang I, Ruth D, Turok N and Yurke B. Cosmology in the laboratory: Defect dynamics in liquid crystals. *Science*, 251, 1336 (1991)

[32] Costagliola G and Vicari E. Critical dynamics in trapped particle systems. *J. Stat. Mech.*, L08001 (2011)

[33] Crecchi F and Vicari E. Quasi-long-range order in trapped systems. *Phys. Rev. A*, 83, 035602 (2011)

[34] Damski B and Zurek W H. Soliton creation during a Bose-Einstein condensation. *Phys. Rev. Lett.*, 104, 160404 (2010)

[35] de Queiroz S L A, dos Santos R R, and Stinchcombe R B. Finite-size scaling behavior in trapped systems. *Phys. Rev. E*, 81, 051122 (2010)

[36] Dehmelt H G. Radiofrequency spectroscopy of stored ions i: Storage. *Advances in Atomic and Molecular Physics*, 3, 53, Academic Press (1968)

[37] del Campo A, De Chiara G, Morigi G, Plenio M B and Retzker A. Structural defects in ion chains by quenching the external potential: The inhomogeneous Kibble-Zurek mechanism. *Phys. Rev. Lett.*, 105, 075701 (2010)

[38] del Campo A, Kibble T W B and Zurek W H. Causality and non-equilibrium second-order phase transitions in inhomogeneous systems. *J. of Phys. Cond. Mat.*, 25, 404210 (2013)

[39] del Campo A and Zurek W H. *Symmetry and Fundamental Physics: Tom Kibble at 80*, chapter from "'Universality of Phase Transition Dynamics: Topological Defects From Symmetry Breaking"', 31–88, World Scientific (2013)

[40] Deshpande V V and Bockrath M. The one-dimensional Wigner crystal in carbon nanotubes. *Nat. Phys.*, 4, 314 (2008)

[41] Diedrich F, Peik E, Chen J M, Quint W and Walther H. Observation of a phase transition of stored laser-cooled ions. *Phys. Rev. Lett.*, 59, 2931 (1987)

[42] Dodd M E, Hendry P C, Lawson N S, McClintock P V E and H. Williams C D H. Nonappearance of vortices in fast mechanical expansions of liquid ^{4}He through the lambda transition. *Phys. Rev. Lett.*, 81, 3703 (1998)

[43] Domb C. *The critical point.* Taylor and Francis (1996)

[44] Dubin D H E and O'Neil T M. Trapped nonneutral plasmas, liquids, and crystals (the thermal equilibrium states). *Rev. Mod. Phys.*, 71, 87 (1999)

[45] Dziarmaga J. Dynamics of a quantum phase transition: Exact solution of the quantum ising model. *Phys. Rev. Lett.*, 95, 245701 (2005)

[46] Dziarmaga J, Laguna P and Zurek W H. Symmetry breaking with a slant: Topological defects after an inhomogeneous quench. *Phys. Rev. Lett.*, 82, 4749 (1999)

[47] Dziarmaga J and Rams M M. Adiabatic dynamics of an inhomogeneous quantum phase transition: the case of a $z > 1$ dynamical exponent. *New J. Phys.*, 12, 103002 (2010)

[48] Dziarmaga J and Rams M M. Dynamics of an inhomogeneous quantum phase transition. *New J. Phys.*, 12, 055007 (2010)

[49] Ejtemaee S and Haljan P C. Spontaneous nucleation and dynamics of kink defects in zigzag arrays of trapped ions. *Phys. Rev. A*, 87, 051401 (2013)

[50] Fisher M. *Scaling, universality and renormalization group theory.* Springer Berlin/Heielberg (1983)

[51] Fishman S, De Chiara G, Calarco T and Morigi G. Structural phase transitions in low-dimensional ion crystals. *Phys. Rev. B*, 77, 064111 (2008)

[52] Friedenauer A, Schmitz H, Glueckert J T, Porras D and Schaetz T. Simulating a quantum magnet with trapped ions. *Nat. Phys.*, 4, 757 (2008)

[53] Nikoghosyan G, Nigmatullin R and Plenio M B. Universality in the dynamics of second-order phase transitions. *arXiv:1311.1543* (2013)

[54] Galván-Moya J E and Peeters F M. Ginzburg-Landau theory of the zigzag transition in quasi-one-dimensional classical wigner crystals. *Phys. Rev. B*, 84, 134106 (2011)

[55] Ghosh P K. *Ion Traps.* Clarendon Press (1995)

[56] Ginzburg V L. *Sov. Phys. - Solid State*, 2, 1824 (1961)

[57] Goldenfeld N. *Theory on Phase Transition and the Renormalization Group.* Addison-Wesley, Advanced Book Program, Reading, Mass. (1992)

[58] Golubchik D, Polturak E and Koren G. Evidence for long-range correlations within arrays of spontaneously created magnetic vortices in a Nb thin-film superconductor. *Phys. Rev. Lett.*, 104, 247002 (2010)

[59] Griffin S M, Lilienblum M, Delaney K T, Kumagai Y, Fiebig M and Spaldin N A. Scaling behavior and beyond equilibrium in the hexagonal manganites. *Phys. Rev. X*, 2, 041022 (2012)

[60] Grimes C C and Adams G. Evidence for a liquid-to-crystal phase transition in a classical, two-dimensional sheet of electrons. *Phys. Rev. Lett.*, 42, 795 (1979)

[61] Häffner H, Roos C F and Blatt R. Quantum computing with trapped ions. *Physics Reports*, 469, 155 (2008)

[62] Hohenberg P C and Halperin B I. Theory of dynamic critical phenomena. *Rev. Mod. Phys.*, 49, 435 (1977)

[63] Huber G, Deuschle T, Schnitzler W, Reichle R, Singer K and Schmidt-Kaler F. Transport of ions in a segmented linear paul trap in printed-circuit-board technology. *New J. Phys.*, 10, 013004 (2008)

[64] Islam R, Senko C, Campbell W C, Korenblit S, Smith J, Lee A, E. Edwards E E, Wang C -C J, Freericks J K and Monroe C. Emergence and frustration of magnetism with variable-range interactions in a quantum simulator. *Science*, 340, 583 (2013)

[65] Janoschek M, Garst M, Bauer A, Krautscheid P, Georgii R, Böni P and Pfleiderer C. Fluctuation-induced first-order phase transition in Dzyaloshinskii-Moriya helimagnets. *Phys. Rev. B*, 87, 134407 (2013)

[66] Wada M, Ohtani S, Okada K, Takayanagi T and Schuessler H A. Observation of ion coulomb crystals in a cryogenic linear octupole rf ion trap. *Physical Review A*, 80, 043405 (2009)

[67] Kadanoff L P. Theories of matter: Infinities and renormalisation. *arXiv:1002.2985* (2010)

[68] Kardar M. *Statistical Physics of Fields.* Cambridge University Press (2007)

[69] Kartashov Y V, Malomed B A and Torner L. Solitons in nonlinear lattices. *Rev. Mod. Phys.*, 83, 247 (2011)

[70] Kaufmann H, Ulm S, Jacob G, Poschinger U, Landa H, Retzker A, Plenio M B and Schmidt-Kaler F Precise Experimental Investigation of Eigenmodes in a Planar Ion Crystal. *Phys. Rev. Lett*, 109, 263003 (2012)

[71] Kibble T W B. Phase-transition dynamics in the lab and the universe. *Physics Today*, 60, 47 (2007)

[72] Kibble T W B. Some implications of a cosmological phase transition. *Physics Reports*, 67, 183 (1980)

[73] Kleinert H. Criterion for dominance of directional over size fluctuations in destroying order. *Phys. Rev. Lett.*, 84, 286 (2000)

[74] Kleinert H and Schulte-Frohlinde V. *Critical Properties of ϕ^4-Theories.* World Scientific (2001)

[75] Kolodrubetz M, Clark B K and Huse D A. Nonequilibrium dynamic critical scaling of the quantum Ising chain. *Phys. Rev. Lett.*, 109, 015701 (2012)

[76] Laguna P and Zurek W H. Density of kinks after a quench: When symmetry breaks, how big are the pieces? *Phys. Rev. Lett.*, 78, 2519 (1997)

[77] Laguna P and Zurek W H. Critical dynamics of symmetry breaking: Quenches, dissipation, and cosmology. *Phys. Rev. D*, 58, 085021 (1998)

[78] Lamporesi G, Donadello S, Serafini S, Dalfovo F and Ferrari G. Spontaneous creation of Kibble-Zurek solitons in a Bose-Einstein condensate. *Nat. Phys.*, 9, 656 (2013)

[79] Landa H, Drewsen M, Reznik B and Retzker A. Classical and quantum modes of coupled Mathieu equations. *J. Phys. A*, 45,455305 (2012)

[80] Landa H, Drewsen M, Reznik B and Retzker A. Modes of oscillation in radiofrequency Paul traps. *New J. Phys.*, 14,093023 (2012)

[81] Landa H, Marcovitch S, Retzker A, Plenio M B and Reznik B. Quantum coherence of discrete kink solitons in ion traps. *Phys. Rev. Lett.*, 104, 043004 (2010)

[82] Landau L D and Khalatnikov I M. On the anomalous absorption of a sound near to points of phase transition of the second kind. *Dokl. Akad. Nauk SSSR*, 96, 469 (1954)

[83] Larson D J, Bergquist J C, Bollinger J J, Itano W M and J. Wineland D J. Sympathetic cooling of trapped ions: A laser-cooled two-species nonneutral ion plasma. *Phys. Rev. Lett.*, 57, 70 (1986)

[84] Levin M A and Wen X G. String-net condensation: A physical mechanism for topological phases. *Phys. Rev. B*, 71, 045110 (2005)

[85] Maniv A, Polturak E and Koren G. Observation of magnetic flux generated spontaneously during a rapid quench of superconducting films. *Phys. Rev. Lett.*, 91, 197001 (2003)

[86] Marciante M, Champenois C, Calisti A and Knoop M. Structural phase transitions in multipole traps. *Appl. Phys. B*, 107, 1117 (2012)

[87] Mermin N D. The topological theory of defects in ordered media. *Rev. Mod. Phys.*, 51, 591 (1979)

[88] Metcaf H J and van der Straten P. *Laser Cooling and Trapping*. Springer (1999)

[89] Mielenz M, Brox J, Kahra S, Leschhorn G, Albert M, Schaetz T, Landa H, and Reznik B. Trapping of topological-structural defects in coulomb crystals. *Phys. Rev. Lett.*, 110, 133004 (2013)

[90] Monaco R, Aaroe M, Mygind J, Rivers R J and Koshelets V P. Experiments on spontaneous vortex formation in josephson tunnel junctions. *Phys. Rev. B*, 74, 144513 (2006)

[91] Monaco R, Mygind J and Rivers R J. Zurek-Kibble domain structures: The dynamics of spontaneous vortex formation in annular Josephson tunnel junctions. *Phys. Rev. Lett.*, 89, 080603 (2002)

[92] Monaco R, Mygind J, Rivers R J and Koshelets V P. Spontaneous fluxoid formation in superconducting loops. *Phys. Rev. B*, 80, 180501 (2009)

[93] Morfill G E and Ivlev A V. Complex plasmas: An interdisciplinary research field. *Rev. Mod. Phys.*, 81, 1353 (2009)

[94] Morigi G and Eschner J. Doppler cooling of a coulomb crystal. *Phys. Rev. A*, 64, 063407 (2001)

[95] Morigi G and Fishman S. Dynamics of an ion chain in a harmonic potential. *Phys. Rev. E*, 70, 066141 (2004)

[96] Morigi G and Fishman S. Eigenmodes and thermodynamics of a coulomb chain in a harmonic potential. *Phys. Rev. Lett.*, 93, 170602 (2004)

[97] Martinez E, Freitas N and Paz J P. Heat transport through ion crystals. *arXiv:1312.6644* (2013)

[98] Nigmatullin R. Phase transitions in ion traps. Master's thesis, Imperial College London (2011)

[99] O F Oxtoby O F, D E Pelinovsky D E and I V Barashenkov I V. Travelling kinks in discrete ϕ^4 models. *Nonlinearity*, 19, 217 (2006)

[100] Partner H L, Nigmatullin R, Burgermeister T, Pyka K, Keller J, Retzker A, Plenio M B and Mehlstäubler T E. Dynamics of topological defects in ion coulomb crystals. *New J. Phys.*, 15, 103013 (2013)

[101] Paul W. Electromagnetic traps for charged and neutral particles. *Rev. Mod. Phys.*, 62, 531 (1990)

[102] Penning F M. Die Glimmentladung bei niedrigem Druck zwischen koaxialen Zylindern in einem axialen Magnetfeld. *Physica*, 3, 873 (1936)

[103] Piacente G, Schweigert I V, Betouras J J and Peeters F M. Generic properties of a quasi-one-dimensional classical Wigner crystal. *Phys. Rev. B*, 69, 045324 (2004)

[104] Piacente G, Schweigert I V, Betouras J J and Peeters F M. Generic properties of a quasi-one-dimensional classical Wigner crystal. *Phys. Rev. B*, 69, 045324 (2004)

[105] Polkovnikov A, Sengupta K, Silva A and Vengalattore M. *Colloquium:* Nonequilibrium dynamics of closed interacting quantum systems. *Rev. Mod. Phys.*, 83, 863 (2011)

[106] Pollet L, Prokof'ev N V and Svistunov B V. Criticality in trapped atomic systems. *Phys. Rev. Lett.*, 104, 245705 (2010)

[107] Pruttivarasin T, Ramm M, Talukdar I, Kreuter A and Häffner H. Trapped ions in optical lattices for probing oscillator chain models. *New J. Phys.*, 13, 075012 (2011)

[108] Pyka K, Keller J, Partner H L, Nigmatullin R, Burgermeister T, Meier D M, Kuhlmann K, Retzker A, Plenio M B, Zurek W H, del Campo A and Mehlstäubler T E. Topological defect formation and spontaneous symmetry breaking in ion coulomb crystals. *Nat. Commun.*, 4, 2291 (2013)

[109] Pyka K, Herschbach N, Keller J and Mehlstäubler T E. A high-precision segmented paul trap with minimized micromotion for an optical multiple-ion clock. *Applied Physics B*, 114, 231 (2014).

[110] Retzker A, Thompson R C, Segal D M and Plenio M B. Double well potentials and quantum phase transitions in ion traps. *Phys. Rev. Lett.*, 101, 260504 (2008)

[111] Ruiz A, Alonso D, Plenio M B and del Campo A. Tuning heat transport in trapped-ion chains across a structural phase transition. *arXiv:1401.5480* (2014)

[112] Rutkowski P X, Michelini M C, Bray T H, Russo N, Maralo J and Gibson J K. Hydration of gas-phase Ytterbium ion complexes studied by experiment and theory. *Theoretical Chemistry Accounts*, 129, 575 (2011)

[113] Ruutu V M H, Eltsov V B, Gill A J, Kibble T W B, Krusius M, G. Makhlin Yu G, Placais B, Volovik G E and Xu W. Vortex formation in neutron-irradiated superfluid ^{3}He as an analogue of cosmological defect formation. *Nature*, 382, 334 (1996)

[114] Sachdev S. *Quantum Phase Transitions*. Cambridge University Press, Cambridge, UK (1999)

[115] Sadler L E, Higbie J M, Leslie S R, Vengalattore M and M. Stamper-Kurn D M. Spontaneous symmetry breaking in a quenched ferromagnetic spinor Bose-Einstein condensate. *Nature*, 443, 312 (2006)

[116] Schiffer J P. Phase transitions in anisotropically confined ionic crystals. *Phys. Rev. Lett.*, 70, 818 (1993)

[117] Schneider C, Porras D and Schaetz T. Experimental quantum simulations of many-body physics with trapped ions. *Reports on Progress in Physics*, 75, 024401 (2012)

[118] Shimshoni E, Morigi G and Fishman S. Quantum zigzag transition in ion chains. *Phys. Rev. Lett.*, 106, 010401 (2011)

[119] Silvi P, De Chiara G, Calarco T, Morigi G and Montangero S. Full characterization of the quantum linear-zigzag transition in atomic chains. *Annalen der Physik*, 525, 827 (2013)

[120] Skeel R D and Izaguirre J S A. An impulse integrator for Langevin dynamics. *Mol. Phys*, 100, 3885 (2002)

[121] Snigirev V G, Voronel' A V and Chashkin Yu R. Behavior of the specific heat C_v of pure substances near the critical point. *JETP*, 653 (1965)

[122] Sondhi S L, Girvin S M, Carini J P and Shahar D. Continuous quantum phase transitions. *Rev. Mod. Phys.*, 69, 315 (1997)

[123] Stenholm S. The semiclassical theory of laser cooling. *Rev. Mod. Phys.*, 58, 699 (1986)

[124] Straube A V, Dullens R P A, Schimansky-Geier L and Louis A A. Zigzag transitions and nonequilibrium pattern formation in colloidal chains. *J. Chem. Phys.*, 139, 134908 (2013).

[125] Sugiyama K and Yoda J. Disappearance of Yb^+ in excited states from rf trap by background gases. *Jpn. J. Appl. Phys.*, 34, 584 (1995)

[126] Sugiyama K and Yoda J. Production of YbH^+ by chemical reaction of Yb^+ in excited states with H_2 gas. *Phys. Rev. A*, 55, R10 (1997)

[127] Tatarkova S A, Carruthers A E and Dholakia K. One-dimensional optically bound arrays of microscopic particles. *Phys. Rev. Lett.*, 89, 283901 (2002)

[128] Tomboulis E. Canonical quantization of nonlinear waves. *Phys. Rev. D*, 12, 1678 (1975)

[129] Ulm S, Rossnagel J, Jacob G, Degünther C, Dawkins S T, G. Poschinger U G, Nigmatullin R, Retzker A, Plenio M B, Schmidt-Kaler F and Singer K. Observation of the Kibble-Zurek scaling law for defect formation in ion crystals. *Nat. Commun.*, 4, 2290 (2013)

[130] Vicari E. Entanglement and particle correlations of fermi gases in harmonic traps. *Phys. Rev. A*, 85, 062104 (2012)

[131] Waki I, Kassner S, Birkl G and Walther H. Observation of ordered structures of laser-cooled ions in a quadrupole storage ring. *Phys. Rev. Lett.*, 68, 2007 (1992)

[132] Walther A, Ziesel F, Ruster T, Dawkins S T, Ott K, Hettrich M, Singer K, Schmidt-Kaler F and Poschinger U. Controlling fast transport of cold trapped ions. *Phys. Rev. Lett.*, 109, 080501 (2012)

[133] Weiler C N, Neely T W, Scherer D R, Bradley A S, Davis M J and Anderson B P. Spontaneous vortices in the formation of Bose-Einstein condensates. *Nature*, 455, 948 (2008)

[134] Wigner E. On the interaction of electrons in metals. *Phys. Rev.*, 46, 1002 (1934)

[135] Wineland D J, Bergquist J C, Itano W M, Bollinger J J and Manney C H. Atomic-ion coulomb clusters in an ion trap. *Phys. Rev. Lett.*, 59, 2935 (1987)

[136] Wuerker R F, Shelton H and Langmuir R V. Electrodynamic containment of charged particles. *J. of Appl. Phys.*, 30, 342 (1959)

[137] Yates A and Zurek W H. Vortex formation in two dimensions: When symmetry breaks, how big are the pieces? *Phys. Rev. Lett.*, 80, 5477 (1998)

[138] Zurek W H. Cosmological experiments in superfluid helium? *Nature*, 317, 505 (1985)

[139] Zurek W H. Cosmic strings in laboratory superfluids and the topological remnants of other phase transition. *Acta Phys. Pol. B*, 24, 1301 (1993)

[140] Zurek W H. Causality in condensates: Gray solitons as relics of BEC formation. *Phys. Rev. Lett.*, 102, 105702 (2009)

[141] Zurek W H, Dorner U and Zoller P. Dynamics of a quantum phase transition. *Phys. Rev. Lett.*, 95, 105701 (2005)

Appendix A

Experimental methods

A.1 PTB experiment

The ion trap is a three dimensional segmented linear radio frequency (rf) Paul trap. It offers full control to compensate stray fields in 3D and, in particular, has low axial micromotion over a large range of several hundreds of micrometers [109]. The ions are trapped in a loading segment via photoionization and then shuttled to a spectroscopy segment, which is protected from the atomic beam. Avoiding contamination of the electrodes makes it possible to perform measurements with highly reproducible experimental parameters. The axial and radial secular frequencies in this segment were measured repeatedly, and a maximum deviation of respectively 0.5 kHz and 1 kHz over several weeks was observed. For a linear crystal of 29 ± 2 ions with length ~ 300 μm the maximum axial rf field component along the crystal is as low as 500 V/m, whereas the radial field does not exceed 200 V/m, corresponding to a total micromotion amplitude of only 12 nm. The ion crystal is imaged with a lens system optimized for minimum aberrations onto an EMCCD camera with a magnification of 28 and an experimentally estimated resolution of about 1.5 μm over the full ion chain length of 300 μm. At the given axial trap frequency, about 30 ions can be imaged in the zigzag configuration. The rf voltage driving the radial confinement is amplitude modulated by a control signal using an rf mixer. Its actual amplitude on the ion trap electrodes is monitored by a short antenna inside the helical resonator (U_{mon}) which impedance matches the amplified rf voltage U_{rf} to the trap capacitance [109]. By observing parametric heating of the ions the radial as well as axial secular frequencies are measured directly as a function of the trap voltages with a relative precision of 10^{-3}. To drive quenches of the radial confinement, a linear function, shown schematically figure A.1a, is applied as a control signal to the rf mixer. Due to the characteristics of the mixer, the measured slope of the ramp deviates from the ideal slope and therefore is fitted manually to the monitored signal U_{mon}, see figure A.1b, to obtain the effective quench time used in simulations. The characteristic time constant of the resonant circuit of 7 μs limits the

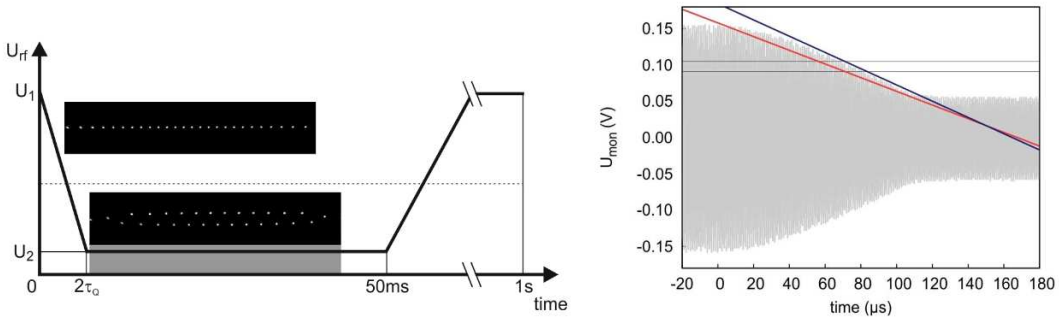

(a) **(b)**

Figure A.1: a) Experimental sequence of the radial quench. The radial trapping potential is steered by a linear ramp on the trapping voltage U_{rf}. The ramp of length $2\tau_Q$ starts at $t = 0$. Immediately after the quench an image of the Coulomb crystal is taken with an exposure time of 40 ms, then ν_t returns to its initial value. The ions are laser cooled and fluoresce throughout the whole sequence. After 1 second the cycle is repeated. b) Record of the monitored rf signal during the radial quench. The linear control signal (red line) has a ramp time of 105 μs. The actual rf voltage ramp (light gray line) deviates from this due to the non-linearity of the rf mixer. Its slope is determined by a manual fit (blue line) and corresponds to an effective ramp time of 88.4 μs. Also shown is the region of the linear to zigzag transition (area between the horizontal grey lines) for $N = 29 \pm 2$ ions. [The diagrams were taken from [108].]

fastest possible quench time, but its effect on the ramps used in this work is negligible.

A.2 Mainz experiment

Segmented linear Paul trap

The experiments are performed in an X-shaped micro-fabricated segmented Paul trap based on four gold-coated laser-cut alumina chips, each with 11 electrodes (see figure A.2) with a thickness of 125 mm. The segment width is 200 μm with isolating gaps of 30μm. The radial distance of the segmented electrodes to the center of the trap measures 960 μm, whereas the length of the whole trap is 2.9 mm. The radial confinement is generated by applying a radiofrequency voltage of $\sim$450 V_{pp} at a drive frequency of $\Omega/(2\pi) = 22$ MHz, resulting in a relevant radial trap frequency of $\omega_{\mathrm{rad}}/(2\pi) = 1.4$ MHz. The axial potential is generated by a superposition of static potentials applied to these segmented electrodes and variable voltages applied to the conical end-cap electrodes allowing for axial frequencies ($\omega_{\mathrm{ax}}/(2\pi)$ within a range of 167–344 kHz. The base pressure in the vacuum chamber is 1×10^{-9} mbar. Optical detection is achieved

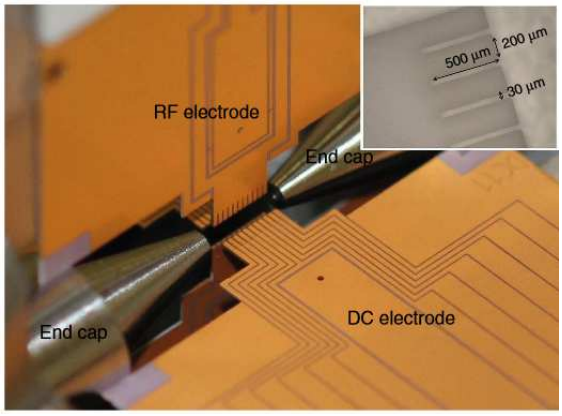

Figure A.2: Photograph of the segmented ion trap with gold-coated alumina chips and conical endcaps. On the right-hand side, one sees a direct current (DC) electrode with voltage supplies for the individual segments. On the top an radio frequency electrode is shown, segmented for symmetry reasons. The angle of view corresponds to the direction of the cooling laser beam. [The photograph was taken from [129].]

using an electron-multiplying charge-coupled device camera with a 10 ms exposure time, oriented at 45° to the planar structure of the crystal. The camera has an optical chip with 128×128 pixels and a pixel size of 24×24 μm^2. An objective lens leads to an effective pixel size in the acquired images of 1.7 μm.

Experimental sequence and set-up.

To allow for high statistics and a large number of data points in maintainable time, a high repetition rate of the whole experimental sequence was ensured by implementing a fully automated real-time experimental control system. A field programmable gate array (FPGA) controls the timing of the lasers [63, 132], the electron multiplying charge coupled device (EMCC) camera and the AFG, which has 16-bit amplitude resolution at a sample rate of 200 M samples per second for fast and glitch-free voltage ramps with variable time constants. The experimental sequence starts with the loading of ions. For this purpose, Ca atoms in a thermal atom beam cross the centre of the trap and are ionized with resonantly enhanced two-photon ionization at wavelengths of 423 and 375 nm. The cloud of trapped ions is Doppler-cooled by laser radiation red detuned to the cycling dipole transition $^2S_{1/2} -^2 P_{1/2}$, leading to a condensation of the ions into a linear crystal. To drive the cooling transition, we use a diode laser near 397 nm with a power of 0.15 mW and a beam direction that has a projection on all three trap axes. The cooling laser is switched on during the whole sequence of the experiment, and the

resonance fluorescence is used for the image acquisition. Ion losses can occur because of background gas collisions and possible losses during the relaxation ramp. With the fully automated sequence, we reach a repetition rate of one experiment per second. To achieve automated control, a first image is taken and the number of ions in the chain is evaluated. If the count is lower than 16, another pulse of the ionization lasers increases the number of ions. In the case where the number of ions is higher than 16, the axial trapping potential is temporarily lowered to reduce the ion number. Only if the number of ions in the chain is exactly 16, does the sequence continue with the ramp of the axial confining potential. The FPGA then triggers the AFG, which controls the ramp of the voltage at the endcaps and thus increases the axial trap frequency. Because of noise on external signal filters, we observe a temporal jitter of the start of the voltage ramp of about 80 ms. To guarantee that the images are taken after the ramp, the image acquisition exposure of 10 ms starts with a delay of 100 ms. Subsequent to the ramp and the image acquisition, the axial potential is ramped back slowly to the initial value, such that the crystal relaxes again into a linear configuration. Another image is taken to verify the number of ions. If the number still equals 16, the ramping sequence is started again. Otherwise, the sequence continues with reloading.